

A λ 3 mm line survey towards the circumstellar envelope of the carbon-rich AGB star IRC +10216 (CW Leo)

JUAN TUO,^{1,2} XIAOHU LI* ,^{1,3} JIXIAN SUN,^{4,5} TOM J. MILLAR,⁶ YONG ZHANG ,^{1,7,8} JIANJIE QIU ,⁷
DONGHUI QUAN,^{1,9} JARKEN ESIMBEK,^{1,3} JIANJUN ZHOU ,^{1,3} YU GAO[‡],^{10,4,5} QIANG CHANG,¹¹ LIN XIAO ,¹²
YANAN FENG,^{1,2} ZHENZHEN MIAO,^{1,3} RONG MA,^{1,2} RYSZARD SZCZERBA,^{1,13} AND XUAN FANG^{1,14,8}

¹*Xinjiang Astronomical Observatory, Chinese Academy of Sciences, 150 Science 1-Street, Urumqi, Xinjiang 830011, China*

²*University of Chinese Academy of Sciences, Beijing 100049, China*

³*Xinjiang Key Laboratory of Radio Astrophysics, 150 Science1-Street, Urumqi, Xinjiang 830011, China*

⁴*Purple Mountain Observatory, Chinese Academy of Sciences, Nanjing 210034, China*

⁵*Key Laboratory of Radio Astronomy, Chinese Academy of Sciences, Nanjing 210034, China*

⁶*Astrophysics Research Centre, School of Mathematics and Physics, Queen's University Belfast, Belfast, BT7 1NN, UK*

⁷*School of Physics and Astronomy, Sun Yat-sen University, Guangzhou 510275, China*

⁸*Laboratory for Space Research, Faculty of Science, The University of Hong Kong, Hong Kong, China*

⁹*Astronomical Computing Research Center, Zhejiang Laboratory, Hangzhou 311100, China*

¹⁰*Department of Astronomy, Xiamen University, Xiamen, Fujian 361005, China*

¹¹*School of Physics and Optoelectronic Engineering, Shandong University of Technology, Zibo, Shandong 255000, China*

¹²*College of Science, Changchun Institute of Technology, Changchun, Jilin 130012, China*

¹³*Nicolaus Copernicus Astronomical Center, Rabiańska 8, 87-100 Toruń, Poland*

¹⁴*National Astronomical Observatories, Chinese Academy of Sciences, A20, Datun Road, Chaoyang District, 100012 Beijing, China*

ABSTRACT

We present an unbiased λ 3 mm spectral line survey (between 84.5 and 115.8 GHz), conducted by the Purple Mountain Observatory 13.7 meter radio telescope, together with updated modeling results, towards the carbon-rich Asymptotic Giant Branch star, IRC +10216 (CW Leo). A total of 75 spectral lines (96 transitions) are detected, and identified to arise from 19 molecules: C₂H, *l*-C₃H, C₄H, CN, C₃N, HC₃N, HC₅N, HCN, HNC, CH₃CN, MgNC, CO, *c*-C₃H₂, SiC₂, SiO, SiS, CS, C₂S, C₃S, and their isotopologues. Among them, one molecular emission line (H¹³CCCN $J = 13 - 12$) is discovered in IRC +10216 for the first time. The excitation temperature, column density, and fractional abundance of the detected species are deduced by assuming they are in local thermodynamic equilibrium. In addition, the isotopic ratios of [¹²C]/[¹³C], [³²S]/[³⁴S], [²⁸Si]/[²⁹Si], and [¹²C³⁴S]/[¹³C³²S] are obtained and found to be consistent with previous studies. Finally, we summarize all of the 106 species detected in IRC +10216 to date with their observed and modeled column densities for the convenience of future studies.

Keywords: Stars (251) — IRC +10216 (1736) — radio lines (1868) — identification (804)

1. INTRODUCTION

One of the most important stages in the evolution of intermediate and low mass stars ($0.8 - 8 M_{\odot}$) is the asymptotic giant branch (AGB) stage. During the AGB phase the mass-loss rate is about $10^{-8} - 10^{-4} M_{\odot} \text{ yr}^{-1}$ (De Beck et al. 2010). The ejected material forms a dense circumstellar envelope (CSE) composed of gas and dust. Based on the carbon to oxygen abundance ratio ($[C]/[O]$), AGB stars can be divided into carbon-rich AGB stars (C-rich, $[C]/[O] > 1$), oxygen-rich AGB stars (O-rich, $[C]/[O] < 1$), and S-type AGB stars ($[C]/[O] \approx 1$) (Olofsson 1996).

*Corresponding author: X. Li, E-mail address: xiaohu.li@xao.ac.cn

‡Prof. Yu Gao passed away on 21 May 2022

Table 1. A summary of the 106 detected species (excluding isotopologues) toward the CSE of the carbon-rich AGB star, IRC+10216, together with their total column density from both observation ($N_{\text{Obs.}}$) and an astrochemical model ($N_{\text{Mod.}}$) that has been updated from Li et al. (2014) and is briefly described in Section 4.3.

No.	Species	$N_{\text{Obs.}}$ (cm^{-2})	Ref.	$N_{\text{Mod.}}$ (cm^{-2})
(1)	C(CI)	$(4.0 - 7.0) \times 10^{15}$	Keene et al. (1993)	2.19×10^{16}
	C (CI)	2.5×10^{16}	van der Veen et al. (1998)	2.19×10^{16}
	C (CI)		Jeste et al. (2023)	2.19×10^{16}
(2)	C ⁺ (CII)	$(4.0 \pm 0.6) \times 10^{17}$	Reach et al. (2022)	3.83×10^{16}
	C ⁺ (CII)		Jeste et al. (2023)	3.83×10^{16}
(3)	C ₂	7.9×10^{14}	Bakker et al. (1997)	4.79×10^{15}
(4)	OH		Ford et al. (2003)	2.96×10^{14}
(5)	HF		Agúndez et al. (2011)	1.02×10^{14}
(6)	AlF ^a	$(0.3 - 1.1) \times 10^{15}$	Ziurys et al. (1994)	
	AlF		Cernicharo & Guélin (1987)	
(7)	HCl		Cernicharo et al. (2010a)	1.25×10^{15}
(8)	KCl		Cernicharo & Guélin (1987)	
(9)	NaCl	5×10^{12}	Cernicharo & Guélin (1987)	
(10)	AlCl		Cernicharo & Guélin (1987)	
(11)	CP ^a	5×10^{12}	Halfen et al. (2008)	2.16×10^{12}
	CP	8×10^{13}	Guélin et al. (1990)	2.16×10^{12}
(12)	PN	6.3×10^{12}	Halfen et al. (2008)	3.89×10^{12}
	PN		Milam et al. (2008)	3.89×10^{12}
	PN	1.6×10^{12}	Agúndez et al. (2007)	3.89×10^{12}
	PN		Guélin et al. (2000)	3.89×10^{12}
	PN		Cernicharo et al. (2000)	3.89×10^{12}
(13)	CN	$(1.08 \pm 0.42) \times 10^{15}$	This work	3.25×10^{15}
	CN	2×10^{15}	Agúndez et al. (2010)	3.25×10^{15}
	CN	6.2×10^{14}	Groesbeck et al. (1994)	3.25×10^{15}
	CN	7.6×10^{14}	Avery et al. (1992)	3.25×10^{15}
	CN	1.7×10^{15}	Wootten et al. (1982)	3.25×10^{15}
	CN		Wilson et al. (1971)	3.25×10^{15}
(14)	SiN	3.8×10^{13}	Turner (1992)	3.72×10^{11}
(15)	CS	$(1.57 \pm 0.46) \times 10^{15}$	This work	1.02×10^{16}
	CS	5.9×10^{15}	Kawaguchi et al. (1995)	1.02×10^{16}
	CS	3.0×10^{15}	Groesbeck et al. (1994)	1.02×10^{16}
	CS ^a	4×10^{15}	Cernicharo et al. (1987a)	1.02×10^{16}
	CS	1.8×10^{15}	Morris et al. (1975)	1.02×10^{16}
	CS		Penzias et al. (1971)	1.02×10^{16}
(16)	SiC	$(4.9 \pm 2.3) \times 10^{13}$	He et al. (2008)	1.95×10^{13}
	SiC ^a	6×10^{13}	Cernicharo et al. (1989)	1.95×10^{13}
(17)	FeC		Koelemay & Ziurys (2023)	

Table 1 continued on next page

Table 1 (*continued*)

No.	Species	$N_{\text{Obs.}}$ (cm^{-2})	Ref.	$N_{\text{Mod.}}$ (cm^{-2})
(18)	SiO	$(4.84 \pm 1.13) \times 10^{14}$	This work	1.74×10^{15}
	SiO	4.1×10^{14}	Morris et al. (1975)	1.74×10^{15}
	SiO	5.4×10^{14}	Kawaguchi et al. (1995)	1.74×10^{15}
	SiO	2.1×10^{14}	Groesbeck et al. (1994)	1.74×10^{15}
	SiO	5.4×10^{14}	Kawaguchi et al. (1995)	1.74×10^{15}
(19)	SiS	$(5.86 \pm 1.74) \times 10^{15}$	This work	2.17×10^{16}
	SiS	4.7×10^{15}	Kawaguchi et al. (1995)	2.17×10^{16}
	SiS	3.0×10^{15}	Groesbeck et al. (1994)	2.17×10^{16}
	SiS	$(6.5 \pm 0.5) \times 10^{15}$	Avery et al. (1992)	2.17×10^{16}
	SiS	7×10^{15}	Cernicharo et al. (1987a)	2.17×10^{16}
	SiS	1.6×10^{15}	Morris et al. (1975)	2.17×10^{16}
(20)	CO	$(4.03 \pm 1.51) \times 10^{17}$	This work	1.35×10^{19}
	CO	2.0×10^{18}	Groesbeck et al. (1994)	1.35×10^{19}
	CO		Solomon et al. (1971)	1.35×10^{19}
(21)	H ₂ O		Melnick et al. (2001)	3.22×10^{16}
(22)	KCN	$(1 \pm 0.2) \times 10^{12}$	Pulliam et al. (2010)	
(23)	NaCN	$(8.5 \pm 1.7) \times 10^{12}$	Pardo et al. (2022)	
	NaCN	3.8×10^{14}	Kawaguchi et al. (1995)	
	NaCN	$(2.0 - 3.8) \times 10^{13}$	Turner et al. (1994)	
(24)	MgCN	$(7.4 \pm 2) \times 10^{11}$	Cabezas et al. (2013)	
	MgCN ^a	2×10^{12}	Ziurys et al. (1995)	
(25)	SiCN ^a	2×10^{12}	Guélin et al. (2000)	
(26)	FeCN	8.6×10^{11}	Zack et al. (2011)	
(27)	MgNC	$(3.20 \pm 0.51) \times 10^{13}$	This work	
	MgNC	$(3.9 \pm 1.5) \times 10^{13}$	Gong et al. (2015)	
	MgNC	$(1.3 \pm 0.3) \times 10^{13}$	Cabezas et al. (2013)	
	MgNC	7.8×10^{13}	He et al. (2008)	
	MgNC	2.5×10^{13}	Kawaguchi et al. (1993)	
	MgNC		Guélin et al. (1993)	
	MgNC		Guélin et al. (1986)	
(28)	AlNC	9×10^{11}	Ziurys et al. (2002)	
(29)	SiNC	2×10^{12}	Guélin et al. (2004)	9.35×10^8
(30)	CaNC	2×10^{11}	Cernicharo et al. (2019a)	
(31)	HNC	$(1.11 \pm 0.08) \times 10^{14}$	This work	1.17×10^{14}
	HNC		Brown et al. (1976)	1.17×10^{14}
(32)	HCN	$(7.36 \pm 0.92) \times 10^{14}$	This work	2.51×10^{17}
	HCN	2.8×10^{16}	Groesbeck et al. (1994)	2.51×10^{17}
	HCN		Morris et al. (1971)	2.51×10^{17}
(33)	MgC ₂	$(1.0 \pm 0.3) \times 10^{12}$	Changala et al. (2022)	
(34)	SiC ₂	$(1.41 \pm 0.34) \times 10^{15}$	This work	6.30×10^{15}

Table 1 continued on next page

Table 1 (continued)

No.	Species	$N_{\text{Obs.}}$ (cm^{-2})	Ref.	$N_{\text{Mod.}}$ (cm^{-2})
	SiC ₂	$(1.87 \pm 1.34) \times 10^{15}$	Zhang et al. (2017)	6.30×10^{15}
	SiC ₂	$(1.2 \pm 0.0) \times 10^{15}$	Gong et al. (2015)	6.30×10^{15}
	SiC ₂ ^b	$(2.35 \pm 0.36) \times 10^{15}$	He et al. (2008)	6.30×10^{15}
	SiC ₂ ^c	$(5.40 \pm 0.88) \times 10^{14}$	He et al. (2008)	6.30×10^{15}
	SiC ₂ ^d	1.04×10^{15}	He et al. (2008)	6.30×10^{15}
	SiC ₂ ^e	5.3×10^{15}	He et al. (2008)	6.30×10^{15}
	SiC ₂	2.2×10^{14}	Kawaguchi et al. (1995)	6.30×10^{15}
	SiC ₂	3.7×10^{14}	Groesbeck et al. (1994)	6.30×10^{15}
	SiC ₂	(cold range) 9.5×10^{14}	Avery et al. (1992)	6.30×10^{15}
	SiC ₂	(warm range) 1.9×10^{15}	Avery et al. (1992)	6.30×10^{15}
	SiC ₂ ^a	2×10^{15}	Cernicharo et al. (1987a)	6.30×10^{15}
	SiC ₂	1.5×10^{14}	Thaddeus et al. (1984)	6.30×10^{15}
(35)	SiCSi ^f	$(1.4 \pm 0.4) \times 10^{15}$	Cernicharo et al. (2015b)	
	SiCSi ^g	$(3.0 \pm 0.7) \times 10^{15}$	Cernicharo et al. (2015b)	
	SiCSi ^h	$(3.2 \pm 0.9) \times 10^{15}$	Cernicharo et al. (2015b)	
(36)	C ₃	1×10^{15}	Hinkle et al. (1988)	1.93×10^{14}
(37)	H ₂ S ^a	1×10^{13}	Cernicharo et al. (1987a)	5.11×10^{13}
(38)	HCP	$(1.0 - 1.4) \times 10^{14}$	Halfen et al. (2008)	3.17×10^{14}
	HCP	1.3×10^{15}	Agúndez et al. (2007)	3.17×10^{14}
(39)	C ₂ H	$(8.14 \pm 2.29) \times 10^{15}$	This work	1.01×10^{16}
	C ₂ H	$(3.84 \pm 0.09) \times 10^{15}$	De Beck et al. (2012)	1.01×10^{16}
	C ₂ H	5.0×10^{15}	Cernicharo et al. (2000)	1.01×10^{16}
	C ₂ H	4.6×10^{15}	Groesbeck et al. (1994)	1.01×10^{16}
	C ₂ H	5.4×10^{15}	Avery et al. (1992)	1.01×10^{16}
	C ₂ H		Tucker et al. (1974)	1.01×10^{16}
(40)	C ₂ P	1.2×10^{12}	Halfen et al. (2008)	8.99×10^9
(41)	C ₂ S	$(1.59 \pm 0.73) \times 10^{14}$	This work	1.84×10^{13}
	C ₂ S	$(4.0 \pm 0.7) \times 10^{13}$	Pardo et al. (2022)	1.84×10^{13}
	C ₂ S	$(2.3 \pm 0.8) \times 10^{14}$	Gong et al. (2015)	1.84×10^{13}
	C ₂ S	$(5.0 \pm 0.3) \times 10^{13}$	Agúndez et al. (2014)	1.84×10^{13}
	C ₂ S	1.5×10^{14}	Kawaguchi et al. (1995)	1.84×10^{13}
	C ₂ S	$(9 \pm 2) \times 10^{13}$	Bell et al. (1993)	1.84×10^{13}
	C ₂ S	1.5×10^{14}	Cernicharo et al. (1987a)	1.84×10^{13}
(42)	C ₂ N	$(1.1 \pm 0.6) \times 10^{13}$	Anderson & Ziurys (2014)	1.46×10^{13}
(43)	<i>l</i> -C ₃ H	$(1.25 \pm 0.22) \times 10^{14}$	This work	1.42×10^{14}
	<i>l</i> -C ₃ H	$(1.32 \pm 0.34) \times 10^{14}$	He et al. (2008)	1.42×10^{14}
	<i>l</i> -C ₃ H	7.0×10^{13}	Cernicharo et al. (2000)	1.42×10^{14}
	<i>l</i> -C ₃ H	5.6×10^{13}	Kawaguchi et al. (1995)	1.42×10^{14}
	<i>l</i> -C ₃ H	2.8×10^{13}	Thaddeus et al. (1985a)	1.42×10^{14}
(44)	<i>c</i> -C ₃ H		Cernicharo et al. (2000)	

Table 1 continued on next page

Table 1 (continued)

No.	Species	$N_{\text{Obs.}}$ (cm^{-2})	Ref.	$N_{\text{Mod.}}$ (cm^{-2})
(45)	H ₂ CO	5×10^{12}	Ford et al. (2004)	2.80×10^{11}
(46)	NH ₃ (para)	$(2.3, 2.7) \times 10^{14}$	Gong et al. (2015)	2.50×10^{16}
	NH ₃ (ortho)	$(1.5, 2.9) \times 10^{14}$	Gong et al. (2015)	2.50×10^{16}
	NH ₃	4.2×10^{13}	Nguyen-Q-Rieu et al. (1984)	2.50×10^{16}
	NH ₃	1×10^{17}	Betz et al. (1979)	2.50×10^{16}
(47)	C ₃ S	$(3.27 \pm 0.16) \times 10^{13}$	This work	1.55×10^{13}
	C ₃ S	$(2.58 \pm 3.60) \times 10^{13}$	Pardo et al. (2022)	1.55×10^{13}
	C ₃ S	$(2.2 \pm 0.4) \times 10^{13}$	Gong et al. (2015)	1.55×10^{13}
	C ₃ S	$(1.7 \pm 0.1) \times 10^{13}$	Agúndez et al. (2014)	1.55×10^{13}
	C ₃ S	$(4.9 \pm 0.3) \times 10^{13}$	Kawaguchi et al. (1995)	1.55×10^{13}
	C ₃ S	$(5.8 \pm 2.7) \times 10^{12}$	Bell et al. (1993)	1.55×10^{13}
	C ₃ S	1.1×10^{14}	Cernicharo et al. (1987a)	1.55×10^{13}
(49)	C ₃ N	$(4.25 \pm 0.81) \times 10^{14}$	This work	5.85×10^{14}
	C ₃ N	$(3.1 \pm 0.3) \times 10^{14}$	Gong et al. (2015)	5.85×10^{14}
	C ₃ N	$(4.54 \pm 2.13) \times 10^{14}$	He et al. (2008)	5.85×10^{14}
	C ₃ N	2.5×10^{14}	Cernicharo et al. (2000)	5.85×10^{14}
	C ₃ N	4.1×10^{14}	Kawaguchi et al. (1995)	5.85×10^{14}
(49)	C ₂ H ₂	3×10^{19}	Ridgway et al. (1976)	9.94×10^{17}
(50)	H ₂ CS ^a	1.0×10^{13}	Agúndez et al. (2008b)	5.01×10^{11}
(51)	SiC ₃	(cold range) 4.3×10^{12}	Apponi et al. (1999)	2.03×10^{12}
	SiC ₃	(warm range) 4.3×10^{12}	Apponi et al. (1999)	2.03×10^{12}
(52)	C ₃ O	1.2×10^{12}	Tenenbaum et al. (2006)	1.07×10^{12}
(53)	HC ₂ N	1.4×10^{13}	Cernicharo et al. (2004)	
	HC ₂ N	1.8×10^{13}	Kawaguchi et al. (1995)	
	HC ₂ N	1.2×10^{13}	Guélin & Cernicharo (1991)	
(54)	HMgNC	6×10^{11}	Cabezas et al. (2013)	
(55)	MgCCH	2×10^{12}	Agúndez et al. (2014)	
	MgCCH	2×10^{12}	Cernicharo et al. (2019b)	
(56)	NCCP*	7×10^{11}	Agúndez et al. (2014)	
(57)	PH ₃		Agúndez et al. (2008a)	
	PH ₃		Tenenbaum & Ziurys (2008)	
(58)	C ₅	1×10^{14}	Bernath et al. (1989)	1.61×10^{14}
(59)	<i>c</i> -C ₃ H ₂ (ortho)	$(1.14 \pm 0.15) \times 10^{14}$	This work	5.85×10^{13}
	<i>c</i> -C ₃ H ₂ (para)	$(8.02 \pm 4.54) \times 10^{13}$	This work	5.85×10^{13}
	<i>c</i> -C ₃ H ₂	$(1.39 \pm 1.07) \times 10^{14}$	Zhang et al. (2017)	5.85×10^{13}
	<i>c</i> -C ₃ H ₂ (ortho)	$(1.2 \pm 0.3) \times 10^{14}$	Gong et al. (2015)	5.85×10^{13}
	<i>c</i> -C ₃ H ₂ (para)	$(8.9 \pm 0.5) \times 10^{13}$	Gong et al. (2015)	5.85×10^{13}
	<i>c</i> -C ₃ H ₂ (ortho)	$(4.82 \pm 4.14) \times 10^{14}$	He et al. (2008)	5.85×10^{13}
	<i>c</i> -C ₃ H ₂ (para)	$(1.22 \pm 2.03) \times 10^{14}$	He et al. (2008)	5.85×10^{13}
	<i>c</i> -C ₃ H ₂	1.6×10^{13}	Kawaguchi et al. (1995)	5.85×10^{13}

Table 1 continued on next page

Table 1 (*continued*)

No.	Species	$N_{\text{Obs.}}$ (cm^{-2})	Ref.	$N_{\text{Mod.}}$ (cm^{-2})
(60)	H ₂ C ₃	2.6×10^{12}	Cernicharo et al. (1991a)	1.20×10^{13}
(61)	HC ₃ N	$(1.18 \pm 0.08) \times 10^{15}$	This work	4.79×10^{14}
	HC ₃ N	$(1.94 \pm 0.21) \times 10^{15}$	Zhang et al. (2017)	4.79×10^{14}
	HC ₃ N	$(1.4 \pm 0.2) \times 10^{15}$	Gong et al. (2015)	4.79×10^{14}
	HC ₃ N	$(8.0 \pm 1.5) \times 10^{14}$	He et al. (2008)	4.79×10^{14}
	HC ₃ N	1.7×10^{15}	Kawaguchi et al. (1995)	4.79×10^{14}
	HC ₃ N	(cold range) $(7.9 \pm 0.2) \times 10^{14}$	Bell (1993)	4.79×10^{14}
	HC ₃ N	(warm range) $(2.1 \pm 1.4) \times 10^{14}$	Bell (1993)	4.79×10^{14}
	HC ₃ N	5.9×10^{14}	Gensheimer (1997a)	4.79×10^{14}
	HC ₃ N	1.1×10^{15}	Gensheimer (1997b)	4.79×10^{14}
	HC ₃ N	$(1.6 \pm 0.4) \times 10^{15}$	Jewell & Snyder (1984)	4.79×10^{14}
	HC ₃ N	1.8×10^{15}	Morris et al. (1975)	4.79×10^{14}
(62)	HNC ₃ ^a	1×10^{12}	Gensheimer (1997a)	7.32×10^{11}
(63)	HC ₂ NC	$2.8, 3.6 \times 10^{12}$	Gensheimer (1997a)	
	HC ₂ NC ^a	8.4×10^{12}	Gensheimer (1997b)	
(64)	CH ₂ CN	$(8.6 \pm 1.4) \times 10^{12}$	Agúndez et al. (2008b)	2.58×10^{11}
(65)	CH ₂ NH	9×10^{12}	Tenenbaum et al. (2010a)	2.56×10^{11}
(66)	C ₄ H	$(2.75 \pm 0.36) \times 10^{15}$	This work	6.57×10^{14}
	C ₄ H	$(1.84 \pm 0.25) \times 10^{14}$	Pardo et al. (2022)	6.57×10^{14}
	C ₄ H	$(2.4 \pm 0.2) \times 10^{15}$	Gong et al. (2015)	6.57×10^{14}
	C ₄ H	$(8.1 \pm 1.1) \times 10^{15}$	He et al. (2008)	6.57×10^{14}
	C ₄ H	3.0×10^{14}	Cernicharo et al. (2000)	6.57×10^{14}
	C ₄ H	$(0.4 - 3) \times 10^{15}$	Guélin et al. (1978)	6.57×10^{14}
	C ₄ H	2.4×10^{15}	Kawaguchi et al. (1995)	6.57×10^{14}
	C ₄ H	5.6×10^{15}	Avery et al. (1992)	6.57×10^{14}
(67)	CH ₄	2.5×10^{17}	Hall & Ridgway (1978)	4.41×10^{16}
	CH ₄	1.8×10^{16}	Clegg et al. (1982)	4.41×10^{16}
(68)	SiH ₄	2×10^{15}	Goldhaber & Betz (1984)	2.78×10^{15}
(69)	SiC ₄	$(6.2 \pm 1.0) \times 10^{12}$	Pardo et al. (2022)	2.45×10^{11}
	SiC ₄	$(1.46 \pm 0.92) \times 10^{13}$	Zhang et al. (2017)	2.45×10^{11}
	SiC ₄	$(1.1 \pm 0.4) \times 10^{13}$	Gong et al. (2015)	2.45×10^{11}
	SiC ₄	7×10^{12}	Kawaguchi et al. (1995)	2.45×10^{11}
	SiC ₄	$(7 \pm 1) \times 10^{12}$	Ohishi et al. (1989)	2.45×10^{11}
(70)	NaC ₃ N	$(1.2 \pm 0.2) \times 10^{11}$	Cabezas et al. (2023)	
(71)	MgC ₃ N	$(5.2 \pm 0.6) \times 10^{12}$	Pardo et al. (2022)	
	MgC ₃ N	(cold range) $(5.7 \pm 1.0) \times 10^{12}$	Cernicharo et al. (2019b)	
	MgC ₃ N	(warm range) $(3.6 \pm 0.6) \times 10^{12}$	Cernicharo et al. (2019b)	
(72)	MgC ₄ H	$(1.5 \pm 1.3) \times 10^{13}$	Pardo et al. (2022)	
	MgC ₄ H	$(2.2 \pm 0.5) \times 10^{13}$	Cernicharo et al. (2019b)	
(73)	HMgC ₃ N	$(3.0 \pm 0.6) \times 10^{12}$	Cabezas et al. (2023)	

Table 1 continued on next page

Table 1 (*continued*)

No.	Species	$N_{\text{Obs.}}$ (cm^{-2})	Ref.	$N_{\text{Mod.}}$ (cm^{-2})
(74)	$\text{C}_5\text{H } ^2\Pi_{1/2}$	$(2.7 \pm 0.5) \times 10^{13}$	Pardo et al. (2022)	4.40×10^{13}
	$\text{C}_5\text{H } ^2\Pi_{3/2}$	$(2.52 \pm 2.48) \times 10^{14}$	Pardo et al. (2022)	4.40×10^{13}
	$\text{C}_5\text{H } ^2\Pi_{1/2}$	$(2.96 \pm 1.21) \times 10^{14}$	Zhang et al. (2017)	4.40×10^{13}
	$\text{C}_5\text{H } ^2\Pi_{1/2}$	$(2.9 \pm 0.6) \times 10^{13}$	Gong et al. (2015)	4.40×10^{13}
	$\text{C}_5\text{H } ^2\Pi_{3/2}$	$(1.2 \pm 2.3) \times 10^{14}$	Gong et al. (2015)	4.40×10^{13}
	C_5H	4.4×10^{13}	Cernicharo et al. (2000)	4.40×10^{13}
	$\text{C}_5\text{H } ^2\Pi_{1/2}$	$(2.9 \pm 0.3) \times 10^{14}$	Kawaguchi et al. (1995)	4.40×10^{13}
	$\text{C}_5\text{H } ^2\Pi_{3/2}$	$(2.0 \pm 0.1) \times 10^{14}$	Kawaguchi et al. (1995)	4.40×10^{13}
(75)	C_2H_4	(cold) $(1.7 \pm 0.4) \times 10^{15}$	Fonfría et al. (2017)	8.59×10^{14}
	C_2H_4	(warm) $(4.8 \pm 1.3) \times 10^{15}$	Fonfría et al. (2017)	8.59×10^{14}
	C_2H_4	4×10^{15}	Goldhaber et al. (1987)	8.59×10^{14}
	C_2H_4	10^{16}	Betz (1981)	8.59×10^{14}
(76)	HC_4N	$(3.9 \pm 3.7) \times 10^{12}$	Pardo et al. (2022)	
	HC_4N^a	1.5×10^{12}	Cernicharo et al. (2004)	
(77)	H_2C_4	3×10^{12}	Kawaguchi et al. (1995)	
	H_2C_4	1.6×10^{13}	Cernicharo et al. (1991b)	
(78)	C_5N^a	6.3×10^{12}	Cernicharo et al. (2000)	2.91×10^{13}
	C_5N^a	3.1×10^{11}	Guélin et al. (1998)	2.91×10^{13}
(79)	CH_3CN	$(6.81 \pm 3.51) \times 10^{13}$	This work	4.88×10^{12}
	CH_3CN	$(2.6 \pm 0.6) \times 10^{13}$	He et al. (2008)	4.88×10^{12}
	CH_3CN	6×10^{12}	Kawaguchi et al. (1995)	4.88×10^{12}
	CH_3CN	6×10^{12}	Guélin & Cernicharo (1991)	4.88×10^{12}
	CH_3CN		Johansson et al. (1984)	4.88×10^{12}
(80)	SiH_3CN	1×10^{12}	Agúndez et al. (2014)	
(81)	C_5S	$(0.2 - 1.4) \times 10^{13}$	Agúndez et al. (2014)	
	C_5S^a	3.6×10^{13}	Bell et al. (1993)	
(82)	$\text{C}_6\text{H } ^2\Pi_{1/2}$	$(1.23 \pm 0.18) \times 10^{13}$	Pardo et al. (2022)	6.01×10^{14}
	$\text{C}_6\text{H } ^2\Pi_{3/2}$	$(1.51 \pm 0.14) \times 10^{13}$	Pardo et al. (2022)	6.01×10^{14}
	$\text{C}_6\text{H } ^2\Pi_{1/2}$	$(1.85 \pm 0.90) \times 10^{13}$	Zhang et al. (2017)	6.01×10^{14}
	$\text{C}_6\text{H } ^2\Pi_{1/2}$	$(1.0 \pm 0.2) \times 10^{14}$	Gong et al. (2015)	6.01×10^{14}
	$\text{C}_6\text{H } ^2\Pi_{3/2}$	$(1.0 \pm 0.1) \times 10^{14}$	Gong et al. (2015)	6.01×10^{14}
	$\text{C}_6\text{H } ^2\Pi_{3/2}$	$(6.6 \pm 2.0) \times 10^{13}$	Cernicharo et al. (2007)	6.01×10^{14}
	C_6H	5.5×10^{13}	Cernicharo et al. (2000)	6.01×10^{14}
	$\text{C}_6\text{H } ^2\Pi_{1/2}$	$(1.13 \pm 0.06) \times 10^{14}$	Kawaguchi et al. (1995)	6.01×10^{14}
	$\text{C}_6\text{H } ^2\Pi_{3/2}$	$(1.67 \pm 0.07) \times 10^{14}$	Kawaguchi et al. (1995)	6.01×10^{14}
	$\text{C}_6\text{H } ^2\Pi_{1/2}$	$(3 \pm 1) \times 10^{13}$	Saito et al. (1987)	6.01×10^{14}
	$\text{C}_6\text{H } ^2\Pi_{3/2}$	$(1_{-0.5}^{+1.5}) \times 10^{13}$	Saito et al. (1987)	6.01×10^{14}
	C_6H^a	3×10^{14}	Cernicharo et al. (1987b)	6.01×10^{14}
(83)	HC_5N	$(5.41 \pm 0.56) \times 10^{14}$	This work	1.39×10^{14}

Table 1 continued on next page

Table 1 (*continued*)

No.	Species	$N_{\text{Obs.}}$ (cm^{-2})	Ref.	$N_{\text{Mod.}}$ (cm^{-2})
	HC ₅ N	$(4.2 \pm 0.4) \times 10^{14}$	Pardo et al. (2022)	1.39×10^{14}
	HC ₅ N	$(5.47 \pm 0.77) \times 10^{14}$	Zhang et al. (2017)	1.39×10^{14}
	HC ₅ N	$(4.6 \pm 0.2) \times 10^{14}$	Gong et al. (2015)	1.39×10^{14}
	HC ₅ N	$(2.3 - 5.47) \times 10^{14}$	Kawaguchi et al. (1995)	1.39×10^{14}
	HC ₅ N	(warm range) $(2.3 - 5.47) \times 10^{14}$	Bell (1993)	1.39×10^{14}
	HC ₅ N	(cold range) 3.2×10^{14}	Bell et al. (1992b)	1.39×10^{14}
	HC ₅ N	(warm range) 3.7×10^{14}	Bell et al. (1992b)	1.39×10^{14}
	HC ₅ N	4×10^{14}	Winnewisser & Walmsley (1978)	1.39×10^{14}
	HC ₅ N		Churchwell et al. (1978)	1.39×10^{14}
(84)	SiC ₆ *	1.3×10^{12}	Pardo et al. (2022)	
(85)	CH ₂ CHCN	5.5×10^{12}	Agúndez et al. (2008b)	4.71×10^{11}
(86)	CH ₃ CCH ^a	1.8×10^{13}	Agúndez et al. (2008b)	1.44×10^{12}
(87)	MgC ₅ N	4.7×10^{12}	Pardo et al. (2022, 2021)	
(88)	MgC ₆ H	2.0×10^{13}	Pardo et al. (2022, 2021)	
(89)	CH ₃ SiH ₃		Cernicharo et al. (2017)	
(90)	C ₇ H ² Π _{1/2}	$(5.1 \pm 1.0) \times 10^{12}$	Pardo et al. (2022)	7.11×10^{13}
	C ₇ H ² Π _{3/2}	$(3.2 \pm 2.0) \times 10^{12}$	Pardo et al. (2022)	7.11×10^{13}
	C ₇ H	2.2×10^{12}	Cernicharo et al. (2000)	7.11×10^{13}
	C ₇ H	2×10^{12}	Guélin et al. (1997)	7.11×10^{13}
(91)	C ₆ H ₂		Guélin et al. (2000, 1997)	6.96×10^{14}
(92)	HC ₇ N	$(1.95 \pm 0.11) \times 10^{14}$	Pardo et al. (2022)	4.61×10^{13}
	HC ₇ N	$(1.52 - 6.21) \times 10^{14}$	Zhang et al. (2017)	4.61×10^{13}
	HC ₇ N	$(3.7 \pm 0.4) \times 10^{14}$	Gong et al. (2015)	4.61×10^{13}
	HC ₇ N	$(1.29 \pm 0.06) \times 10^{14}$	Kawaguchi et al. (1995)	4.61×10^{13}
	HC ₇ N ^a	2×10^{14}	Winnewisser & Walmsley (1978)	4.61×10^{13}
(93)	C ₈ H ¹ Π _{3/2}	$(1.15 \pm 1.38) \times 10^{13}$	Pardo et al. (2022)	1.38×10^{14}
	C ₈ H ² Π _{3/2}	$(8.9 \pm 0.9) \times 10^{12}$	Pardo et al. (2022)	1.38×10^{14}
	C ₈ H ² Π _{3/2}	$(5.00 \pm 1.008) \times 10^{13}$	Zhang et al. (2017)	1.38×10^{14}
	C ₈ H ² Π _{3/2}	$(8.4 \pm 1.4) \times 10^{13}$	Gong et al. (2015)	1.38×10^{14}
	C ₈ H	$(8 \pm 3) \times 10^{12}$	Remijan et al. (2007)	1.38×10^{14}
	C ₈ H	1.0×10^{13}	Cernicharo et al. (2000)	1.38×10^{14}
	C ₈ H	5.5×10^{12}	Cernicharo & Guélin (1996)	1.38×10^{14}
(94)	HC ₉ N	$(4.5 \pm 0.6) \times 10^{13}$	Pardo et al. (2022)	1.31×10^{13}
	HC ₉ N	$(5.88 \pm 1.28) \times 10^{13}$	Zhang et al. (2017)	1.31×10^{13}
	HC ₉ N	$(2.5 \pm 1.4) \times 10^{13}$	Gong et al. (2015)	1.31×10^{13}
	HC ₉ N	$(2.7 \pm 0.9) \times 10^{13}$	Kawaguchi et al. (1995)	1.31×10^{13}
	HC ₉ N	4×10^{13}	Bell et al. (1992a)	1.31×10^{13}
(95)	CN ⁻	5×10^{12}	Agúndez et al. (2010)	5.56×10^{10}
(96)	HCO ⁺		Pulliam et al. (2011)	1.98×10^{12}
	HCO ⁺		Tenenbaum et al. (2010b)	1.98×10^{12}

Table 1 continued on next page

Table 1 (continued)

No.	Species	$N_{\text{Obs.}}$ (cm^{-2})	Ref.	$N_{\text{Mod.}}$ (cm^{-2})
(97)	C_3N^-	1.6×10^{12}	Thaddeus et al. (2008)	3.07×10^{11}
(98)	C_4H^-	$(7.1 \pm 2.0) \times 10^{11}$	Cernicharo et al. (2007)	1.28×10^{13}
(99)	MgC_3N^+	$(1.2 \pm 0.2) \times 10^{11}$	Cernicharo et al. (2023a)	
(100)	MgC_4H^+	$(4.8 \pm 0.3) \times 10^{11}$	Cernicharo et al. (2023a)	
(101)	C_5N^-	$(4.9 \pm 1.6) \times 10^{12}$	Pardo et al. (2022)	3.58×10^{12}
	C_5N^-	$(3.4 - 4.9) \times 10^{12}$	Cernicharo et al. (2008)	3.58×10^{12}
	C_5N^-	$(5.7 \pm 0.2) \times 10^{12}$	Cernicharo et al. (2023b)	3.58×10^{12}
(102)	C_6H^-	$(4.3 \pm 0.6) \times 10^{12}$	Pardo et al. (2022)	8.71×10^{13}
	C_6H^-	$(6.11 \pm 2.99) \times 10^{12}$	Zhang et al. (2017)	8.71×10^{13}
	C_6H^-	$(5.8 \pm 0.5) \times 10^{12}$	Gong et al. (2015)	8.71×10^{13}
	C_6H^-	$(6.1 - 8.0) \times 10^{12}$	Kasai et al. (2007)	8.71×10^{13}
	C_6H^-	$(4.1 \pm 1.5) \times 10^{12}$	Cernicharo et al. (2007)	8.71×10^{13}
	C_6H^-	4×10^{12}	McCarthy et al. (2006)	8.71×10^{13}
(103)	MgC_5N^+	$(1.1 \pm 0.2) \times 10^{11}$	Cernicharo et al. (2023a)	
(104)	MgC_6H^+	$(2.5 \pm 0.3) \times 10^{11}$	Cernicharo et al. (2023a)	
(105)	C_7N^-	$(2.4 \pm 0.2) \times 10^{12}$	Cernicharo et al. (2023b)	
(106)	C_8H^-	$(1.1 \pm 0.4) \times 10^{12}$	Pardo et al. (2022)	3.30×10^{12}
	C_8H^-	$(8 \pm 3) \times 10^{12}$	Remijan et al. (2007)	3.30×10^{12}
	C_8H^-	$(1.5 \pm 0.6) \times 10^{12}$	Kawaguchi et al. (2007)	3.30×10^{12}

NOTE—^(a) Assumed rotational temperature. ^(*) The detection of SiC_6 is marginal and the identification of NCCP is tentative. ^(b) The range of data for SiC_2 fitting is $J_{(up)} = 6, 7$; $K_a = 0, 2, 4$. ^(c) The range of data for SiC_2 fitting is $J_{(up)} = 9, 10, 11, 12$; $K_a = 0, 2, 4$. ^(d) The range of data for SiC_2 fitting is $J_{(up)} = 10, 11$; $K_a = 6$. ^(e) The range of data for SiC_2 fitting is $J_{(up)} = 10, 11$; $K_a = 8$. ^(f) The range of upper level energy for SiCSi fitting is $E_u < 60$ K. ^(g) The range of upper level energy for SiCSi fitting is $60 \text{ K} < E_u < 200 \text{ K}$. ^(h) The range of upper level energy for SiCSi fitting is $E_u > 200 \text{ K}$.

IRC +10216 (CW Leo), a C-rich AGB star, is the brightest astronomical source at $5 \mu\text{m}$ outside the Solar System (Becklin et al. 1969). Its mass-loss rate is about $2 \times 10^{-5} M_{\odot} \text{ yr}^{-1}$ at a distance of 130 pc to Earth (Crosas & Menten 1997; Menten et al. 2012). As summarized in Table 1, 106 molecular species (note that these are 35% of the overall-known 300 molecules in space^a), have been detected in the CSE of IRC +10216 (Agúndez et al. 2014; Cernicharo et al. 2017; Fonfría et al. 2018; McGuire 2018; Cernicharo et al. 2019a,b; McGuire 2022; Pardo et al. 2022). Molecules that were observed in the CSE of IRC +10216 and the column densities of these molecules calculated by our CSE chemical model (see Sect. 4.3) are listed in Table 1. The detected molecules include a large number of linear carbon-chain molecules such as C_nH ($n = 2 - 8$) (Tucker et al. 1974; Guélin et al. 1978; Thaddeus et al. 1985a; Cernicharo et al. 1986a; Saito et al. 1987; Cernicharo & Guélin 1996; Guélin et al. 1997), HC_nN ($n = 1, 2, 3, 4, 5, 7, 9$) (Morris et al. 1971, 1975; Churchwell et al. 1978; Winnewisser & Walmsley 1978; Guélin & Cernicharo 1991; Bell et al. 1992b; Cernicharo et al. 2004), C_nS ($n = 1, 2, 3, 5$) (Penzias et al. 1971; Cernicharo et al. 1987a; Bell et al. 1992b), negatively and positively charged molecules such as C_nH^- ($n = 4, 6, 8$) (McCarthy et al. 2006; Cernicharo et al. 2007; Remijan et al. 2007), C_nN^- ($n = 1, 3, 5$) (Cernicharo et al. 2008; Thaddeus et al. 2008; Agúndez et al. 2010) and HCO^+ (Tenenbaum et al. 2010b), metal cyanides/isocyanides such as KCN, CaNC, NaCN, MgNC, MgCN, AlNC, FeCN, SiCN, SiNC, HMgNC and SiH₃CN (Kawaguchi et al. 1993; Turner et al. 1994; Ziurys et al. 1995, 2002;

^(a) <https://cdms.astro.uni-koeln.de/classic/molecules/>

Table 2. Published radio line surveys toward IRC+10216.* Note that a collection of line surveys of evolved stars at λ 3 mm wavelength band can be found in Table 7.

Covered Frequencies (GHz)	Telescope	Reference
4 – 6	Arecibo–305 m	Araya et al. (2003)
13.3 – 18.5	TMRT–65 m	Zhang et al. (2017)
17.8 – 26.3	Effelsberg–100 m	Gong et al. (2015)
18 – 50	VLA	Keller et al. (2015)
20 – 25	Nobeyama–45 m	Zhang et al. (2020)
28 – 50	Nobeyama–45 m	Kawaguchi et al. (1995)
31.3 – 50.6	Yebes–40 m	Tercero et al. (2021)
31.3 – 50.3	Yebes–40 m	Pardo et al. (2022)
72.2 – 91.1	Onsala–20 m	Johansson et al. (1984, 1985)
84.5 – 115.8	PMO–13.7 m	This work
129.0 – 172.5	IRAM–30 m	Cernicharo et al. (2000)
131.2 – 160.3	ARO–12 m	He et al. (2008)
214.5 – 285.5	SMT–10 m	Tenenbaum et al. (2010b)
219.5 – 245.5 and 251.5 – 267.5	SMT–10 m	He et al. (2008)
222.4 – 267.92 ^a	JCMT–15 m	Avery et al. (1992)
253 – 261	CARMA	Fonfría et al. (2014)
255.3 – 274.8	ALMA	Cernicharo et al. (2013)
255.3 – 274.8	ALMA	Velilla Prieto et al. (2015)
293.9 – 354.8	SMA	Patel et al. (2011)
330.2 – 358.1	CSO–10.4 m	Groesbeck et al. (1994)
339.6 – 364.6	JCMT–15 m	Avery et al. (1992)
554.5 – 636.5	Herschel/HIFI	Cernicharo et al. (2010b)

NOTE— (*) Unpublished work is not included in this table; for instance, the 3 mm IRAM–30 m and ALMA surveys toward IRC+10216 mentioned in the papers of Agúndez et al. (2014, 2017). ^(a) The line survey was discontinuously conducted in the listed frequency range and contains significant gaps.

Guélin et al. 2000, 2004; Pulliam et al. 2010; Zack et al. 2011; Cabezas et al. 2013; Cernicharo et al. 2017, 2019a), and even metal halides such as NaCl, AlCl, KCl and AlF (Cernicharo & Guélin 1987). Some of these molecules, such as the metal halides and the metal-bearing molecules, were identified during line surveys, covering a significant part of the radio and (sub-)millimeter spectrum (Cernicharo et al. 2011). Therefore, unbiased spectral line surveys are of fundamental importance to the systematic evaluation of the molecular composition and in particular to those species whose chemistries are poorly studied. For example, the first identified Ca-bearing species in space, CaNC, was discovered by a full-spectral line survey despite not being expected from chemical models (Cernicharo et al. 2019a).

Multiple transition lines of each molecular species observed in different spectral line surveys have greatly improved estimates of molecular abundances and excitation temperatures, thus better estimating the physical conditions in which each molecular species occurs. By fitting several spectral lines of C₃S, HC₃N, and HC₅N in the CSE of IRC+10216 in different wavebands, it was found that these molecules all have both cold and warm excitation temperature components (Bell et al. 1992b; Bell 1993; Bell et al. 1993). Later, Zhang et al. (2017) fitted the spectral line survey data of HC₅N, HC₇N, and HC₉N in three different frequency ranges and found that the high rotational transitions of these molecules

trace the warmer molecular regions and that the thermal structure is stratified, which is consistent with the results for HC₅N from the CSE of the C-rich AGB star CIT6 (Chau et al. 2012).

Molecular line surveys are a powerful tool to analyzing the physical and chemical parameters of astronomical sources. IRC +10216 is the definitive source for studying the circumstellar chemistry in the late stages of stellar evolution (Zhang et al. 2020), and there have been many reports on its detailed and high sensitivity surveys at centimeter, millimeter, and submillimeter wavelengths. Based on the works of Gong et al. (2015), and Zhang et al. (2017), we collected the published line surveys toward IRC +10216 and list them in Table 2. We find that Johansson et al. (1984) carried out the first survey toward IRC +10216 with the OSO–20m telescope at ~ 3.8 mm (72.2 – 91.1 GHz), and they reviewed the excitation conditions and relative abundances of molecules in the CSE of IRC +10216. Agúndez et al. (2014) mainly reconfirmed three transitions of C₅S and preliminarily identified four transitions of MgCCH, three transitions of NCCP, and six transitions of SiH₃CN within the $\lambda \sim 3$ mm region of IRC +10216, while Agúndez et al. (2017) mainly explored the growth mechanism of carbon chain molecules in IRC +10216 based on data in this band.

Note, however, that a systematic spectral line survey in the frequency range from 91 GHz to 116 GHz is still missing, with the original survey of Johansson et al. (1984, 1985) only covering frequencies up to 91 GHz (see Table 2). Therefore, we present a spectral line survey of the C-rich AGB star IRC +10216 in the λ 3 mm (84.5 – 115.8 GHz) region using the Purple Mountain Observatory 13.7 meter radio telescope (PMO–13.7m).

We describe the observations and data reduction process in Section 2. and present the identification of the emission lines in Section 3. Section 4 contains the observationally-deduced and modeled excitation temperatures, column densities, and the fractional abundances of detected species, together with their isotopic ratios. The conclusions are given in Section 5. Further information is included in the six Appendices. The complete spectra of the survey of IRC +10216 range from 84.5 to 115.8 GHz and are shown in Appendix A. The spectral line parameters of all the identified species from this survey are presented in Appendix B. All the observed spectral profiles are included in Appendix C. A detailed description of the detected molecules from this survey, as well as from previous observations, is included in Appendix D. Appendix E presents the rotational diagrams for the identified species, while the stratified thermal structures of a few molecules can be found in Appendix F. Detailed comparisons of emission lines obtained with different angular resolutions are included in Appendix G.

2. OBSERVATIONS AND DATA REDUCTION

The spectral line survey of IRC +10216 between 84.5 and 115.8 GHz was carried out in August 2019 using the PMO 13.7m millimeter-wave radio telescope of the Purple Mountain Observatory at Delingha in China. The typical system temperature was about 150 – 300 K (Li et al. 2013). The frontend of the receiver uses a nine-beam sideband separation Superconduction Spectroscopic Array Receiver system, and the backend consists of 18 high resolution digital spectrum analyzer Fast Fourier Transform Spectrometers (FFTSs). Each FFTS provides 16384 channels with a total bandwidth of 1 GHz (Shan et al. 2012). The beam separation of the nine beams of the PMO-13.7m telescope is 3'. The observations adopted the position switching mode using the standard chopper wheel calibration method. The position switching mode uses only one beam, while the other beams point to other parts of the sky. On- and off-source integration times were one minute each per scan. The temperature scale is antenna temperature (T_A^*) after correction of atmospheric absorption and ohmic loss. The T_A^* scale is related to the main beam brightness temperature (T_{mb}) via the main beam efficiency (η), i.e. $T_{mb} = T_A^*/\eta$; the value of η is ~ 0.6 ^b. The half-power bandwidths (HPBW_s) are 51'' and 49'' at 110 GHz and 115 GHz, respectively. The velocity resolution is $\sim 0.16 - 0.17$ km s⁻¹. The total observing time of the spectral line survey is about 32.5 hours, which includes overhead due to telescope movement. The pointing accuracy was better than 5''.

The data were reduced using the GILDAS^c software package, including CLASS and GREG. Linear baseline subtractions were used for all the spectra. Since the edges of the spectral range may have unknown defects, channels closer than 150 MHz to each edge of a spectral window were discarded. Velocity is given relative to the local standard of rest. Except for CO, CS, and HCN, molecular lines were smoothed (combined channels) to improve signal-to-noise (S/N) ratios for individual channels. The rms noise of the smoothed spectra is about 0.014 (or ~ 0.135) K in 1.759 (or ~ 0.402) km s⁻¹ wide channels for the detected species (or CO, CS, and HCN).

3. RESULTS

^(b) <http://www.radioast.nsd.c.cn/zhuangtaibaogao.php>

^(c) GILDAS is developed and distributed by the Observatoire de Grenoble and IRAM.

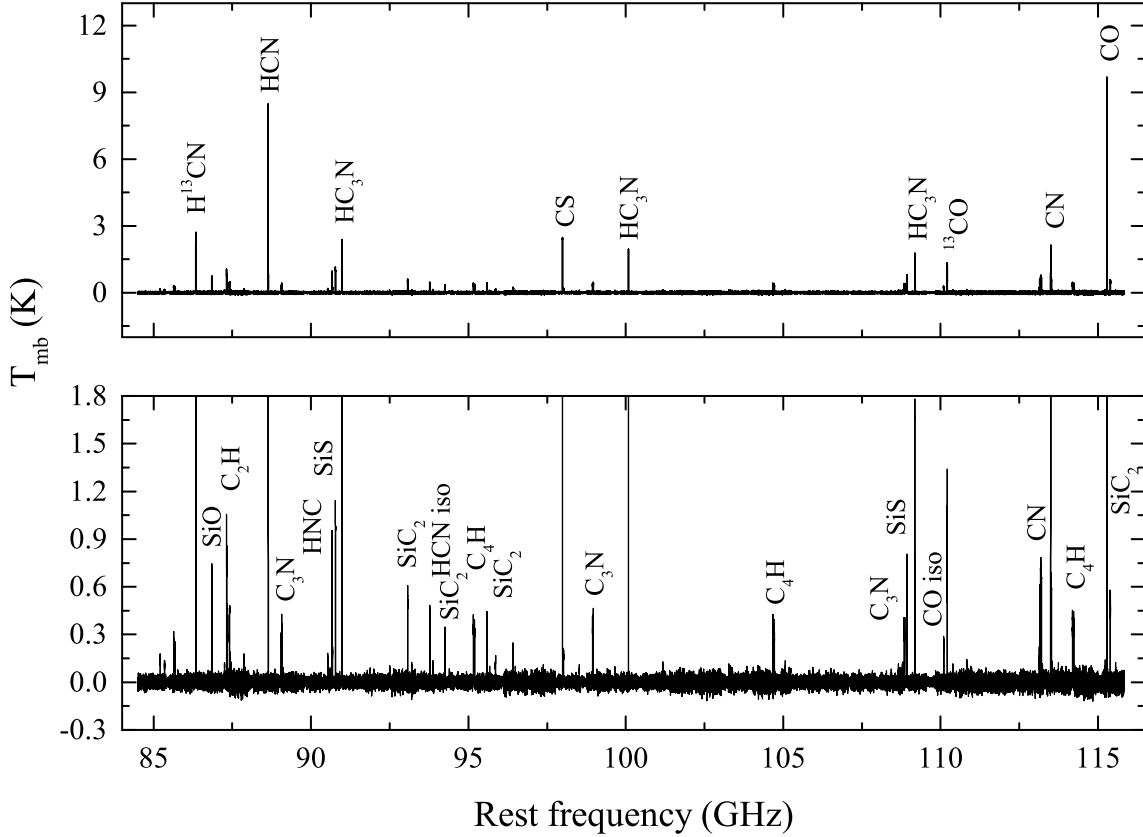


Figure 1. An overall spectral line survey towards IRC +10216 in the 3 mm band by the PMO–13.7 m radio telescope. The rest frequency scale was obtained by adopting a radial velocity of -26.5 km s^{-1} . The X-axis denotes the rest frequency (GHz), and the Y-axis depicts T_{mb} (K). On the upper panel, spectral lines with T_{mb} greater than 1.3 K are marked, while those with T_{mb} greater than 350 mK are marked on the lower panel.

3.1. The overall survey

Figure 1 presents an overview of the spectral line survey toward IRC +10216 in λ 3 mm band, which is displayed in consecutive 475 MHz frequency segments with 0.244 MHz spectral resolution in Appendix A. We find 96 transitions, and the identified lines are assigned to 19 different molecular species and their isotopologues. The line identification was performed by using the Jet Propulsion Laboratory ^d (JPL, Pickett et al. 1998), Cologne Database for Molecular Spectroscopy catalogs ^e (CDMS, Müller et al. 2005), and splatalogue databases ^f as well as the online Lovas line list ^g (Lovas 2004) for astronomical spectroscopy. The local standard of rest radial velocity (V_{lsr}) of -26.5 km s^{-1} is adopted to derive the rest frequency of the observed lines (Zhang et al. 2017). This paper discusses the lines detected with S/N of at least three (Fonfría et al. 2014).

We used the SHELL fitting routine in CLASS to fit the spectral line profiles and obtain the relevant parameters (Gong et al. 2015). The fitted spectral line parameters include peak intensity, integrated intensity, and expansion velocity, defined as the halfwidth at zero power (Gong et al. 2015; Zhang et al. 2017). For the lines with hyperfine

^(d) <http://spec.jpl.nasa.gov>

^(e) <http://www.astro.uni-koeln.de/cdms/catalog>

^(f) <https://splatalogue.online//advanced.php>

^(g) <http://www.nist.gov/pml/data/micro/index.cfm>

structure (hfs, like HCN, H^{13}CN , etc.), only their primary components are fitted with the routine to obtain their expansion velocities, and the integrated intensity is a sum over all hyperfine components. All detected transitions and the line parameters are listed in Table B1. The rms noise on a main beam brightness temperature (T_{mb}) scale is obtained from the statistics in regions free of noticeable spectral lines, and the measurement uncertainty of the integrated intensity given in this work is calculated as the product of the rms noise and the line width (Zhang et al. 2017).

Table 3. An overview over previous studies on molecules identified within our measured λ 3 mm band towards IRC +10216. Note that in this work we have provided all of the information on all of the species listed here.

No.	Molecule	Rest Freq. (MHz)	Detected?	Spectrum?	T_{ex} obtained?	N or f^a obtained?	Ref.
(1)	HC_5N	85201.346	✓	✓	✓	✓	1, 2, 3, 4, 5
(2)	$c\text{-C}_3\text{H}_2$	85338.906	✓	✓		✓	2, 6, 7
(3)	C_4H	85634.000	✓	✓	✓	✓	2, 5, 7, 8
(4)	C_4H	85672.570	✓	✓	✓	✓	2, 5, 8
(5)	^{29}SiO	85759.188	✓	✓	✓	✓	2, 9, 10, 11, 12
(6)	H^{13}CN	86338.737	✓	✓			4, 6, 9, 13
(7)	H^{13}CN	86340.176	✓	✓		✓	4, 6, 9, 13, 14, 15, 16
(8)	H^{13}CN	86342.255	✓	✓			4, 6, 9, 13
(9)	SiO	86846.995	✓	✓	✓	✓	2, 6, 9, 11, 12, 17
(10)	C_2H	87284.156	✓	✓	✓	✓	2, 4, 10, 18, 19
(11)	C_2H	87316.925	✓	✓	✓	✓	2, 4, 10, 16, 18, 19, 20, 21
(12)	C_2H	87328.624	✓	✓	✓	✓	2, 4, 5, 10, 16, 18, 19, 20
(13)	C_2H	87402.004	✓	✓	✓	✓	2, 4, 10, 16, 18, 19, 20
(14)	C_2H	87407.165	✓	✓	✓	✓	2, 4, 10, 18, 19, 20
(15)	C_2H	87446.512	✓	✓	✓	✓	2, 4, 10, 18, 19
(16)	HC_5N	87863.630	✓	✓	✓	✓	1, 2, 3, 5, 9
(17)	H^{13}CCCN	88166.808	✓	✓			2, 3, 4, 9
(18)	HCN	88630.416	✓	✓			2, 4, 6, 9, 13
(19)	HCN	88631.847	✓	✓	✓	✓	2, 4, 6, 9, 13, 14, 16, 15
(20)	HCN	88633.936	✓	✓			2, 4, 6, 9, 13, 22
(21)	C_3N	89045.590	✓	✓	✓	✓	2, 5, 23, 24
(22)	C_3N	89064.360	✓	✓	✓	✓	4, 5, 23, 24
(23)	^{29}SiS	89103.720	✓	✓	✓	✓	4, 10, 11, 12
(24)	HC_5N	90525.890	✓	✓	✓	✓	2, 3, 5, 25, 26
(25)	HC^{13}CCN	90593.059	✓	✓		✓	2, 4, 6
(26)	HCC^{13}CN	90601.791	✓	✓		✓	2, 4, 6
(27)	HNC	90663.450	✓	✓			2, 4, 6, 9, 27, 28
(28)	HNC	90663.574	✓	✓	✓	✓	2, 4, 6, 9, 16, 21, 27, 28
(29)	HNC	90663.656	✓	✓			2, 4, 6, 9, 27, 28
(30)	SiS	90771.561	✓	✓	✓	✓	2, 6, 9, 11, 12, 16, 17, 22, 29, 30
(31)	HC_3N	90978.989	✓	✓	✓	✓	2, 4, 5, 6, 9, 16, 17, 21

Table 3 continued on next page

Table 3 (continued)

No.	Molecule	Rest Freq. (MHz)	Detected?	Spectrum?	T_{ex} obtained?	N or f^a obtained?	Ref.
(32)	^{13}CS	92494.270	✓	✓	✓	✓	11, 12, 15, 31
(33)	SiC_2	93063.639	✓	✓	✓	✓	25, 32, 33, 34, 35
(34)	HC_5N	93188.123	✓	✓	✓	✓	3, 5, 36
(35)	C_4H	93863.300	✓	✓			37
(36)	C_2S	93870.098	✓	✓	✓	✓	31, 38
(37)	SiC_2	94245.393	✓	✓	✓	✓	7, 25, 30, 32, 33, 35
(38)	C_4H	95150.320	✓	✓	✓	✓	5, 6, 8, 34
(39)	C_4H	95188.940	✓	✓	✓	✓	5, 8, 34
(40)	SiC_2	95579.381	✓	✓	✓	✓	25, 32, 33, 35, 39
(41)	HC_5N	95850.335	✓	✓	✓	✓	3, 5
(42)	C^{34}S	96412.950	✓	✓	✓	✓	4, 10, 11, 12
(43)	CS	97980.953	✓	✓		✓	4, 10, 11, 12, 15, 16, 22, 30, 40, 41
(44)	$l\text{-C}_3\text{H}$	97995.212	✓	✓	✓	✓	2, 4, 40
(45)	$l\text{-C}_3\text{H}$	97995.951	✓	✓	✓	✓	2, 4, 6, 40
(46)	$l\text{-C}_3\text{H}$	98011.649	✓	✓	✓	✓	2, 4, 34, 40
(47)	$l\text{-C}_3\text{H}$	98012.576	✓	✓	✓	✓	2, 4, 34, 40
(48)	HC_5N	98512.524	✓	✓	✓	✓	1, 3, 5
(49)	C_3N	98940.020	✓	✓	✓	✓	5, 23, 24, 42
(50)	C_3N	98958.780	✓	✓	✓	✓	5, 23, 24, 42
(51)	HC^{13}CCN	99651.863	✓	✓			7
(52)	HCC^{13}CN	99661.471	✓	✓			7
(53)	HC_3N	100076.386	✓	✓	✓	✓	5, 16
(54)	HC_5N	101174.677	✓				5
(55)	C_4H	103266.081	✓				37
(56)	$l\text{-C}_3\text{H}$	103319.278	✓	✓			37
(57)	$l\text{-C}_3\text{H}$	103319.818	✓	✓			37
(58)	$l\text{-C}_3\text{H}$	103372.506	✓	✓			37
(59)	$l\text{-C}_3\text{H}$	103373.129	✓	✓			37
(60)	HC_5N	103836.817	✓				5
(61)	C_3S	104048.451	✓	✓	✓	✓	31, 42
(62)	C_4H	104666.560	✓	✓	✓	✓	5, 8
(63)	C_4H	104705.100	✓	✓	✓	✓	5, 8
(64)	C_4H	105838.000	✓				37
(65)	Si^{34}S	105941.503	✓				11, 12
(66)	C_4H	106132.800	✓				37
(67)	C_2S	106347.740	✓		✓	✓	31,
(68)	HC_5N	106498.910	✓	✓	✓	✓	3, 5
(69)	MgNC	107399.420	✓	✓	✓	✓	43
(70)	HC^{13}CCN	108710.523	✓			✓	6
(71)	HCC^{13}CN	108721.008	✓			✓	6

Table 3 continued on next page

Table 3 (continued)

No.	Molecule	Rest Freq. (MHz)	Detected?	Spectrum?	T_{ex} obtained?	N or f^a obtained?	Ref.
(72)	C ₃ N	108834.270	✓	✓	✓	✓	2, 5, 6, 22, 23, 24
(73)	C ₃ N	108853.020	✓	✓	✓	✓	2, 5, 22, 23, 24
(74)	SiS	108924.297	✓	✓		✓	2, 6, 11, 12, 17, 22, 29, 44
(75)	HC ₃ N	109173.638	✓	✓	✓	✓	2, 5, 6, 9, 15, 16
(76)	¹³ CO	110201.354	✓	✓			6, 9, 15, 16, 41, 45, 46
(77)	CH ₃ CN	110375.049	✓	✓	✓	✓	7
(78)	CH ₃ CN	110381.400	✓	✓	✓	✓	7
(79)	CH ₃ CN	110383.518	✓	✓	✓	✓	7
(80)	C ₄ H	112922.500	✓				37
(81)	CN	113123.337	✓	✓			16, 18
(82)	CN	113144.192	✓	✓		✓	16, 18
(83)	CN	113170.528	✓	✓		✓	16, 18
(84)	CN	113191.317	✓	✓		✓	16, 18
(85)	C ₄ H	113265.900	✓	✓			37, 47
(86)	CN	113488.140	✓	✓			7, 14, 16, 18
(87)	CN	113490.982	✓	✓		✓	6, 14, 16, 18, 41
(88)	CN	113499.639	✓	✓			5, 14, 16, 18
(89)	CN	113508.944	✓	✓			14, 16, 18
(90)	CN	113520.414	✓	✓			14, 16, 18
(91)	C ₄ H	114182.510	✓	✓	✓	✓	5, 8
(92)	C ₄ H	114221.040	✓	✓	✓	✓	5, 8
(93)	H ¹³ CCCN	114615.021					
(94)	C ₄ H	115216.800	✓				37
(95)	CO	115271.202	✓	✓	✓	✓	6, 9, 15, 16, 41, 48, 49, 50, 45
(96)	SiC ₂	115382.375	✓	✓	✓	✓	32, 33, 35, 51

NOTE— ^(a) N and f depict the total column density and fractional abundance of the molecular species. Since there exist numerous observations toward IRC+10216, here we only provide a few key references containing molecular spectral line profiles, excitation temperature, and column density, which are: (1) Bujarrabal et al. (1981); (2) Johansson et al. (1984); (3) Cernicharo et al. (1986b); (4) Kahane et al. (1988); (5) Agúndez et al. (2017); (6) Nyman et al. (1993); (7) Agúndez et al. (2008b); (8) Guélin et al. (1978); (9) Olofsson et al. (1982); (10) Groesbeck et al. (1994); (11) Agúndez et al. (2012); (12) Velilla-Prieto et al. (2019); (13) Morris et al. (1971); (14) Dayal & Bieging (1995); (15) Wannier & Linke (1978); (16) Park et al. (2008); (17) Morris et al. (1975); (18) Truong-Bach et al. (1987); (19) De Beck et al. (2012); (20) Tucker et al. (1974); (21) Bieging & Rieu (1988); (22) Henkel et al. (1985); (23) Guélin & Thaddeus (1977); (24) Thaddeus et al. (2008); (25) Cernicharo et al. (1986c); (26) Agúndez et al. (2014); (27) Brown et al. (1976); (28) Daniel et al. (2012); (29) Sahai et al. (1984); (30) Lucas et al. (1995); (31) Cernicharo et al. (1987a); (32) Thaddeus et al. (1984); (33) Snyder et al. (1985); (34) Cernicharo et al. (1986a); (35) Cernicharo et al. (2018); (36) Turner et al. (1994); (37) Yamamoto et al. (1987); (38) Cernicharo et al. (2019b); (39) Guélin et al. (1990); (40) Thaddeus et al. (1985a); (41) Wilson et al. (1971); (42) Cernicharo & Guélin (1987); (43) Guélin et al. (1986); (44) Bieging & Nguyen-Quang-Rieu (1989); (45) Kuiper et al. (1976); (46) Knapp & Chang (1985); (47) Cernicharo et al. (2019a); (48) Solomon et al. (1971); (49) Fong et al. (2003); (50) Fong et al. (2006); (51) Tenenbaum et al. (2006).

All detected transitions are shown in Figs: 2, C1, C2, C3, C4, C5, C6, C7, C8, C9, and C10. To clearly present the spectral line profile and $V_{l,sr}$ of each molecule, the X-axis range of the spectral line figure we show varies. For most

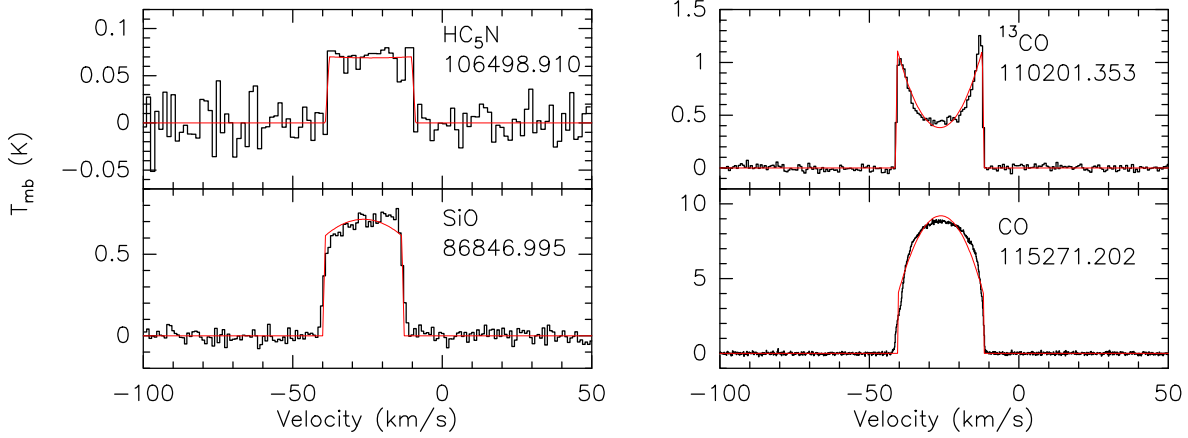


Figure 2. Illustrations of the four typical shapes of the spectral line profiles observed in IRC+10216: flat-topped (e.g. HC_5H , optically thin, spatially unresolved), double-peaked (e.g. ^{13}CO , optically thin, spatially resolved), truncated parabolic (e.g. SiO , optically thick, spatially resolved), and parabolic (e.g. CO , optically thick, spatially unresolved). The solid black line shows the observed spectrum, and the solid red line represents the spectral line profile fitted by the shell function. The rest frequency of separable spectral lines are in MHz, and the molecule’s name is displayed in the upper right corner of each panel. All of the detected spectra from this survey are included in Appendix C.

spectral lines, the velocity range is set from -100 to 50 km s^{-1} , while the velocity range from -50 to 0 km s^{-1} is assumed for transitions shown in Figs. C1, C4 (except for the top right panel where it extends from -200 to 50 km s^{-1}), and C5 (except for the bottom right panel, where the velocity range is the standard one).

The detected lines include six transitions each for C_2H and C_3N , eight transitions for $l\text{-C}_3\text{H}$ as well as C_4H ($\nu = 0$), seven transitions of C_4H ($\nu = 1$), nine transitions for CN as well as HC_5N , two transitions each for H^{13}CCCN , SiS , and C_2S , three transitions each for HC^{13}CCN , HCC^{13}CN , HNC , HCN , H^{13}CN , CH_3CN , and HC_3N , one transition for $c\text{-C}_3\text{H}_2$, CO , ^{13}CO , SiO , ^{29}SiO , Si^{34}S , ^{29}SiS , C_3S , CS , ^{13}CS , C^{34}S , and MgNC , and four transitions of SiC_2 .

Table 3 summarizes previous 3 mm observations towards IRC+10216. We checked if the previous work had detected all of the species we identified, or if they had provided all of the necessary information about these species, such as spectral line profile, excitation temperature (T_{ex}), and the molecular column density (N) or the fractional abundance (f). Clearly, none of them have provided all of these parameters. Therefore, a detailed complete study of the 3 mm molecules in this famous source is highly desirable. Here, we find that the $J = 13 - 12$ transition of H^{13}CCCN is detected in IRC+10216 for the first time.

3.2. Typical spectral line profiles

Typically, in the CSEs of AGB stars, there are four types of molecular spectral line profiles: double-peaked, parabolic, flat topped, and truncated parabolic line shapes (see Figure 2). The different shapes of the observed spectral lines are mainly determined by the optical depth of the transition and the ratio of the angular area of the emitting region to the beam size of the telescope (Zuckerman 1987). Optically thin unresolved and resolved emission lines show flat-topped and double-peaked profiles, while optically thick unresolved and resolved emission lines have parabola and truncated parabola profiles. (Morris et al. 1975; Zuckerman 1987; Habing & Olofsson 2004).

The profiles of the C_2H (Johansson et al. 1984), $l\text{-C}_3\text{H}$, C_4H ($\nu = 0$) (Olofsson et al. 1982; Johansson et al. 1984), C_4H ($\nu = 1$), C_3N (Johansson et al. 1984), $c\text{-C}_3\text{H}_2$ (Zhang et al. 2017), ^{13}CO , H^{13}CCCN (Zhang et al. 2017), HC_5N (Gong et al. 2015; Zhang et al. 2017), MgNC , CH_3CN , HNC , SiC_2 , ^{13}CS , C^{34}S (Grosbeck et al. 1994), C_2S and C_3S emission lines appear to be double-peaked or/and flat-topped, indicating that they are optically thin. The profiles of the HCN , H^{13}CN , and CO emission lines appear to be parabolic, while the CS line is a truncated parabola profile, which implies that they are all optically thick.

Interestingly, the $\text{CN } N = 1 - 0, J = 1/2 - 1/2, F = 1/2 - 1/2$ profile is double-peaked, while other $N = 1 - 0, J = 1/2 - 1/2$ hyperfine transitions of CN ($F = 1/2 - 3/2, F = 3/2 - 1/2, F = 3/2 - 3/2$) show truncated parabolic profiles (see Figure C4). Grosbeck et al. (1994) find that CN ($N = 3 - 2$) lines have prominent double-peaked profiles indicative of low optical depth.

Zhang et al. (2017) found that HC_3N produced a double-peaked profile and was rated to be optically thin. However, we find that the spectral lines of HC_3N are truncated parabola (see Figure C6), which indicates that HC_3N is at least partially saturated (Olofsson et al. 1982).

Our fitting results for SiO (see Figure 2) showed a truncated parabolic shape, indicating that the line is slightly optically thick. ^{29}SiO shows a double-peaked structure (see Figure C8), which indicates that this molecule is optically thin. Judging from the average profile of the ^{29}SiO and ^{30}SiO lines, Kahane et al. (1988) pointed out that the $J = 2 - 1$ rotational transition of SiO seems to be optically thick. However, Olofsson et al. (1982) noted that the SiO $J = 2 - 1$ transition has a flat-topped appearance, albeit that the red-shifted emission is slightly stronger than the blue-shifted emission and resembles the typical rectangular line profile of an unresolved, optically thin molecular shell with a constant velocity gas flow. On the other hand, the spectral lines of the SiO $J = 2 - 1$ to $J = 8 - 7$ transitions observed by Agúndez et al. (2012) have a slight double-peaked structure, but the spectral line profiles simulated by them using radiative transfer are parabolic. This may indicate that the envelope of SiO is slightly unresolved (Agúndez et al. 2012), or more likely that an enhanced density shell should be considered in the IRC +10216 model (see De Beck et al. (2012) and Daniel et al. (2012)), or that more infrared pumping should be added in the model (Agúndez et al. 2012).

The SiS $J = 6 - 5$ spectrum (see Figure. C9) shows an optically thick emission with a parabolic shape. This result is consistent with observations by Johansson et al. (1984) and Fonfría et al. (2018). Johansson et al. (1984) and Olofsson et al. (1982) speculated that the SiS $J = 5 - 4$ double-peaked profile might be due to maser enhanced line wings. Fonfría et al. (2018) find through monitoring of the SiS $J = 5 - 4$ and SiS $J = 6 - 5$ lines in IRC +10216 that the SiS $J = 5 - 4$ spectral line shows narrow peaks at high expansion velocities, which vary strongly with the pulsation of the star, while the remaining line profile is approximately constant over the stellar pulsation period. On the contrary, SiS $J = 6 - 5$ shows neither narrow peaks nor a constant profile over the stellar period at high expansion velocities.

Apparently the line shape of a certain transition of a molecule could be different when being observed by different telescopes. We compared and summarized all of the line profiles related to this work in Appendix G.

4. DISCUSSION

4.1. Rotation-diagram Analysis

4.1.1. Molecular excitation temperature and column density

Assuming local thermal equilibrium (LTE), the column densities (N_{tot}) and excitation temperatures of detected lines were derived by using the following equation:

$$\ln \frac{N_{\text{u}}}{g_{\text{u}}} = \ln \frac{3kW}{8\pi^3\nu S\mu^2} = \ln \frac{N_{\text{tot}}}{Q(T_{\text{ex}})} - \frac{E_{\text{u}}}{kT_{\text{ex}}}, \quad (1)$$

where, N_{u} and g_{u} are the population and statistical weights of the upper level, k is the Boltzmann constant, $W = \int T_{\text{R}} dv$ is the integral of the source brightness temperature (T_{R}) over the line's velocity range, ν is the rest frequency of the line, S is the transition's intrinsic strength, μ is the permanent dipole moment, and Q is the partition function, which is related to T_{ex} , and E_{u} , the excitation energy of the upper level. The values of Q , E_{u}/k and $S\mu^2$ are taken from the "Splatalogue" spectral line catalogs.

In actual astronomical measurements, the observed molecules often do not fill the telescope beam, so it is necessary to consider the correction of the main beam brightness temperature and source brightness temperature by using the beam dilution correction of the molecular source (η_{BD}).

The relationship between the main beam brightness temperature and the source brightness temperature is as follows:

$$T_{\text{R}} = \frac{T_{\text{mb}}}{\eta_{\text{BD}}}, \quad (2)$$

where

$$\eta_{\text{BD}} = \frac{\theta_{\text{s}}^2}{\theta_{\text{s}}^2 + \theta_{\text{beam}}^2}. \quad (3)$$

Here, η_{BD} is the beam dilution factor or beam filling factor, θ_{beam} is the half power beam width of the antenna (HPBW), and θ_{s} is the source size. In our calculations, η_{BD} of all the identified unblended molecular lines and the supplemented data are calculated via equation (3), while data from the blended lines are excluded. When a molecule's excitation temperature is obtained using rotational diagrams, it is required that at least two unblended transition

lines of the same molecule, with significant upper energy difference have been observed. Unfortunately, this does not hold for all our detections. We only observed one line in case of CS, C³⁴S, ¹³CS, C₃S, CO, ¹³CO, SiO, ²⁹SiS, Si³⁴S, MgNC, and *c*-C₃H₂. For molecules like HNC, HCN, H¹³CN, and CH₃CN, we only observed the hyperfine structure of one rotational transition. Because the frequency interval of these fine structure lines is too small, their spectral lines are blended. For CN, SiC₂, *l*-C₃H, C₃N, H¹³CCCN, and C₂H, at least two transitions have been observed, but the energy level spacing of these lines is minimal. It has been reported that the excitation temperatures of HC₃N and HC₅N are related to their energy level transitions (Bell et al. 1992b). Therefore, to calculate these molecules' excitation temperature and column density, we supplemented our data with spectral line surveys of other research groups. The additional frequency ranges with observational data includes 13.3 to 18.5 GHz (Zhang et al. 2017), 17.8 to 26.3 GHz (Gong et al. 2015), 28 to 50 GHz (Kawaguchi et al. 1995), 129.0 to 172.5 GHz (Cernicharo et al. 2000), 131.2 to 160.3 GHz (He et al. 2008), 219.5 to 267.5 GHz (He et al. 2008), and 330 to 358 GHz (Grosbeck et al. 1994). In addition, supplementary data for HNC come from Daniel et al. (2012). For CS, ¹³CS, C³⁴S, SiO, ²⁹SiO, SiS, ²⁹SiS, and Si³⁴S, we have also supplemented the data using observations of Agúndez et al. (2012). Data for HCN from Nyman et al. (1993) are also included. We processed the data of Grosbeck et al. (1994), Kawaguchi et al. (1995), He et al. (2008), Gong et al. (2015), and Zhang et al. (2017), calculating the uncertainty of the integrated intensity as the product of the rms noise and the line width. For other supplementary data, we adopted the integrated intensity and uncertainty values as reported in the original literature. To derive the excitation temperature and column density of a molecule, one needs to know the spatial distribution of the molecular source or the source size. Agúndez et al. (2017) find that the observational results of HC₅N ($J = 32 - 31$ to $J = 43 - 42$) with ALMA are not showing a radial shift in the emission peak between low- J and high- J lines as might reasonably be expected, and all emission distributions of HC₅N appear quite similar. The same is found for HC₃N, C₄H, and C₃N in the λ 3 mm band (Agúndez et al. 2017). The source size employed in this work is taken from previous high resolution maps in the λ 3 mm band of the relevant molecule. If such a study does not exist, the source size is obtained from chemically related species (He et al. 2008; Gong et al. 2015). The employed sizes of the identified molecules, θ_s , and the references are listed in Table 4.

We used the least squares method to perform the linear fitting for the rotational diagrams of these molecules and their isotopes. The fitting results are shown in Figs: E1, E2, E3, E4, and E5. According to the rotational diagrams, it can be seen that most spectra have large dispersion, especially CS, ¹³CS, and C³⁴S. The derived excitation temperatures, column densities, and the molecular fractional abundances relative to H₂ (see Section 4.2) together with observational results from the literature (including line surveys in the 18, 13, 8, 2, and 1.3 mm bands), are summarized in Table 4. The excitation temperatures of the molecules range from 5.3 to 73.4 K and their column densities range from 3.27×10^{13} to 4.15×10^{17} cm⁻².

Compared to observational results in the literature, the molecules with large differences in excitation temperatures include *l*-C₃H, C₄H ($\nu = 0$), C₄H ($\nu = 1$), HC₅N, *c*-C₃H₂, C₂S, and CH₃CN. We also find that column densities, except for C₄H, HCN, and CH₃CN, agree with previously published observational results.

The excitation temperatures of *l*-C₃H in the ² $\Pi_{1/2}$ and ² $\Pi_{3/2}$ states are 8.5 K (Thaddeus et al. 1985a; Kawaguchi et al. 1995) and 52 K (Thaddeus et al. 1985a), respectively. Thaddeus et al. (1985a) pointed out that the low excitation temperature (8.5 K) of the ² $\Pi_{1/2}$ state of *l*-C₃H is due to rapid radiative decay, while the high excitation temperature (52 K) of the ² $\Pi_{3/2}$ state is a consequence of the fact that interconnecting far-IR radiative transitions are only weakly permitted. When we adopt an *l*-C₃H diameter of 30'', the excitation temperatures of the ² $\Pi_{1/2}$ and ² $\Pi_{3/2}$ states of *l*-C₃H are 27.4 ± 9.3 and 14.2 ± 1.7 K, respectively.

The excitation temperature of C₄H ($\nu = 0$) obtained in our work is 45.9 ± 3.1 K, and the excitation temperature of C₄H deduced by Avery et al. (1992) is 48 ± 4 K. Comparing the excitation temperatures and column densities in Table 4, we find that the excitation temperatures derived by others are lower than those derived by us except for that of Avery et al. (1992) and He et al. (2008). For Kawaguchi et al. (1995), and Gong et al. (2015), the difference even amounts to a factor of two. Pardo et al. (2022) derive both the lowest excitation temperature, 4.9 ± 0.6 K, and column density, $(1.84 \pm 0.25) \times 10^{14}$ cm⁻², the latter about an order of magnitude lower than the other values. The excitation temperatures and column densities of the vibrationally excited C₄H ($\nu = 1$) derived by us and He et al. (2008) are obviously much larger than those derived by Pardo et al. (2022). In contrast, Pardo et al. (2022) observed low- J lines of C₄H ($\nu = 1$), which trace the cold component of the gas (see Appendix F for a detailed discussion), resulting in a lower excitation temperature. Although they also used a rotational diagram to derive the excitation temperature and column density of C₄H ($\nu = 1$), they did not consider the effect of the beam dilution factor. The large excitation

temperatures and column densities derived for the $\nu = 0$ and $\nu = 1$ states of C_4H indicate that infrared pumping could be very efficient (Avery et al. 1992; He et al. 2008).

Table 4. A summary of column density (N), excitation temperature (T_{ex}), source size, (θ_s) and fractional abundance relative to H_2 ($f = N/N_{H_2}$), of the detected species in this work and the literature. The derivation of the fractional abundance is discussed in Sec 4.2.

Molecule	This work					Lit. observational		
	T_{ex} (K)	N (cm^{-2})	f	θ_s ($''$)	Ref. (for θ_s)	T_{ex} (K)	N (cm^{-2})	Ref. (for T_{ex}, N)
C_2H	17.0 (2.0)	$8.14 (2.29) \times 10^{15}$	3.37×10^{-6}	32	1	16	4.6×10^{15}	11
$l\text{-}C_3H$	14.3 (0.9)	$1.25 (0.22) \times 10^{14}$	4.84×10^{-8}	30	2	8.5	5.6×10^{13}	11
$C_4H (\nu = 0)$	45.9 (3.1)	$2.75 (0.36) \times 10^{15}$	1.07×10^{-6}	30	2	25 (5)	$1.32 (0.35) \times 10^{14}$	12
						18.5 (7.6)	$2.4 (0.2) \times 10^{15}$	13
						15	2.4×10^{15}	11
						4.9 (0.6)	$1.84 (0.25) \times 10^{14}$	14
$C_4H (\nu = 1)$	64.3 (2.8)	$3.66 (0.74) \times 10^{16}$	1.42×10^{-5}	30	3	53 (3)	$8.1 (1.1) \times 10^{15}$	12
						53 (4)	$5.9 (2.1) \times 10^{15}$	12
						10 (5)	$6.6 (2.0) \times 10^{13}$	14
CN	9.8 (2.0)	$> 1.08 (0.42) \times 10^{15}$	$> 1.4 \times 10^{-6}$	100	4	8.7	6.2×10^{14}	15
C_3N	27.6 (1.9)	$4.25 (0.81) \times 10^{14}$	1.98×10^{-7}	36	5	20.2 (1.1)	$3.1 (0.3) \times 10^{14}$	13
						15	4.1×10^{14}	11
HC_3N	21.2 (0.5)	$> 1.18 (0.08) \times 10^{15}$	$> 4.59 \times 10^{-7}$	30	6	27.2 (19.4)	$1.94 (0.21) \times 10^{15}$	16
						24.7 (18.5)	$1.4 (0.2) \times 10^{15}$	13
						26	1.7×10^{15}	11
						28 (1)	$8.0 (1.5) \times 10^{14}$	12
$H^{13}CCCN$	15.9 (0.9)	$4.38 (0.88) \times 10^{13}$	1.70×10^{-8}	30	3	18.7 (3.3)	$3.25 (1.46) \times 10^{13}$	16
						27	2×10^{13}	12
HC_5N	23.7 (0.5)	$5.41 (0.56) \times 10^{14}$	2.10×10^{-7}	30	6	13.6 (2.1)	$5.47 (0.77) \times 10^{14}$	16
						18.8 (1.3)	$4.6 (0.2) \times 10^{14}$	13
						27 (5)	$2.7 (0.2) \times 10^{14}$	11
						10.1 (0.6)	$4.2 (0.4) \times 10^{14}$	14
HNC	12.1 (0.1)	$1.11 (0.08) \times 10^{14}$	5.76×10^{-8}	40	7			
HCN	16.0 (1.4)	$> 7.36 (0.92) \times 10^{14}$	$> 6.10 \times 10^{-7}$	64	4		2.8×10^{16}	15
$H^{13}CN$	20.8 (5.5)	$> 3.92 (1.17) \times 10^{14}$	$> 2.84 \times 10^{-7}$	56	4		2.8×10^{14}	15
CO	31.9 (10.9)	$> 4.03 (1.51) \times 10^{17}$	$> 1.04 \times 10^{-3}$	200	8		2.0×10^{18}	15
^{13}CO	30.2 (5.4)	$4.12 (0.86) \times 10^{16}$	1.07×10^{-4}	200	3	17	5.0×10^{16}	15
$c\text{-}C_3H_2$ (ortho)	5.3 (0.2)	$1.14 (0.15) \times 10^{14}$	4.44×10^{-8}	30	3	5.7 (1.4)	$4.82 (4.14) \times 10^{14}$	12
$c\text{-}C_3H_2$ (para)	5.7 (0.9)	$8.02 (4.54) \times 10^{13}$	3.11×10^{-8}	30	3	8 (6)	$1.22 (2.03) \times 10^{14}$	12
						6.1 (2.8)	$1.39 (1.07) \times 10^{14}$	16
						5.5 (0.6)	$2.1 (0.4) \times 10^{14}$	13
						20	1.6×10^{13}	11
SiO	29.2 (3.9)	$> 4.84 (1.13) \times 10^{14}$	$> 1.38 \times 10^{-7}$	22	9	29	5.4×10^{14}	11

Table 4 continued on next page

Table 4 (*continued*)

Molecule	This work				Ref.	Lit. observational		Ref.
	T_{ex} (K)	N (cm^{-2})	f	θ_s ($''$)		T_{ex} (K)	N (cm^{-2})	
^{29}SiO	27.7 (3.5)	$3.95 (0.91) \times 10^{13}$	1.13×10^{-8}	22	9	29	2.1×10^{14}	15
						29	2.5×10^{13}	11
						29	1.9×10^{13}	15
^{29}SiS	64.8 (4.6)	$4.39 (0.75) \times 10^{14}$	1.25×10^{-7}	22	9	85	2.1×10^{14}	15
Si^{34}S	72.5 (5.2)	$3.35 (0.59) \times 10^{14}$	9.54×10^{-8}	22	9	79	1.8×10^{14}	15
SiS	73.4 (11.3)	$> 5.86 (1.74) \times 10^{15}$	$> 1.70 \times 10^{-6}$	22	9	70	4.7×10^{15}	11
						70	3×10^{15}	15
CS	22.9 (4.3)	$> 1.57 (0.46) \times 10^{15}$	$> 8.12 \times 10^{-7}$	40	9	28	5.9×10^{15}	11
							3.0×10^{15}	15
^{13}CS	51.4 (15.8)	$8.09 (2.80) \times 10^{13}$	4.19×10^{-8}	40	9			
C^{34}S	26.1 (3.3)	$1.47 (0.26) \times 10^{14}$	7.63×10^{-8}	40	9	28	1.5×10^{14}	15
C_2S	11.2 (1.2)	$1.59 (0.73) \times 10^{14}$	8.22×10^{-8}	40	3	39.2 (135.3)	$2.3 (0.8) \times 10^{14}$	13
						14	1.5×10^{14}	11
						7.9 (1.1)	$4.0 (0.7) \times 10^{13}$	14
						20.4 (13.7)	$2.2 (0.4) \times 10^{13}$	13
C_3S	34.0 (1.2)	$3.27 (0.16) \times 10^{13}$	1.70×10^{-8}	40	3	33	4.9×10^{13}	11
						23.6 (96.85)	$2.58 (3.60) \times 10^{13}$	14
MgNC	18.9 (1.2)	$3.20 (0.51) \times 10^{13}$	1.24×10^{-8}	30	2	25.8 (54.9)	$3.9 (1.5) \times 10^{13}$	13
						15	2.5×10^{13}	11
						8.6	7.8×10^{13}	12
CH_3CN	37.4 (6.4)	$6.81 (3.51) \times 10^{13}$	2.64×10^{-8}	30	3	16	6×10^{12}	11, 17
						35 (4)	$2.6 (0.6) \times 10^{13}$	12
SiC ₂	34.9 (5.5)	$1.41 (0.34) \times 10^{15}$	4.92×10^{-7}	27	10	40.1 (36.2)	$1.87 (1.34) \times 10^{15}$	16
						31.8 (0.9)	$1.2 (0.0) \times 10^{15}$	13

NOTE— The values in parentheses in this table are the 1σ errors associated with the fits to our rotational diagrams. The corresponding references are: (1) Guélin et al. (1999); (2) Guélin et al. (1993); (3) The source size assumed to be the same as its main isotopomer or obtained from chemically related species (He et al. 2008; Gong et al. 2015); (4) Dayal & Bieging (1995); (5) Bieging & Tafalla (1993); (6) Keller et al. (2015); (7) Guélin et al. (1997); (8) Fong et al. (2006); (9) Velilla-Prieto et al. (2019); (10) Lucas et al. (1995); (11) Kawaguchi et al. (1995); (12) He et al. (2008); (13) Gong et al. (2015); (14) Pardo et al. (2022); (15) Groesbeck et al. (1994); (16) Zhang et al. (2017); (17) Guélin & Cernicharo (1991).

The excitation temperature of HC_5N obtained by our rotational diagram analysis is close to that of Kawaguchi et al. (1995), but more than twice that of Pardo et al. (2022). In fact, the excitation temperatures of HC_5N are stratified (see Appendix F for a detailed discussion). The excitation temperature of HC_5N obtained by us is the result of fitting multiple rotational transitions, including low and high rotational transitions, which may result in our excitation temperature being close to the one from Kawaguchi et al. (1995). Kawaguchi et al. (1995) derived a higher excitation temperature than Pardo et al. (2022), likely because the latter did not consider the beam dilution factor. Bell et al. (1992b) pointed out that the moderately high excitation temperature of HC_5N , 25 K, is probably due to the influence of infrared excitation. Warm HC_3N ($T_{\text{ex}} = 48$ K) and warm HC_5N ($T_{\text{ex}} = 35$ K) in the CSE of IRC+10216 may indicate that the excitation is almost entirely due to infrared radiation (Bell 1993).

For ^{13}CO , the excitation temperature and column density obtained by us are consistent with the results of Groesbeck et al. (1994). The column density of CO with opacity corrections obtained by Groesbeck et al. (1994) is about five times larger than our value. Our value of $N(\text{CO})$ in Table 4 is derived from a rotation diagram and is a lower limit as CO is optically thick.

Our HCN column density is much different from that calculated by Groesbeck et al. (1994). Our column density of H^{13}CN is slightly larger than their value, but our value for $N(\text{HCN})$ is only 2.6% of theirs. They derived their value by first using the rotation diagram method for HC^{15}N to obtain T_{ex} and $N(\text{HC}^{15}\text{N})$. Using a $^{12}\text{C}/^{13}\text{C}$ ratio of 44 (Kahane et al. 1988; Cernicharo et al. 1991c) and a $^{14}\text{N}/^{15}\text{N} = 4000$ (Kahane et al. 1988), they derived $N(\text{HCN})$ and $N(\text{H}^{13}\text{CN})$. We detected HC^{15}N with a S/N of less than three, so our observations of HCN and H^{13}CN , which are both optically thick, give lower limits to their column densities in Table 4. Similarly, using the rotation diagram method, Qiu et al. (2022) derived the column density of HCN in C-rich post-AGB star CRL 2688, and they find that this molecule exhibits a much lower observed abundance, which could be attributed to the effect of optical depth.

For CS, Groesbeck et al. (1994) used the same isotopic rotational diagram method to derive its column density using observations of C^{34}S and a $^{32}\text{S}/^{34}\text{S}$ ratio of 20.2, derived by Kahane et al. (1988) from Si^{32}S and Si^{34}S . We used the same method and our determination of $N(\text{C}^{34}\text{S})$ to derive $N(\text{CS}) = 3.0 \times 10^{15} \text{ cm}^{-2}$, agreeing with the value derived by Groesbeck et al. (1994). The excitation temperature of C_2S derived by us is in good agreement with that obtained by Kawaguchi et al. (1995), but the excitation temperature derived by Gong et al. (2015) is three times that of ours. In the work of Gong et al. (2015), the uncertainty in the C_2S excitation temperature is large because the C_2S transitions only cover a narrow energy range. We find that the excitation temperature of C_3S is three times that of C_2S , Agúndez et al. (2014) find that the rotational temperature of C_3S is more than twice that of C_2S , which points to differences in the excitation and may indicate that radiative pumping to vibrationally excited states plays an important role in the case of C_3S (Agúndez et al. 2008b).

In thermal equilibrium, ortho-to-para ratios (OPRs) for species containing two protons with parallel and anti-parallel nuclear spins range from their statistical weight limit of 3:1 at high temperatures ($T \geq 30 \text{ K}$) to infinity or zero as the temperature decreases, depending on the symmetry of the rotational and electronic wave functions (Decin et al. 2010; Khouri et al. 2014; Le Gal et al. 2017; Chapovsky 2021; Tsuge et al. 2021). The statistical OPR of *c*- C_3H_2 derived by He et al. (2008) is approximately 4 (3.95 ± 3.16) while we derived a ratio of 1.42 ± 0.58 , consistent with the result estimated by Gong et al. (2015). However, compared to He et al. (2008) and Gong et al. (2015), we have collected and employed more data, and the excitation temperatures (less than 10 K) of para and ortho-*c*- C_3H_2 are fitted independently. The amounts of ortho-*c*- C_3H_2 and para-*c*- C_3H_2 formed are influenced by the OPR of H_2 and by ion-neutral reactions of C_3H_2 with H^+ and H_3^+ that can exchange protons with it. Both Park et al. (2006) and Morisawa et al. (2006) have observed and modeled the OPR of *c*- C_3H_2 in the dark cloud TMC-1. The latter authors show that this OPR is dependent on the age of the cloud as abundances of species change with time. The situation in IRC +10216 is in part simpler since the OPR in H_2 is likely to be 3 since it forms at high temperature and its flow time through the envelope is too short to change it to any extent. On the other hand, the changing physical conditions of temperature and density, ion abundances, and collision times in the outflow add complexity to the state-selective chemistry that ultimately sets the OPR of molecules such as *c*- C_3H_2 that form in the outer envelope. A detailed study of the ortho-para chemistry of *c*- C_3H_2 in the CSE is needed to understand the observed ratio.

For SiC_2 , we have not added more data. Avery et al. (1992) carefully studied transitions with upper level energies of 10 – 300 K and later He et al. (2008) those with values in the range 20 – 200 K. The excitation temperature and column density of SiC_2 obtained by us agrees with the observed results collected in Table 4.

For the column density of CH_3CN , the result we obtained is in good agreement with that of Agúndez et al. (2008b), He et al. (2008), and Agúndez et al. (2015), but it is one order of magnitude higher than that estimated by Kawaguchi et al. (1995). Unfortunately, we are unable to provide any insight on why we have a larger column density than Kawaguchi et al. (1995). His values are actually taken from Guélin & Cernicharo (1991). However, these authors simply give the values in the text of the article and give no information on how these were derived.

We have discussed all spectral lines with S/N of at least three. Spectral lines whose S/N are between three and five will affect the calculated results of molecular excitation temperature and column density (Gong et al. 2015). Moreover, different transitions of the same molecule have different source sizes (He et al. 2008). We neglected this factor in the calculations of the molecules' excitation temperature and column density given the lack of available high-resolution data and detailed radiative transfer modelling, including radiative pumping, which could allow one to determine the radial extent of the observed transitions. In addition, significant uncertainties will arise when one deals with the optically

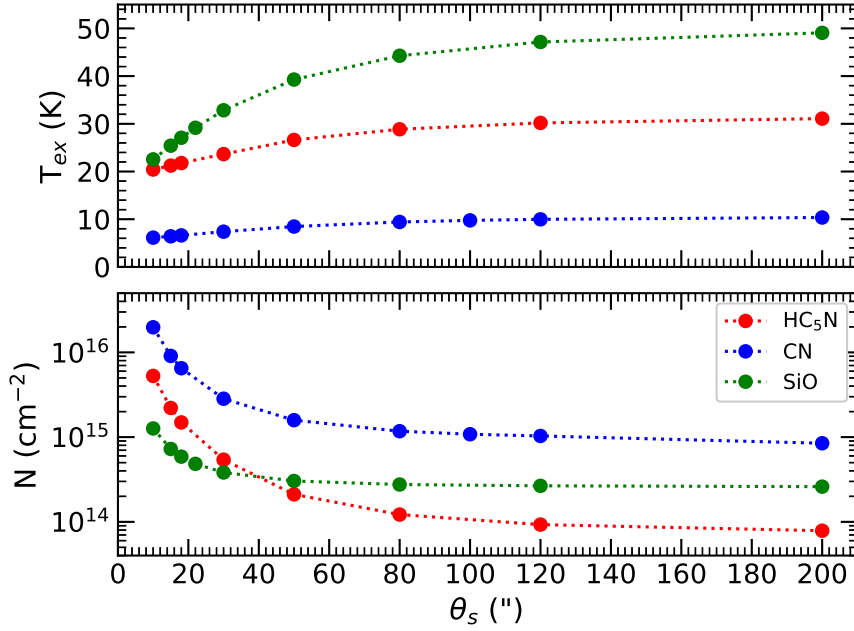


Figure 3. Illustrations for the impact of the employed source size (θ_s) on the calculated excitation temperature (T_{ex}) and column density (N) of HC₅N (in red), CN (in blue), and SiO (in green).

thick lines by employing the rotational diagram method. These factors will cause uncertainties in the observationally deduced excitation temperature and column density of the molecules.

4.1.2. Impact of the source size on molecular excitation temperature and column density

In order to get some handle on the effect of the influence of source size on T_{ex} and column density, we use different source sizes (10", 15", 18", 30", 50", 80", 120", and 200") for all molecules for which we determine these quantities through the rotational diagram method. It is found that as source size increases so do the excitation temperatures while column densities decrease. Figure 3 shows the results for CN, HC₅N, and SiO. Molecular column densities decrease rapidly between source sizes of 10" and 50". The excitation temperatures of molecules vary by a factor of two, while column densities vary by up to three orders of magnitude.

4.2. Observationally deduced fractional abundances

Once the column density of H₂ is known, the molecular fractional abundances relative to H₂ can be obtained. The beam-averaged H₂ column density ($N(\text{H}_2)$) can be calculated from the mass loss rate via the formula (Gong et al. 2015):

$$N_{\text{H}_2} = \frac{\dot{M}R/V_{\text{exp}}}{\pi R^2 m_{\text{H}_2}} = \frac{\dot{M}}{\pi R V_{\text{exp}} \mu m_{\text{H}}}, \quad (4)$$

where \dot{M} , R , V_{exp} , and m_{H} are the mass-loss rate, the radius of the molecular emission, expansion velocity, and the mass of a hydrogen atom, respectively. For IRC+10216, \dot{M} is $2 \times 10^{-5} M_{\odot} \text{ yr}^{-1}$ (Crosas & Menten 1997; Menten et al. 2012); V_{exp} is 14.5 km s^{-1} (Cernicharo et al. 2000); μ is 2.3 amu (Massalkhi et al. 2018). According to Equation (4), the beam-averaged H₂ column density varies with radius (the location of the molecular emission region in the CSE). Due to the large differences in the observed sizes of molecules (e.g., the emission size of CO is over 100" (Fong et al. 2006) while that of HC₃N is about 15" (Keller et al. 2015)), $N(\text{H}_2)$ obtained at different radii can be quite different (up to an order of magnitude (Gong et al. 2015)). We thus calculated the beam-averaged H₂ column density at different radii to obtain the molecular fractional abundances relative to H₂.

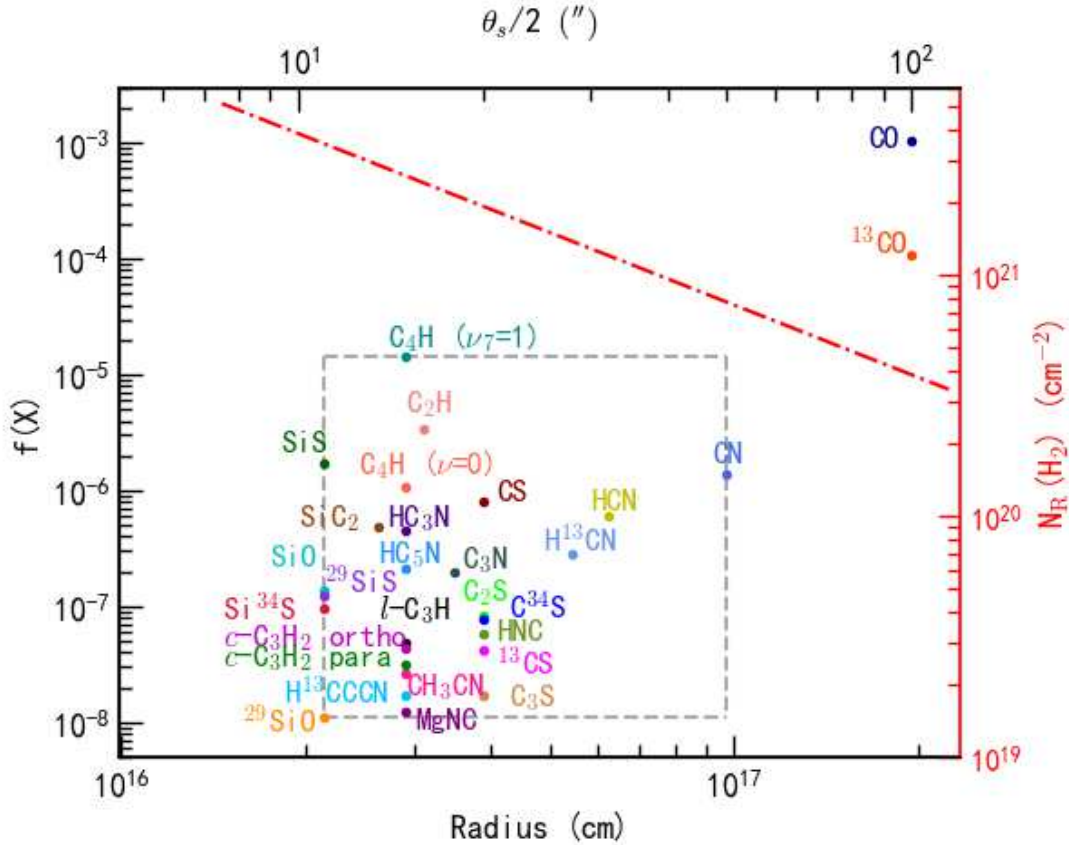


Figure 4. Observationally deduced fractional abundances (f), relative to H_2 , of all the λ 3 mm band detected species (X) toward IRC+10216 by the PMO-13.7 m, as a function of radius (R). In the plot, $f(X) = N(X) / N_R(\text{H}_2)$, where $N(X)$ depicts the total column density of the species (X), and $N_R(\text{H}_2)$ (the red dash-dotted line) represents the beam-averaged H_2 column density at radius R . Except for CO and ^{13}CO , the detected molecules are located within the area marked by the gray-dashed lines.

The observationally-deduced molecular abundance relative to H_2 , along with the beam-averaged H_2 column density that varies with radius, are summarised in Table 4 and plotted in Figure 4. Here, $f(X) = N(X) / N_R(\text{H}_2)$, where $N(X)$ depicts the total column density of the species (X), and $N_R(\text{H}_2)$ represents the beam-averaged H_2 column density at radius R . For those parent species that peak on the central star, the corresponding $N_R(\text{H}_2)$ values are calculated at the maximum emission radii of these species. In the case of daughter species that are distributed in a shell-like structure around the central star, $N_R(\text{H}_2)$ is calculated at the peak emission radii of the molecules.

It is found that in IRC+10216, the fractional abundances of the majority of detected species are between 10^{-8} and 10^{-6} in the λ 3 mm wavelength band. Some parent species, however, are more abundant. Agúndez et al. (2012) used the Large Velocity Gradient (LVG) radiative transfer model to deduce the fractional abundances of CS , SiO , SiS , and CO , which are 7×10^{-7} , 1.8×10^{-7} , 1.3×10^{-6} , and 6×10^{-4} , respectively. These results are very close to our observational results.

4.3. Updated CSE model

Good astrochemical modeling results are valuable in explaining, comparing with, and creating observations. As one of the best-observed “molecular factories” in space, IRC+10216, was frequently modeled for various purposes, e.g.: Millar et al. (2000), Agúndez & Cernicharo (2006), Cordiner & Millar (2009), Li et al. (2014), Agúndez et al. (2017), Van de Sande & Millar (2019), Millar (2020), Van de Sande et al. (2021), Van de Sande & Millar (2022), Reach et al. (2022). We employ the CSE model described in Li et al. (2014), with an update of the initial fractional abundances

Table 5. Initial abundances of parent species relative to H_2 , updated from the CSE model for IRC+10216 (Li et al. 2014).

Species	Abundance	Species	Abundance
N_2	4.0×10^{-5}	SiS	$1.7 \times 10^{-6(a)}$
NH_3	6.0×10^{-8}	CH_4	3.5×10^{-6}
HCN	2.0×10^{-5}	H_2O	2.6×10^{-6}
He	1.7×10^{-1}	PN	3.0×10^{-10}
HF	8.0×10^{-9}	C_2H_4	2.0×10^{-8}
C_2H_2	8.0×10^{-5}	SiH ₄	2.2×10^{-7}
CO	$1.0 \times 10^{-3(a)}$	HCl	1.0×10^{-7}
H_2S	4.0×10^{-9}	HCP	2.5×10^{-8}
CS	$8.1 \times 10^{-7(a)}$	SiC ₂	$4.9 \times 10^{-7(a)}$
SiO	$1.4 \times 10^{-7(a)}$		

NOTE—^(a)The observationally-deduced abundance from this work.

of several parent species listed in Table 5. Unless stated elsewhere, the assumptions and parameters are the same as those described in the model of Li et al. (2014) that accurately calculates the photodissociation of CO and N_2 (the two most abundant molecules after H_2) in the full 3D spherical geometry with isotropic incident radiation calculated by the Draine (1978) radiation field. Initially, parent species are injected at a radius of $r_i = 1 \times 10^{15}$ cm, where the molecular hydrogen number density is $n_{H_2} = 1.3 \times 10^7 \text{ cm}^{-3}$, the visual extinction is $A_V = 13.8$ mag, and the kinetic temperature of the gas is $T = 575$ K. The final radius of the CSE is set at $r_f = 2 \times 10^{17}$ cm, where the gas density decreases to $n_{H_2} = 26 \text{ cm}^{-3}$, with $T = 10$ K, and $A_V = 0.02$ mag. In the calculations, the mass-loss rate of the star is $1.5 \times 10^{-5} M_\odot \text{ yr}^{-1}$ and the outflow expansion velocity is 14.5 km s^{-1} . The gas-phase reaction network of the UMIST database for astrochemistry 2012 (McElroy et al. 2013) is employed. Reasonable good agreements are found between the simulated and observed column densities (within an order of magnitude) for most of the detected species (> 70%), as summarised in Table 1.

4.4. Isotopic ratios

Isotopic ratios are closely related to the physical conditions in the star’s core where the isotopes are formed. Therefore, isotopic ratios provide information on understanding the nucleosynthesis and the Galactic chemical evolution as well as the abundances of the interstellar medium (Kahane et al. 1988; Wilson & Rood 1994; Herwig 2005; Peng et al. 2013). AGB stars play an important role in the chemical evolution of galaxies. Thermal pulsing on the AGB creates a convective envelope, which transfers the products of He-shell burning (light elements, such as C, N and F) and the elements produced by the slow neutron-capture process (s-process) (half of the elements heavier than Fe) to the stellar surface through the third dredge-up (TDU). This alters the composition (isotopic ratios) of the envelope (Busso et al. 1999; Herwig 2005; Cristallo et al. 2009; Zhang et al. 2013; Wasserburg et al. 2017; Battino et al. 2022). Peng et al. (2013) pointed out that the mass and metallicity of a star will affect the composition of its ejected material. This will influence its surrounding interstellar medium and the isotope ratios of its gas. In fact, IRC+10216 is a much younger star (IRC+10216 was born $\sim 1 - 5 \times 10^8$ years ago, assuming masses of $3 - 5 M_\odot$) than the Sun (see Peng et al. (2013) and Portinari et al. (1998)). Although the carbon-rich AGB star IRC+10216 is located in the solar neighbourhood, extensive observational results show that its isotopic composition is remarkably non-solar (Kahane et al. 1988, 1992; Cernicharo et al. 2000). This is likely due to the fact that the shell of IRC+10216 is highly enriched in processed material after the ultimate dredge-ups (Cernicharo et al. 2000).

Here, we also observed some rotational transitions of rare isotopes. We calculated the observed isotopic ratios of these molecules using the integrated intensities ratio of spectral lines and considering the correction factor ν^{-2} (Kahane et al. 1988; Cernicharo et al. 2000) since column density is proportional to ν^{-2} , where ν represents the rest frequency (Linke et al. 1977). Our results and some results from the literature are listed in Table 6. We have provided only a few key references, which include research results from the millimeter, submillimeter, and mid-infrared wavelength ranges. For optically thin molecules, the results obtained by this method are close to the isotopic ratios.

Table 6. Isotopic ratios obtained in IRC +10216, as described in Section 4.4.

Isotope ratio	Method	Value	Local ISM ⁽ⁱ⁾	Solar ^(j)
[²⁸ Si]/[²⁹ Si]	SiS	17.3 ± 5.3		19.7
	SiO	> 10.9 ± 3.7		
	SiS and SiC ₂	18.7 ^{+1.3} _{-1.0} ^(b)		
	SiS and SiC ₂	> 15.4 ± 1.1 ^(c)		
	SiC ₂	17.2 ± 1.1 ^(d)		
	SiS and SiO	18 ± 2 ^(e)		
	SiS	> 15.1 ± 0.7 ^(f)		
	SiS	17 ⁺⁵ ₋₄ ^(g)		
[³² S]/[³⁴ S]	SiS	> 11.4 ± 3.5	24 ± 4	22.1
	CS	> 10.6 ± 1.3		
	SiS	20.2 ^{+2.6} _{-2.1} ^(b)		
	CS and SiS	21.8 ± 2.6 ^(c)		
	²⁹ Si ³² S/ ²⁸ Si ³⁴ S, ³⁰ Si ³² S/ ²⁸ Si ³⁴ S	18.9 ± 1.3 ^(d)		
	SiS	22 ± 2.5 ^(e)		
	SiS	19.6 ± 1.3 ^(f)		
	SiS	> 14 ⁺⁶ ₋₄ ^(g)		
	CS	22 ± 4 ^(h)		
	CS	22 ± 4 ^(h)		
[¹² C]/[¹³ C]	¹² C ³⁴ S/ ¹³ C ³² S ^(a)	46.4 ± 0.1	54 ± 10	89.4
	HC ₃ N	> 24.1 ± 6.9		
	CO	> 9.6 ± 0.3		
	HCN	> 2.7 ± 0.2		
	CS	> 23.1 ± 6.3		
	¹² C ³⁴ S/ ¹³ C ³² S	47 ⁺⁶ ₋₅ ^(b)		
	CS	45 ± 3 ^(c)		
	SiC ₂	34.7 ± 4.3 ^(d)		
	CS	35 ± 3.5 ^(e)		
	CS	40 ⁺¹⁸ ₋₁₀ ^(f)		

NOTE— ^(a) Assuming that the ³⁴S/³²S ratio is solar. ^(b) Kahane et al. (1988). ^(c) Cernicharo et al. (2000). ^(d) He et al. (2008). ^(e) Agúndez et al. (2012). ^(f) Patel et al. (2009). ^(g) Fonfría et al. (2015). ^(h) Wannier & Linke (1978). ⁽ⁱ⁾ The local ISM values refer to 7.5 kpc ≤ R_{GC} ≤ 8.5 kpc, and the data come from Yan et al. (2023). ^(j) Asplund et al. (2009).

Optically thick molecules may lead to a lower limit. In this work, the [²⁸Si]/[²⁹Si] ratio is derived to be 17.3 ± 5.3 from the ²⁸SiS/²⁹SiS ($J = 5 - 4$) transitions, but is only 10.9 ± 3.7 from ²⁸SiO/²⁹SiO ($J = 2 - 1$). Thus the ratio from the SiS ($J = 5 - 4$) transitions is close to the solar system value, 19.7 (Asplund et al. 2009), while the ratio from SiO ($J = 2 - 1$) is considerably smaller. In the following we therefore emphasize ratios (see Table 6), where the lines used to determine isotope ratios are both (almost) optically thin. For the [³²S]/[³⁴S] ratio with a solar system ratio of 22.1 (Asplund et al. 2009), this holds when analysing the sulfur isotopic ratios which yield calculated by optically thin spectral lines and are thus also close to the ratios obtained in the local ISM (Cernicharo et al. 2000; He et al. 2008; Patel et al. 2009; Agúndez et al. 2012). Fonfría et al. (2015) used the Texas Echelon-cross-Echelle Spectrograph at the NASA Infrared Telescope Facility to obtain high resolution mid-infrared spectra of SiS in the innermost envelope of IRC +10216. They find that the [²⁸Si]/[²⁹Si] and [³²S]/[³⁴S] ratios in the vicinity of the star are compatible with the previously measured values for the outer shells of the envelope.

We have also derived [¹²C]/[¹³C] ratios from four carbon-bearing molecules: HC₃N, CO, HCN, and CS, and obtain lower limits in that these species are optically thick. The [¹²C]/[¹³C] ratios deduced from HC₃N/H¹³CCCN ($J = 10 - 9$),

$^{12}\text{CO}/^{13}\text{CO}$ ($J = 1 - 0$), $\text{H}^{12}\text{CN}/\text{H}^{13}\text{CN}$ ($J = 1 - 0$), and $^{12}\text{CS}/^{13}\text{CS}$ are 24.1 ± 6.9 , 9.6 ± 0.3 , 2.7 ± 0.2 , and 23.1 ± 6.3 , respectively. Unlike the optically thick species, we also observed C^{34}S and ^{13}CS , both of which are optically thin. Therefore we are able to deduce a reliable isotopic ratio of $[^{12}\text{C}^{34}\text{S}]/[^{13}\text{C}^{32}\text{S}] = 2.1 \pm 0.7$, rather than a lower limit. Because the $[^{32}\text{S}]/[^{34}\text{S}]$ ratio in IRC+10216 is confirmed to be consistent with the solar value, 22.1, (Asplund et al. 2009), we estimate a $[^{12}\text{C}]/[^{13}\text{C}]$ ratio of 46.4 ± 0.1 . This value is in good agreement with existing results (Kahane et al. 1988, 1992; Cernicharo et al. 2000; Agúndez et al. 2012). Therefore, we confirm that the $[^{12}\text{C}]/[^{13}\text{C}]$ ratio in IRC+10216 is much smaller than the solar value (89.4, see Asplund et al. 2009) and local ISM value (54 ± 10 , see Yan et al. 2023). This indicates that there is a nonstandard mixing mechanism or cool bottom processing (Charbonnel 1995; Zhang et al. 2013) in the CSE of IRC+10216. A more detailed discussion on the effect of $[^{12}\text{C}]/[^{13}\text{C}]$ for AGB nucleosynthesis can be found in Milam et al. (2009). All of the isotopic ratios discussed here are included in Table 6.

In IRC+10216, the sulfur and silicon isotope ratio calculated by the optically thin spectral lines are close to solar while the carbon isotope ratio is non-solar (Cernicharo et al. 2000; He et al. 2008). Fonfría et al. (2015) pointed out that in the past 1000 yr, the nucleosynthesis of the most abundant silicon and sulfur isotopes are not expected to change significantly. In this work, we detected in several cases the same transitions and obtained close results to those described by Kahane et al. (1988), Kahane et al. (1992), and Park et al. (2008). Note that we ignored the impact of the beam dilution and did not consider the time-variation of the intensities of the spectra. These effects might be important in some cases (He et al. 2017, 2019; Pardo et al. 2018), and might lead to discrepancies in the observationally-deduced isotopic ratios.

4.5. Line surveys toward other evolved stars

In addition to the widely studied AGB star IRC+10216, detailed studies of other carbon stars have also been reported. For instance, IRAS 15194-5115 (II Lup), the brightest carbon star in the Southern hemisphere at $12 \mu\text{m}$, and also the third brightest in both hemispheres, with only IRC+10216 and CIT 6 being brighter (Epchtein et al. 1987), was also well investigated. Nyman et al. (1993) used the 15-meter Swedish-ESO Submillimeter Telescope (SEST) to make a molecular line survey in the 3 and 1.3 mm bands toward II Lup, and find that the gas composition of this object is very similar to that of IRC+10216. Subsequently, Woods et al. (2003) conducted a detailed study of the molecules in seven carbon stars with high mass-loss rate (IRAS 15082-4808, IRAS 07454-7112, CIT 6, AFGL 3068, IRC+40540, IRC+10216, and II Lup) in the northern and southern skies. They found that the chemical compositions of these carbon stars were similar, too. However, there was a significant difference in the $[^{12}\text{C}]/[^{13}\text{C}]$ ratio, which is related to nucleosynthesis and reflects the evolutionary status of these stars. Moreover, Zhang et al. (2009a,b, 2020) conducted spectral line surveys toward CIT6 and CRL 3068, and find that only the most abundant molecules could be detected and that the gas compositions of these two sources were very similar to IRC+10216, too.

In short, it is found that the gas compositions of the evolved stars are highly determined by their chemical types (namely their $[\text{C}]/[\text{O}]$ ratios), and could be simply classified as C-rich, O-rich, and S-type cases. In principle, the gas compositions of all three types of AGB stars will be well simulated by the corresponding chemical models based on the parent species and physical conditions. This conclusion is further confirmed by the results of other line surveys toward other types of evolved stars in the λ 3 mm band, as summarized in Table 7.

5. CONCLUSIONS

We present the first unbiased λ 3 mm (between 84.5 and 115.8 GHz) line survey toward the carbon-rich envelope of IRC+10216 using the PMO-13.7m telescope, and provide a comprehensive analysis of the molecular spectra by making use of the results from previous studies. A total of 75 spectral lines were detected and assigned to 19 different molecules. The detected molecules are C_2H , $l\text{-C}_3\text{H}$, C_4H , CN, C_3N , HC_3N , HC_5N , HCN, HNC, CH_3CN , MgNC , CO, $c\text{-C}_3\text{H}_2$, SiC_2 , SiO, SiS, CS, C_2S , C_3S . The $J = 13 - 12$ transition of H^{13}CCCN is detected in IRC+10216 for the first time. The excitation temperatures and column densities of these molecules are derived by assuming LTE with excitation temperatures ranging from 5.3 to 73.4 K, and molecular column densities ranging from 3.27×10^{13} to $4.03 \times 10^{17} \text{ cm}^{-2}$. Except for HCN, the observationally deduced excitation temperatures and column densities roughly agree with previous studies. We find that the fractional abundances of the detected species range between 1.14×10^{-8} and 1.04×10^{-3} . We also find that HC_5N , HC_7N and HC_9N , together with higher J transitions of HC_3N , C_3S , CH_3CN ,

Table 7. Published radio line surveys of evolved stars around the λ 3 mm band. Note that the published line surveys toward IRC +10216 are summarised in Table 2.

Sources Name	Evolutiona stage	Chemical type	Covered Frequencies (GHz)	Telescope	Reference
IK Tau	AGB	O-rich	79 – 116	IRAM–30 m	Velilla Prieto et al. (2017)
IRC +10216	AGB	C-rich	84.5 – 115.8	PMO–13.7 m	This work
IRC +10216	AGB	C-rich	72.2 – 91.1	Onsala–20 m	Johansson et al. (1984, 1985)
II Lup	AGB	C-rich	80.5 – 115.5 ^c	Mopra–22 m	Smith et al. (2015)
RAFGL 4211	AGB	C-rich	80.5 – 115.5 ^c	Mopra–22 m	Smith et al. (2015)
AI Vol	AGB	C-rich	80.5 – 115.5 ^c	Mopra–22 m	Smith et al. (2015)
RAFGL 4211	AGB	C-rich	~ 85.10 – 115.75 ^d	SEST–15 m	Woods et al. (2003)
RAFGL 4078	AGB	C-rich	~ 85.10 – 115.75 ^d	SEST–15 m	Woods et al. (2003)
CIT 6	AGB	C-rich	~ 85.10 – 115.75 ^d	SEST–15 m	Woods et al. (2003)
CIT 6	AGB	C-rich	90 – 116	ARO–12 m	Yang et al. (2023)
AFGL 3068	AGB	C-rich	~ 85.10 – 115.75 ^d	SEST–15 m	Woods et al. (2003)
IRC +40540	AGB	C-rich	~ 85.10 – 115.75 ^d	SEST–15 m	Woods et al. (2003)
II Lup	AGB	C-rich	~ 85.10 – 115.75 ^d	SEST–15 m	Nyman et al. (1993)
Red Rectangle	post-AGB	O-rich	84.50 – 92.25	IRAM–30 m	Gallardo Cava et al. (2022)
HD 52961	post-AGB	O-rich	84.40 – 92.15	IRAM–30 m	Gallardo Cava et al. (2022)
AI Canis Minoris	post-AGB	O-rich	84.40 – 92.15	IRAM–30 m	Gallardo Cava et al. (2022)
IRAS 20056 +1834	post-AGB	O-rich	84.40 – 92.20	IRAM–30 m	Gallardo Cava et al. (2022)
R Scuti	post-AGB	O-rich	83.40 – 92.30	IRAM–30 m	Gallardo Cava et al. (2022)
89 Herculis	post-AGB	C-rich	83.40 – 92.50	IRAM–30 m	Gallardo Cava et al. (2022)
CRL 2688	post-AGB	C-rich	75.7–83.5 and 91.4–99.2	IRAM–30 m	Qiu et al. (2022)
CRL 2688	post-AGB	C-rich	71–111	ARO–12 m	Zhang et al. (2013)
CRL 2688	post-AGB	C-rich	85–116	TRAO–14 m	Park et al. (2008)
CRL 618	post-AGB	C-rich	80.25–115.75	IRAM–30 m	Pardo et al. (2007)
AC Herculis	post-AGB	O-rich	84.40–92.15	IRAM–30 m	Gallardo Cava et al. (2022)
IRAS 19157 -0257	post-AGB		84.40–92.20	IRAM–30 m	Gallardo Cava et al. (2022)
IRAS 18123 +0511	post-AGB		84.40–92.15	IRAM–30 m	Gallardo Cava et al. (2022)
IRAS 19125 +0343	post-AGB		84.40–92.15	IRAM–30 m	Gallardo Cava et al. (2022)
NGC 7027	PN	C-rich	71–111	ARO–12 m	Zhang et al. (2008)
IC 4406	PN	O-rich	80.5–115.5 ^c	Mopra–22 m	Smith et al. (2015)
NGC 6537	PN	O-rich	80.5–115.5 ^c	Mopra–22 m	Smith et al. (2015)
NML Cyg	RSG ^a	O-rich	68–116	OSO–20 m	Andrews et al. (2022)
IRC +10420	YHG ^b	N-rich	~ 83.2–117.1	IRAM–30 m	Quintana-Lacaci et al. (2016)

NOTE— ^a Red supergiant (RSG) star. ^b Yellow hypergiant (YHG) star. ^c Note that 98.5 – 107.5 GHz is uncovered in the observation. ^d Frequency range is directly taken from the reference.

SiS, C₄H ($\nu = 0$) and C₄H ($\nu = 1$), trace the warmer molecular layers in IRC +10216. Moreover, we detected several isotopologues and derived their isotopic ratios. The $^{28}\text{Si}/^{29}\text{Si}$ ratio, for example, is found to be 17.3 ± 5.3 , which is roughly consistent with earlier determinations and close to solar system value. Last but not least, we have summarised all of the 106 species detected in IRC +10216 to date with their observed and modeled column densities for the convenience of future studies.

We are extremely grateful to the anonymous reviewer for the fruitful and insightful comments, along with valuable inputs to this manuscript, which greatly helped improving the quality of this paper. We thank Prof. Y. Xu (PMO) and Prof. C. Walsh (Univ. of Leeds) for their constructive suggestions on this work. We appreciate the assistance of the PMO–13.7 m telescope operators during the observations. X. Li acknowledges support from the Xinjiang Tianchi Talent project (2019). This work was also funded by National Key R&D Program of China under grant No.2022YFA1603103, the NSFC under grants 11973076, 12173023, 11973075, the Natural Science Foundation of Xinjiang Uygur Autonomous Region 2022D01B221. Y. Gao thanks the Project of Xinjiang Uygur Autonomous Region of China for Flexibly Fetching in Upscale Talents. TJM thanks the Leverhulme Trust for the award of an Emeritus Fellowship. Astrophysics at QUB is supported by the STFC through grant ST/T000198/1. Y. Zhang and X. Fang thank the Xinjiang Tianchi Talent Program (2023).

APPENDIX

A. ZOOM-IN PLOTS OF OBSERVED SPECTRA

This appendix includes the spectra of the survey of IRC +10216 ranging from 84.5 to 115.8 GHz, displayed in consecutive 475 MHz frequency segments with 0.244 MHz frequency resolution. The observed molecular spectral lines whose S/N is greater than 3 are marked in blue. Molecules marked with a ? indicate that the S/N of the spectral line is between 2 and 3.

B. SPECTRAL LINE PARAMETERS OF ALL THE IDENTIFIED SPECIES

The spectral line parameters of all the identified species from this survey towards IRC +10216 are listed in Table B1.

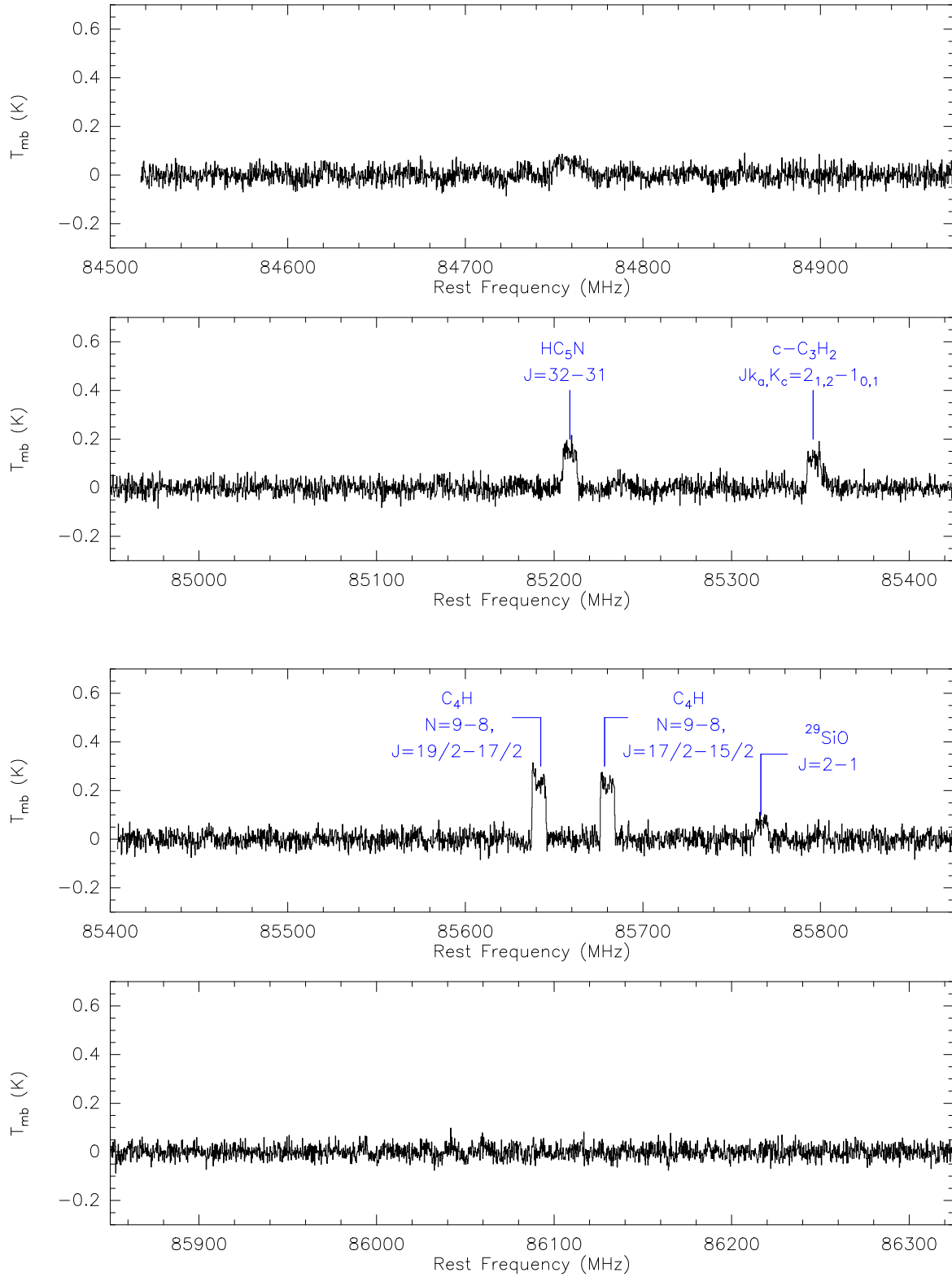


Figure A1. 84.5 – 115.8 GHz spectrum of IRC +10216 displayed in consecutive 475 MHz frequency segments with 0.244 MHz spectral resolution.

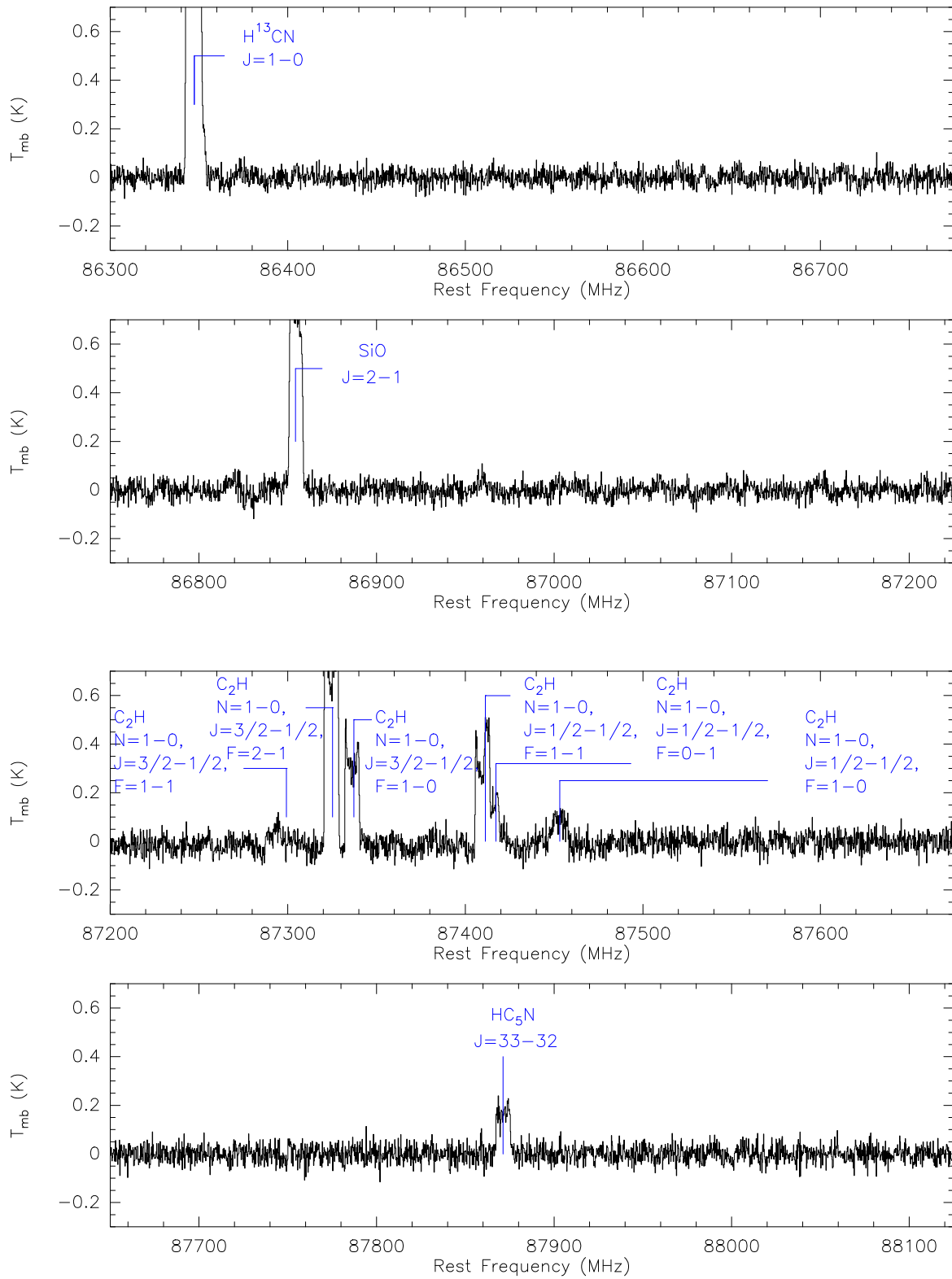


Figure A2. Same as Figure A1.

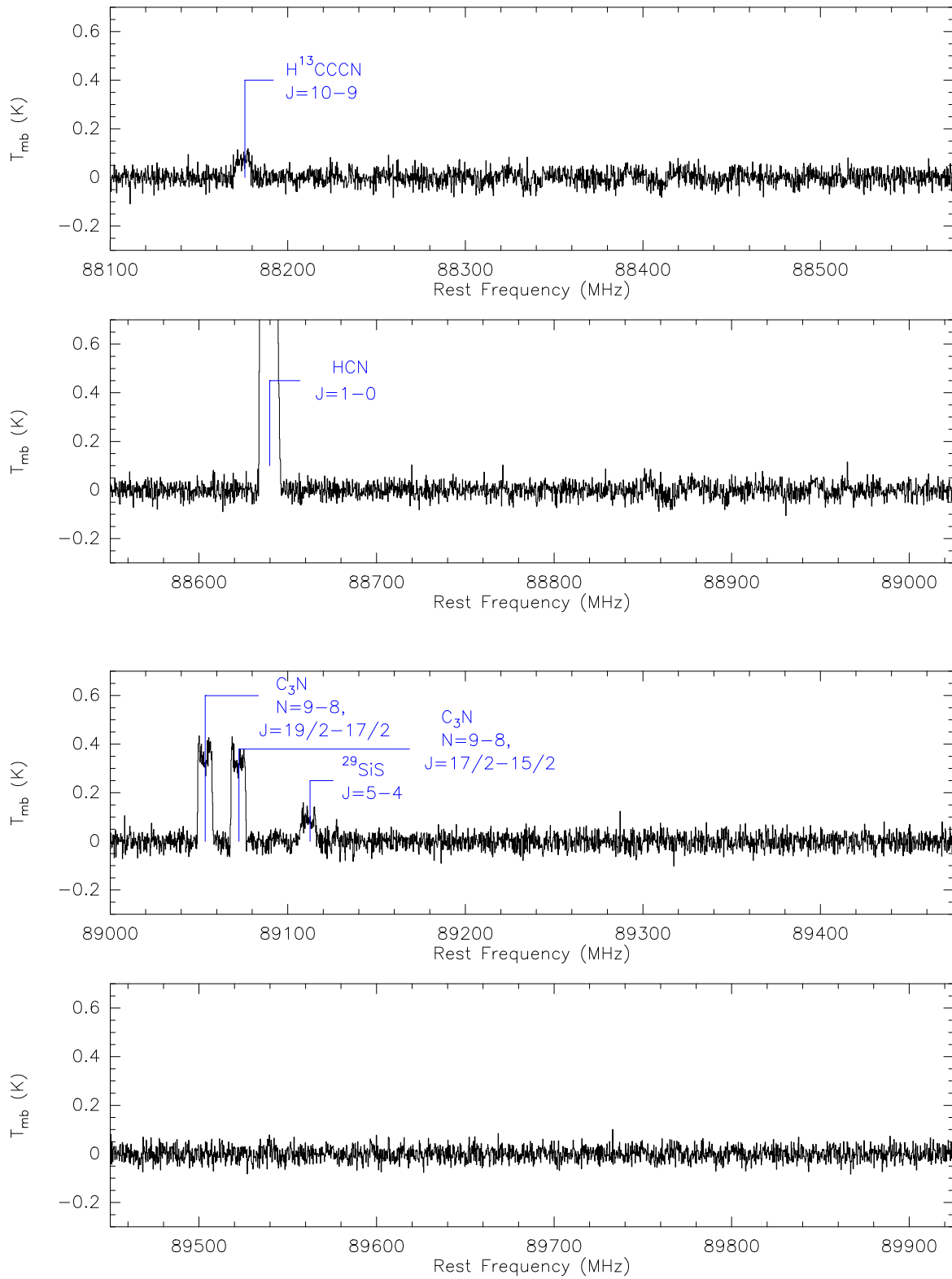


Figure A3. Same as Figure A1.

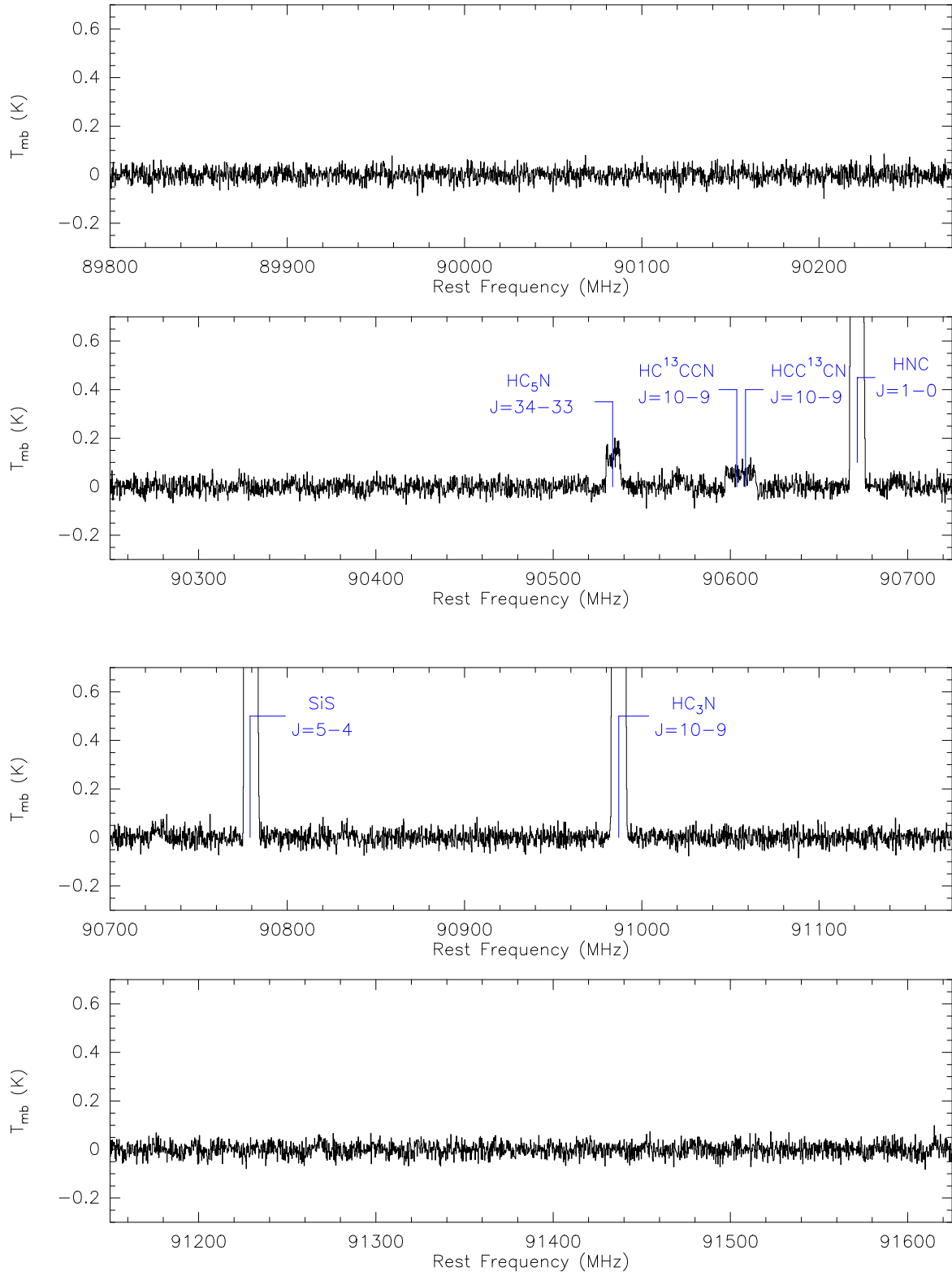


Figure A4. Same as Figure A1.

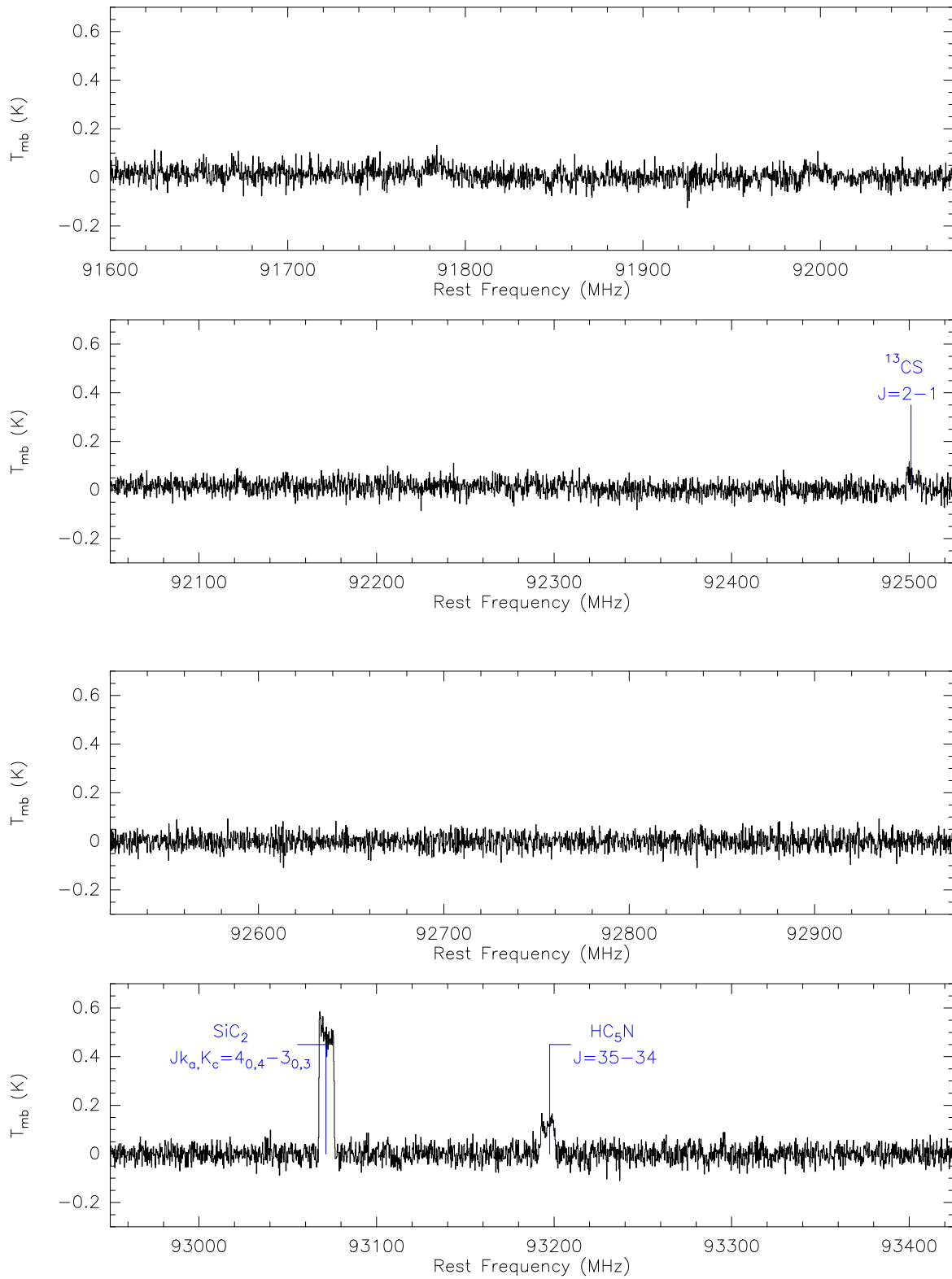


Figure A5. Same as Figure A1.

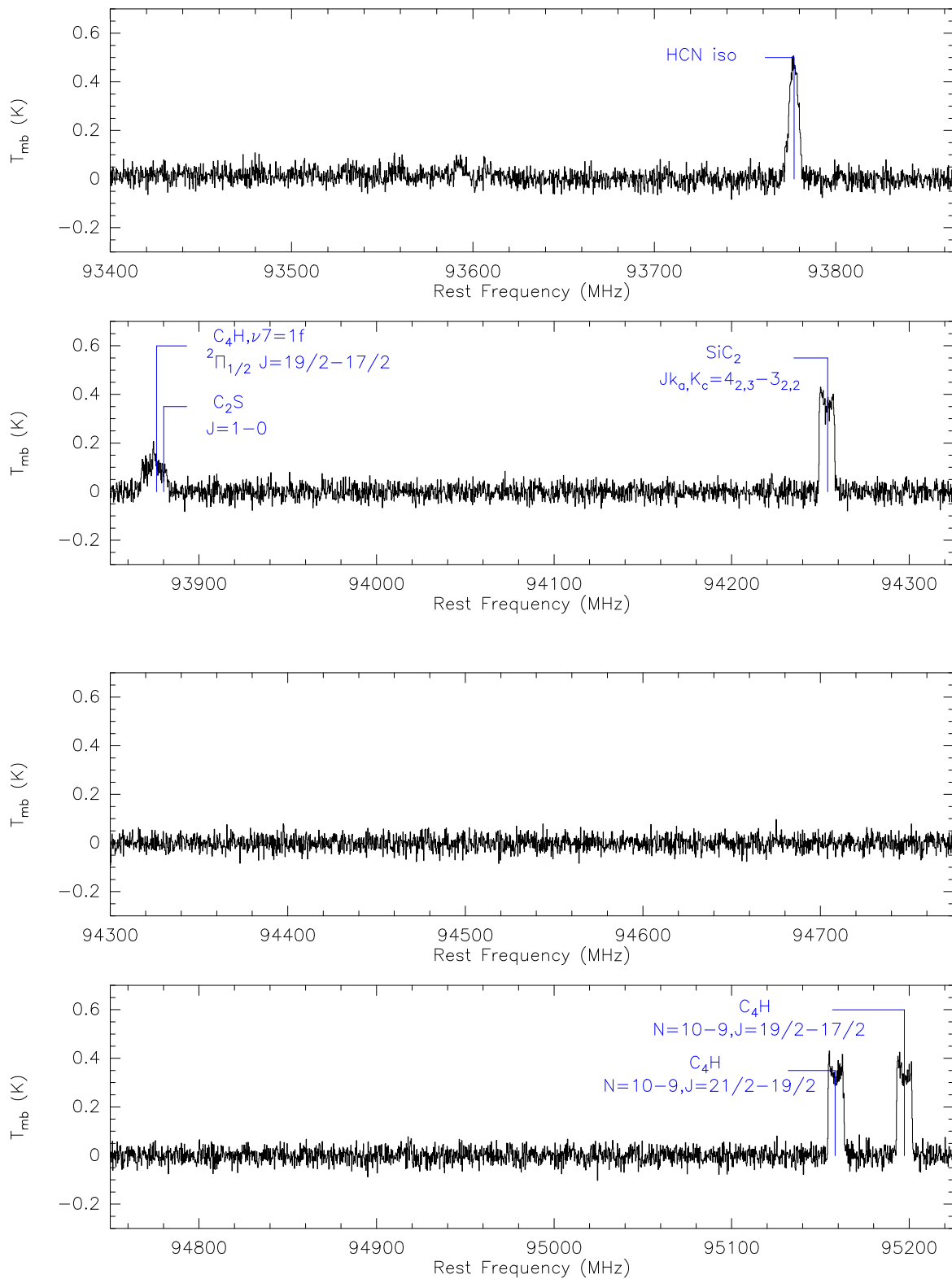


Figure A6. Same as Figure A1.

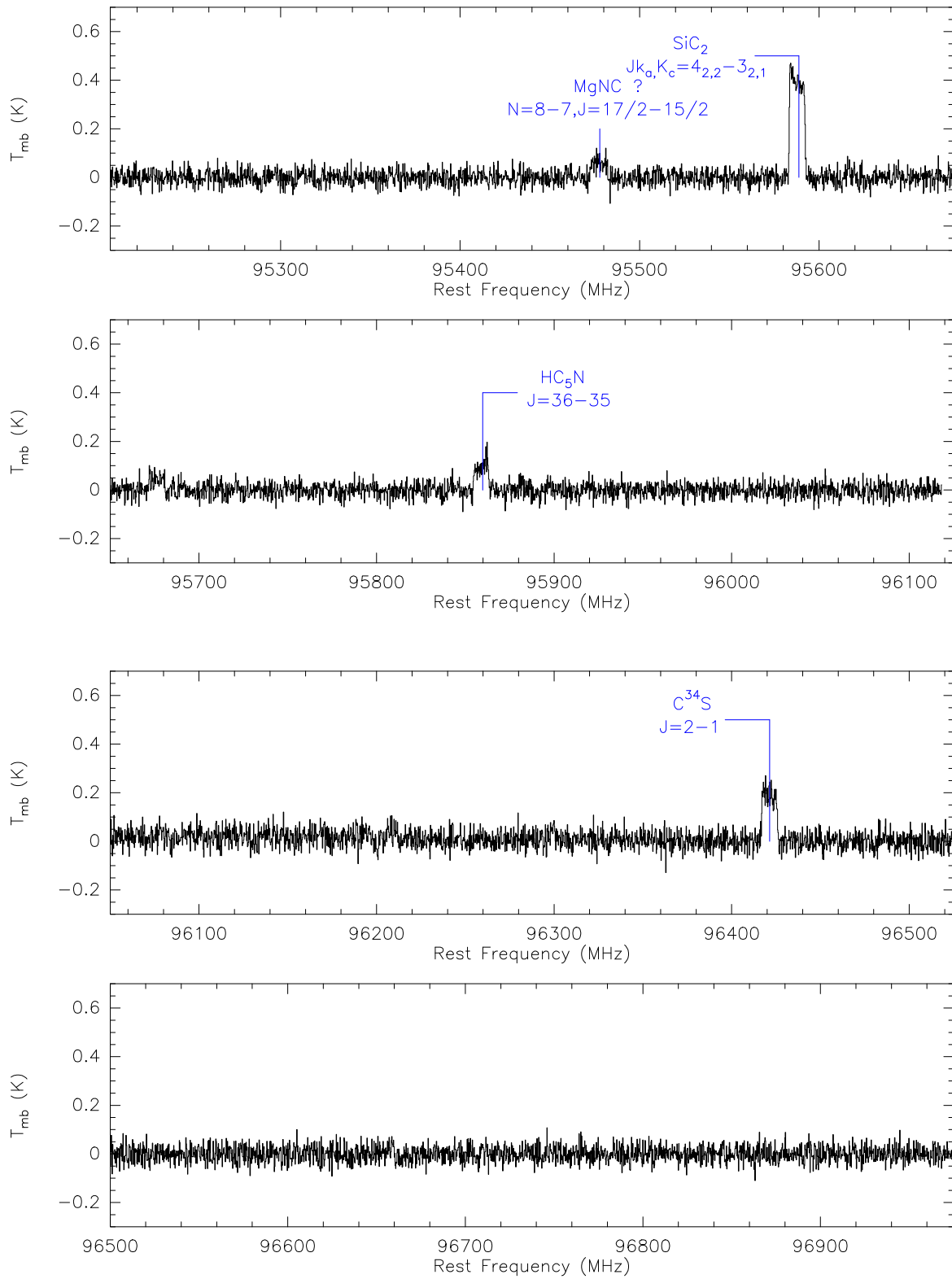


Figure A7. Same as Figure A1.

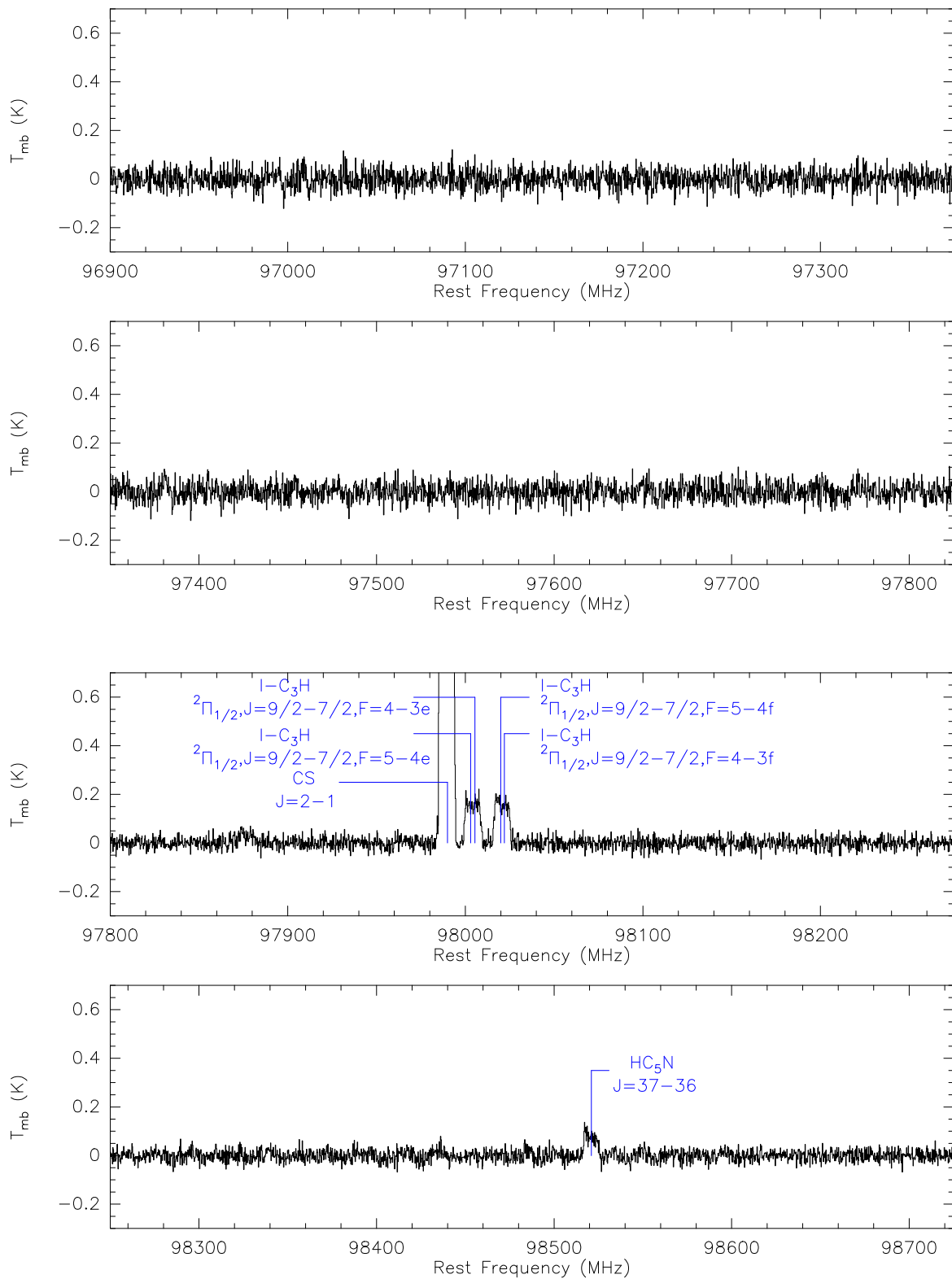


Figure A8. Same as Figure A1.

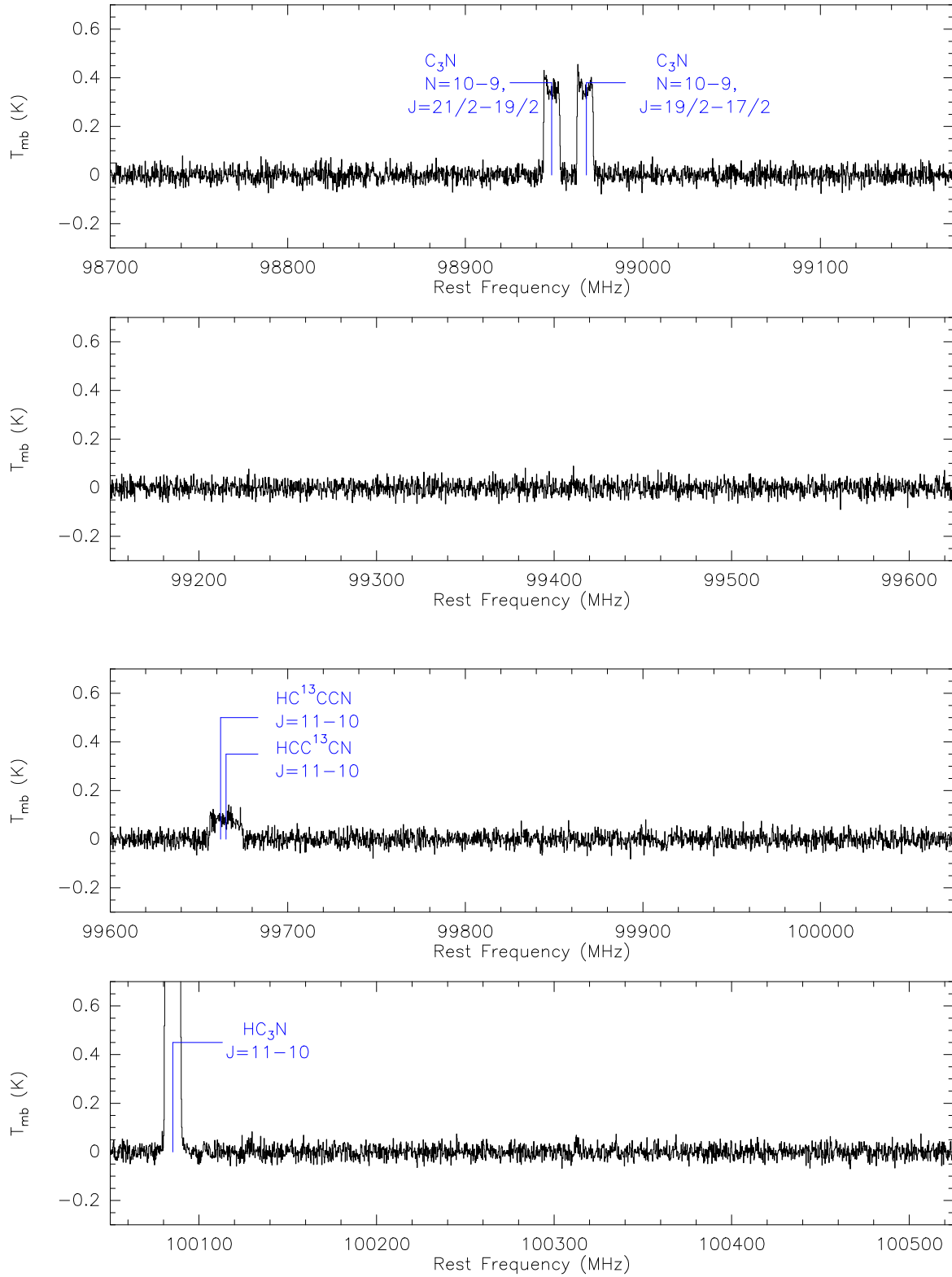


Figure A9. Same as Figure A1.

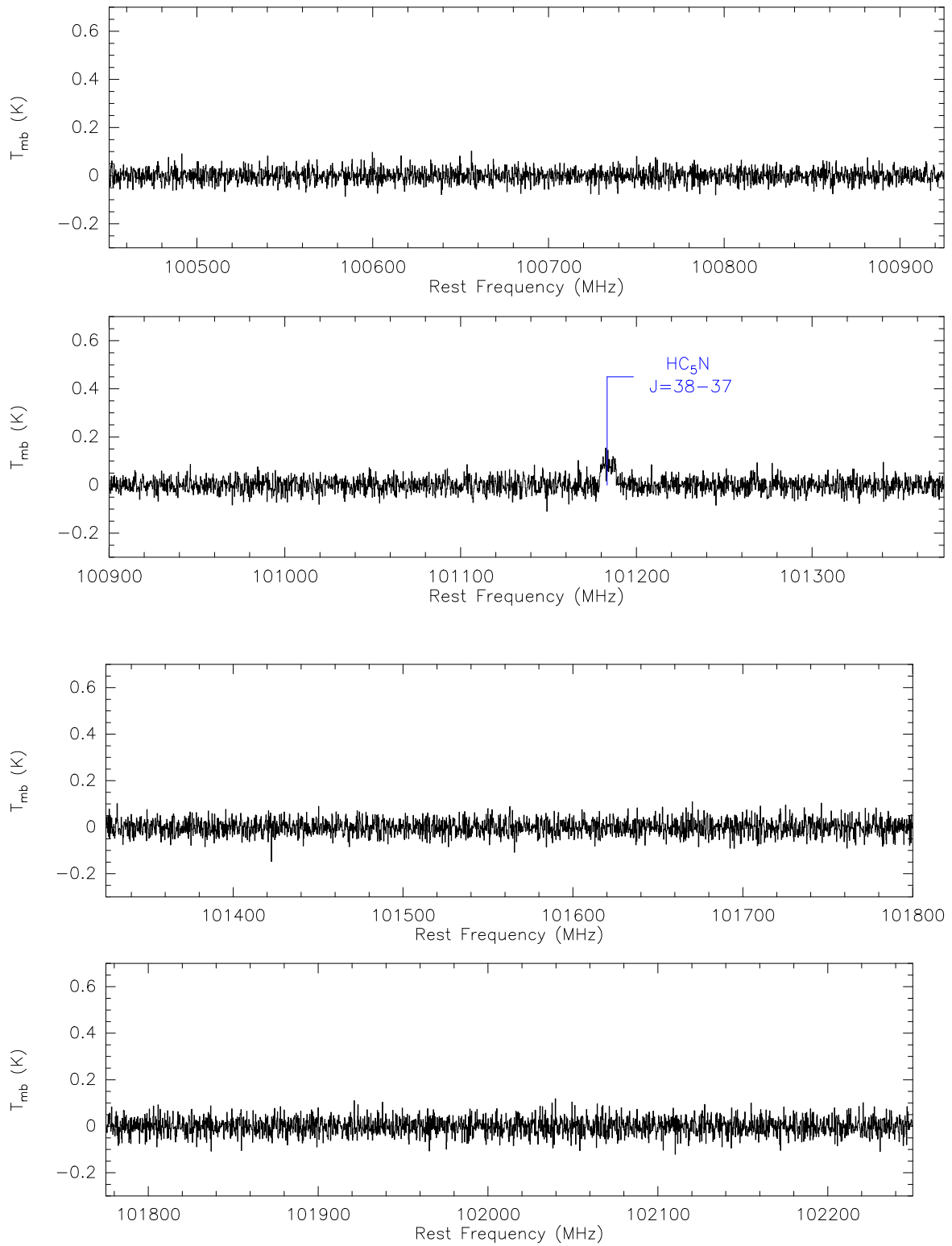


Figure A10. Same as Figure A1.

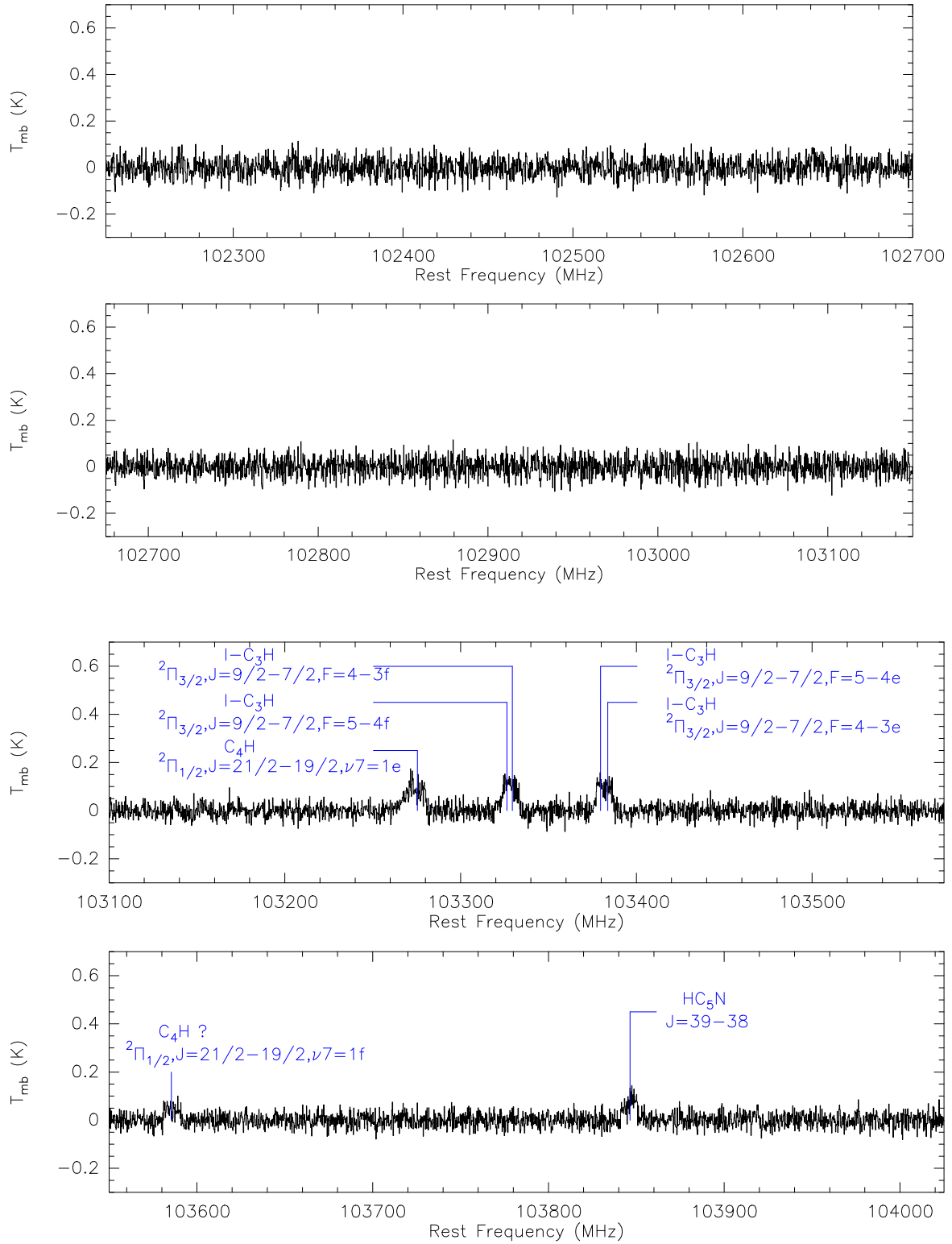


Figure A11. Same as Figure A1.

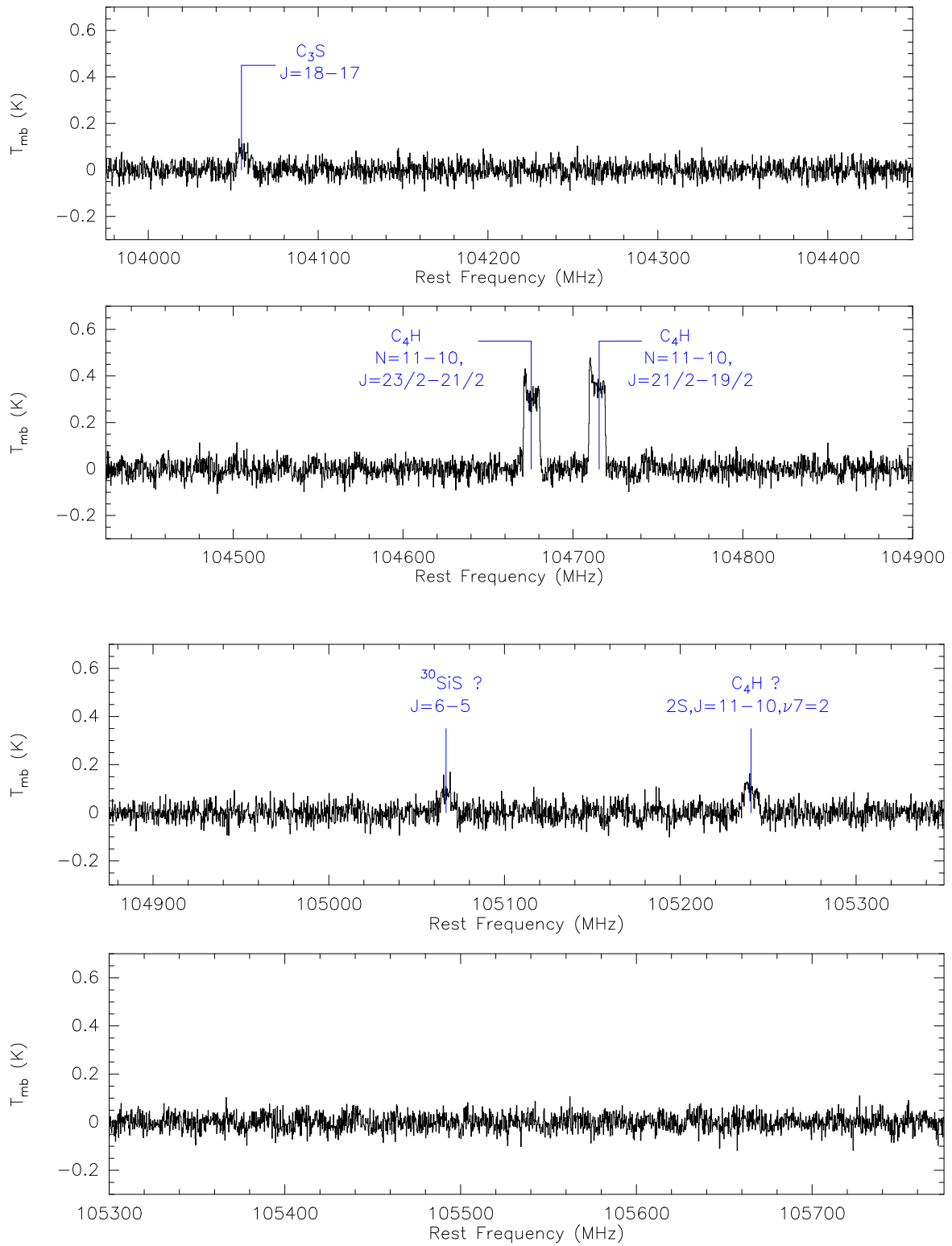


Figure A12. Same as Figure A1.

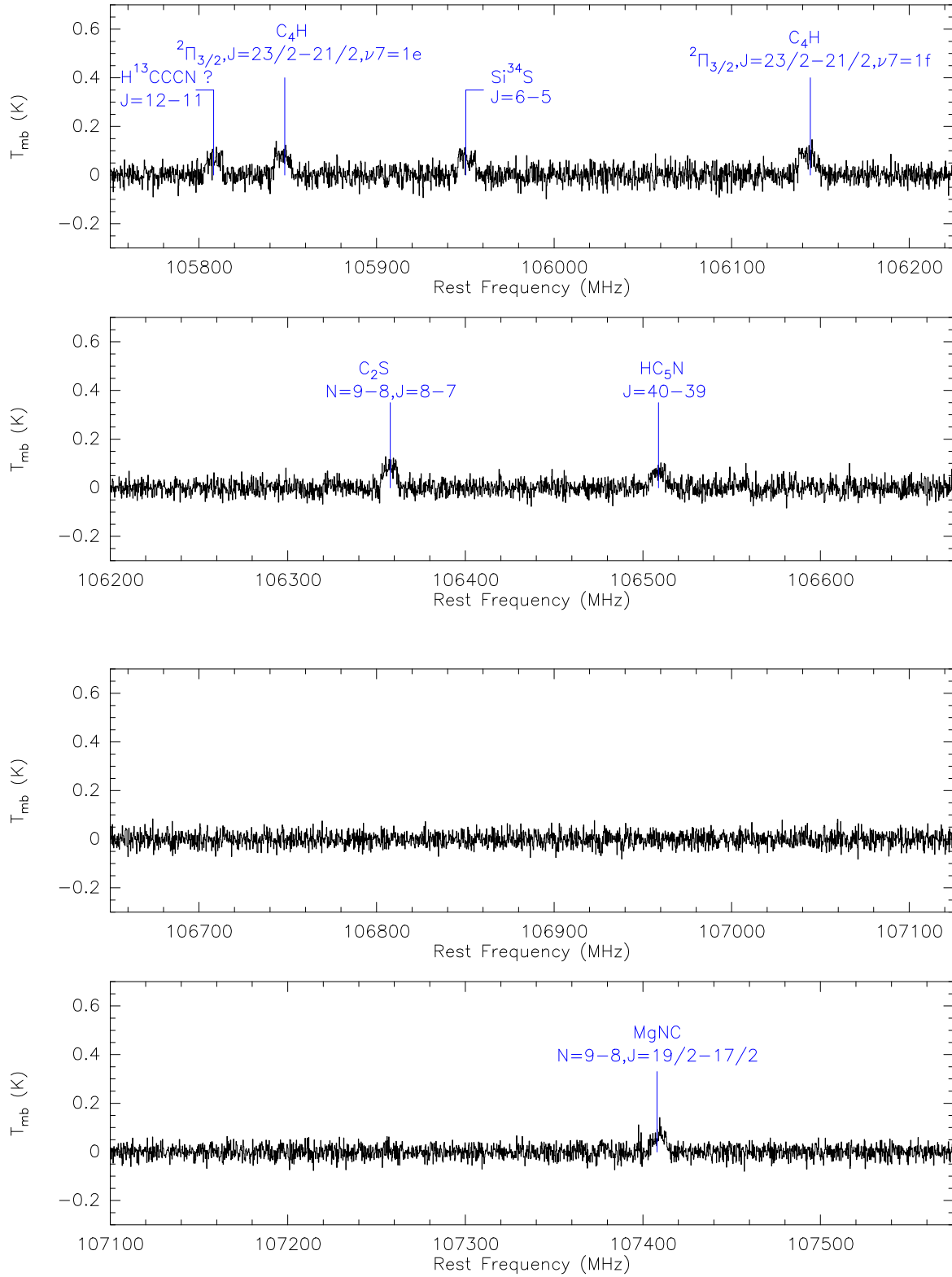


Figure A13. Same as Figure A1.

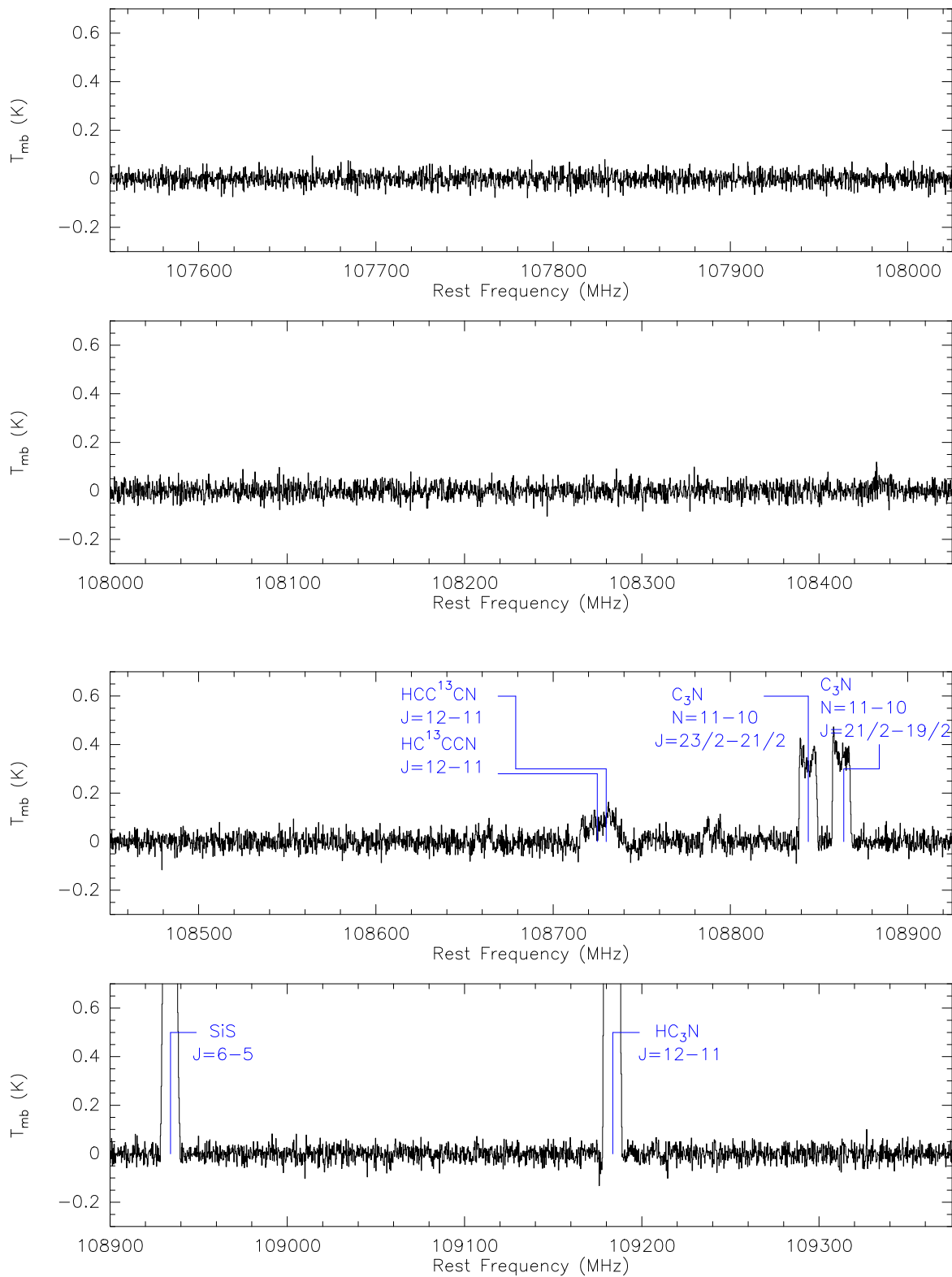


Figure A14. Same as Figure A1.

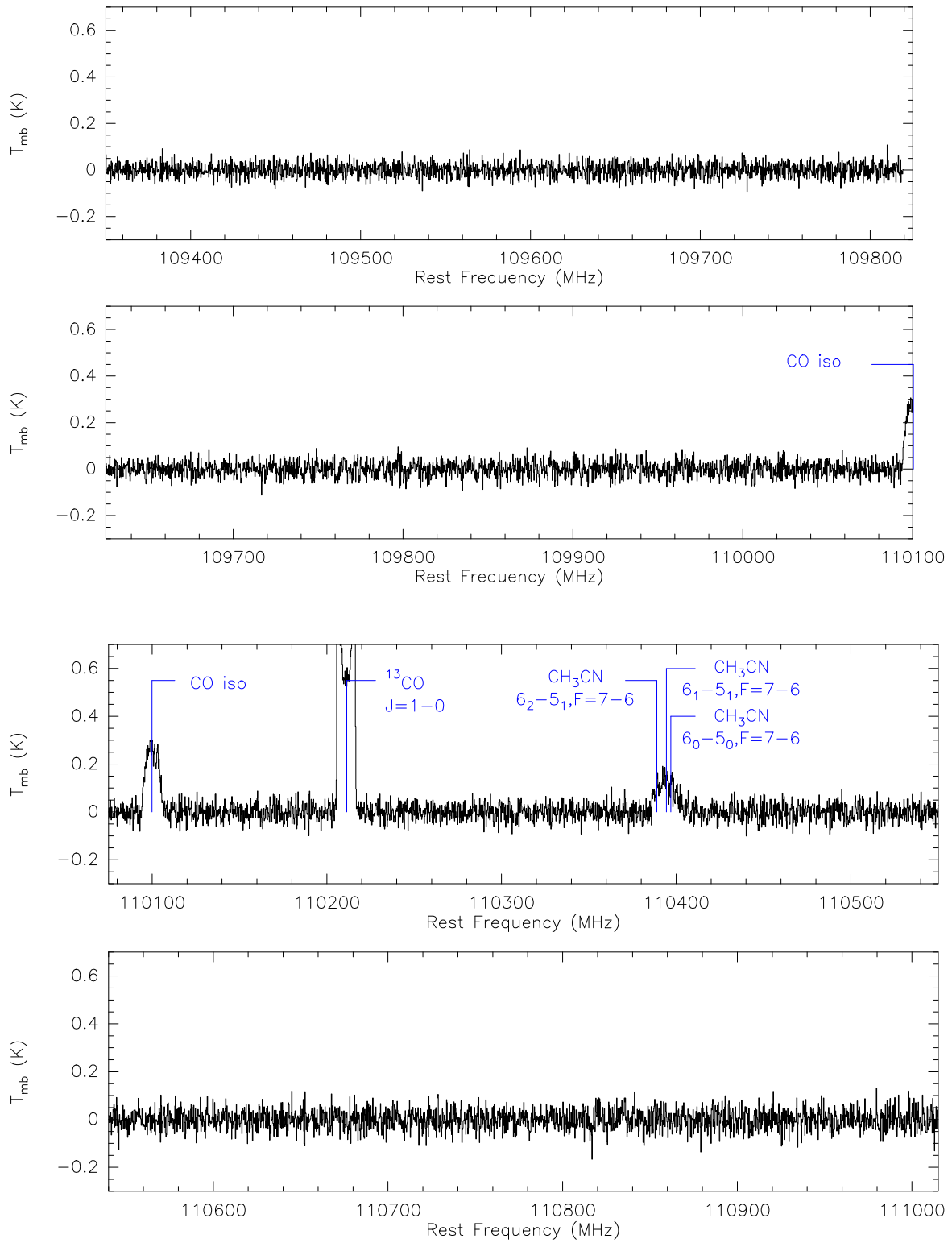


Figure A15. Same as Figure A1.

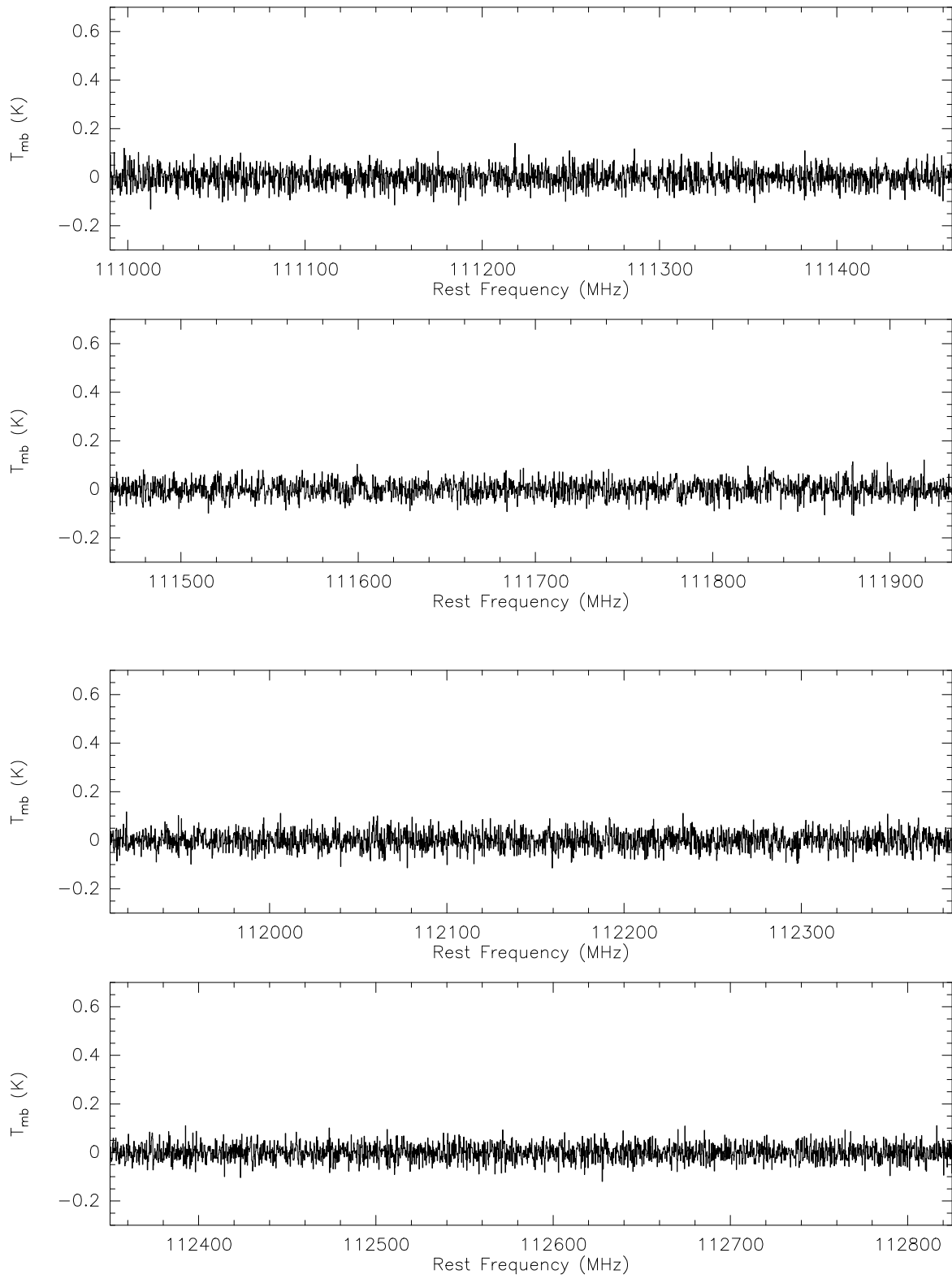


Figure A16. Same as Figure A1.

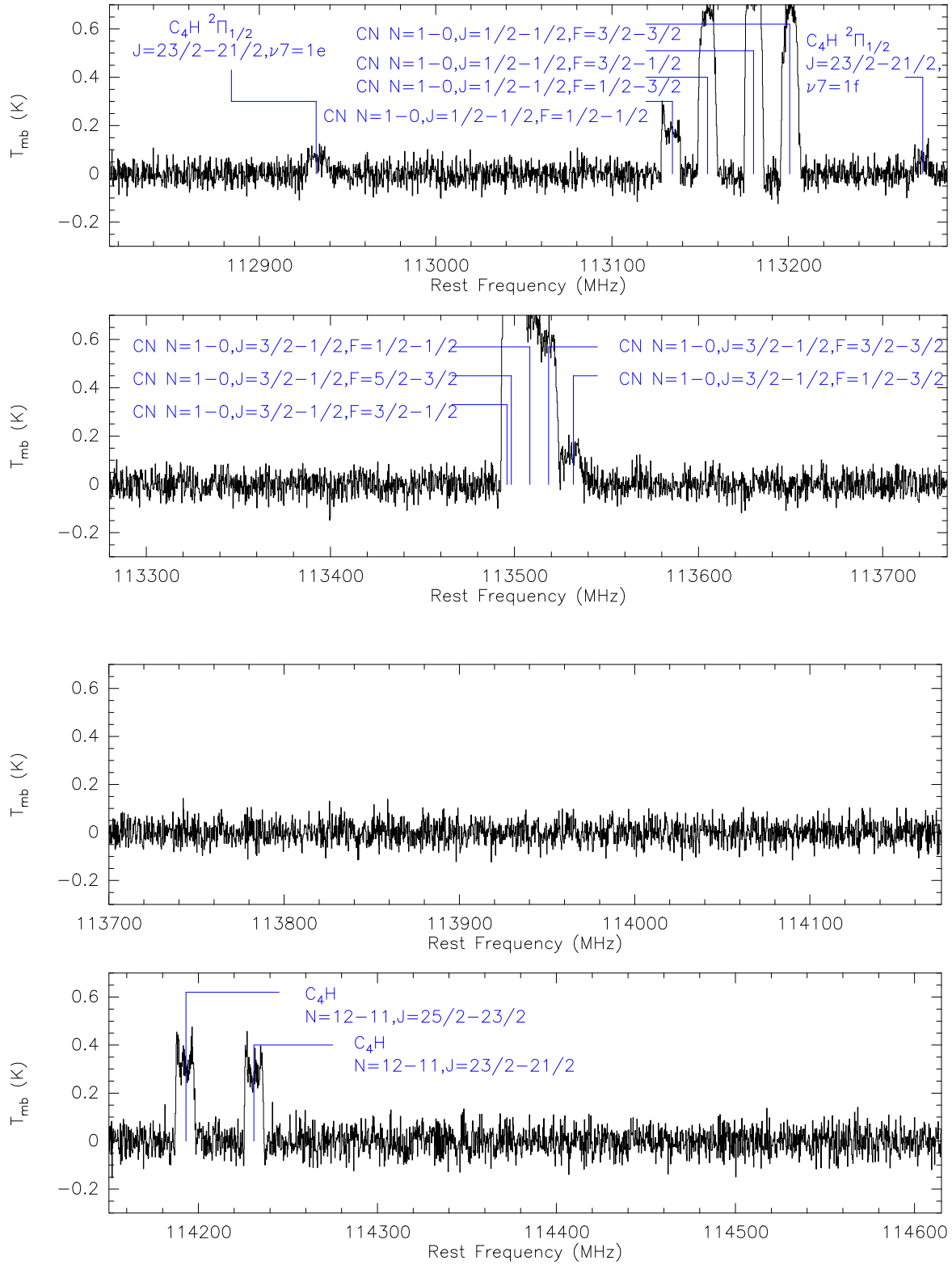


Figure A17. Same as Figure A1.

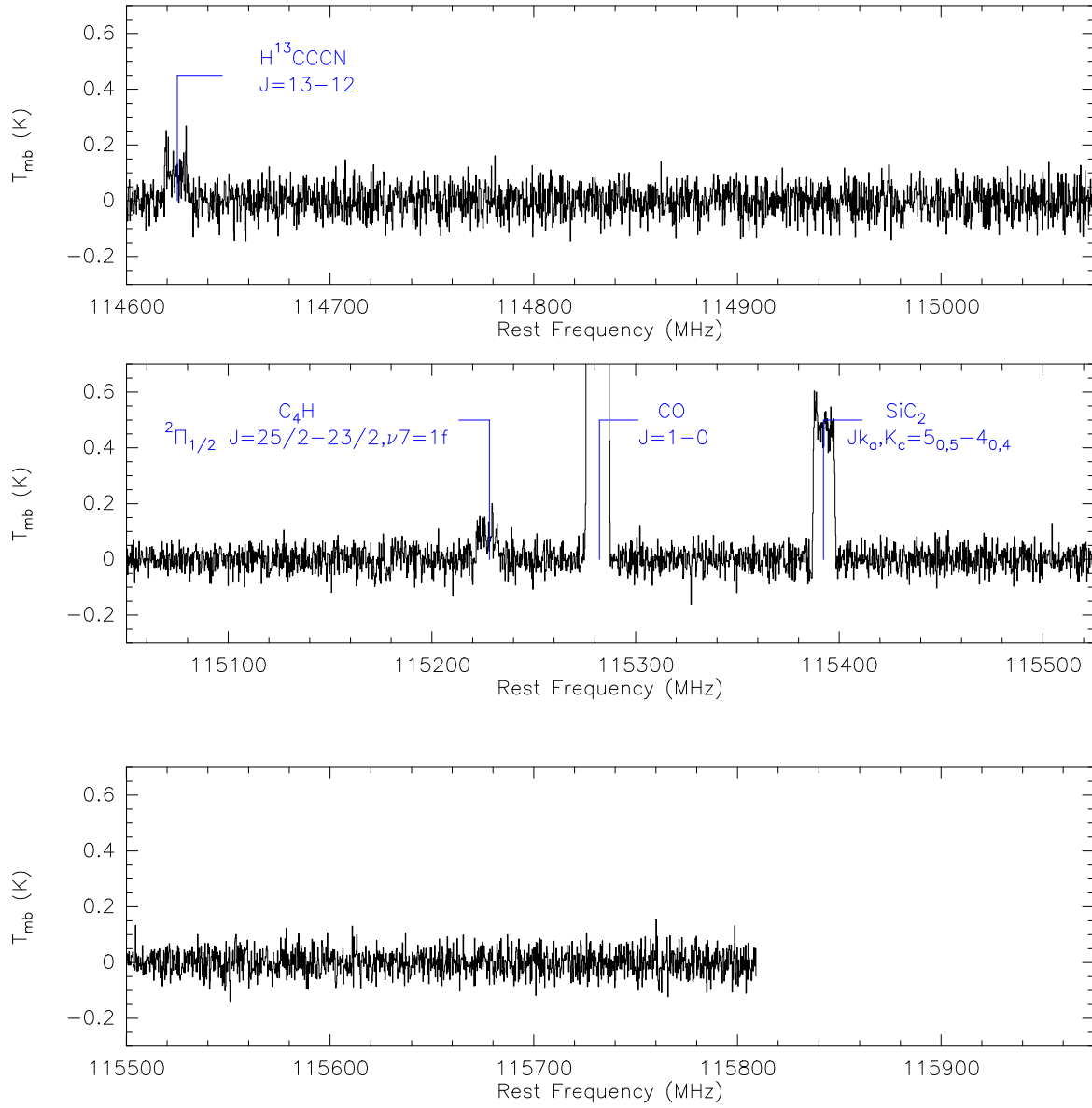


Figure A18. Same as Figure A1.

Table B1. Spectral line parameters of all the identified species from this survey towards IRC+10216.

No.	Molecule	Transitions	Rest Freq.	$\int T_{\text{mb}} dv$	V_{lsr}	V_{exp}	T_{mb}	Notes
			(MHz)	(K km s ⁻¹)	(km s ⁻¹)	(km s ⁻¹)	(K)	
(1)	C ₂ H	$N = 1 - 0, J = 3/2 - 1/2, F = 1 - 1$	87284.156	2.15(0.606)	-25.96(0.839)	14.988(0.157)	0.066(0.021)	
(2)	C ₂ H	$N = 1 - 0, J = 3/2 - 1/2, F = 2 - 1$	87316.925	22.00(0.904)	-25.75(0.419)	14.035(0.094)	0.693(0.031)	
(3)	C ₂ H	$N = 1 - 0, J = 3/2 - 1/2, F = 1 - 0$	87328.624	9.38(1.070)	-25.44(0.419)	13.830(0.028)	0.281(0.037)	
(4)	C ₂ H	$N = 1 - 0, J = 1/2 - 1/2, F = 1 - 1$	87402.004	13.40(0.837)	*	*	0.341(0.037)	1
(5)	C ₂ H	$N = 1 - 0, J = 1/2 - 1/2, F = 0 - 1$	87407.165	1
(6)	C ₂ H	$N = 1 - 0, J = 1/2 - 1/2, F = 1 - 0$	87446.512	1.86(0.599)	-23.94(0.837)	14.461(0.008)	0.070(0.021)	
(7)	l-C ₃ H	$^2\Pi_{1/2}, J = 9/2 - 7/2, F = 5 - 4e$	97995.212	4.01(0.599)	-26.87(0.747)	14.137(0.094)	0.142(0.021)	1
(8)	l-C ₃ H	$^2\Pi_{1/2}, J = 9/2 - 7/2, F = 4 - 3e$	97995.951	
(9)	l-C ₃ H	$^2\Pi_{1/2}, J = 9/2 - 7/2, F = 5 - 4f$	98011.649	4.60(0.667)	-26.79(0.747)	14.552(0.080)	0.167(0.023)	1
(10)	l-C ₃ H	$^2\Pi_{1/2}, J = 9/2 - 7/2, F = 4 - 3f$	98012.576	
(11)	l-C ₃ H	$^2\Pi_{3/2}, J = 9/2 - 7/2, F = 5 - 4f$	103319.278	2.31(0.667)	-26.67(0.708)	13.754(0.181)	0.079(0.023)	1
(12)	l-C ₃ H	$^2\Pi_{3/2}, J = 9/2 - 7/2, F = 4 - 3f$	103319.818	
(13)	l-C ₃ H	$^2\Pi_{3/2}, J = 9/2 - 7/2, F = 5 - 4e$	103372.506	2.24(0.725)	-24.96(0.708)	13.452(0.145)	0.075(0.025)	1
(14)	l-C ₃ H	$^2\Pi_{3/2}, J = 9/2 - 7/2, F = 4 - 3e$	103373.129	
(15)	C ₄ H	$N = 9 - 8, J = 19/2 - 17/2$	85634.000	6.73(0.552)	-25.73(1.709)	13.692(0.068)	0.282(0.019)	
(16)	C ₄ H	$N = 9 - 8, J = 17/2 - 15/2$	85672.570	6.26(0.651)	-26.63(1.709)	14.227(0.102)	0.217(0.022)	
(17)	C ₄ H	$N = 10 - 9, J = 21/2 - 19/2$	95150.320	9.69(0.623)	-26.45(1.528)	14.332(0.068)	0.326(0.021)	
(18)	C ₄ H	$N = 10 - 9, J = 19/2 - 17/2$	95188.940	8.63(0.605)	-25.94(1.528)	13.840(0.071)	0.289(0.021)	
(19)	C ₄ H	$N = 11 - 10, J = 23/2 - 21/2$	104666.560	8.17(0.893)	-26.31(0.699)	13.894(0.046)	0.262(0.031)	
(20)	C ₄ H	$N = 11 - 10, J = 21/2 - 19/2$	104705.100	10.3(0.824)	-25.62(0.699)	13.924(0.038)	0.351(0.028)	
(21)	C ₄ H	$N = 12 - 11, J = 25/2 - 23/2$	114182.510	8.99(0.984)	-26.11(1.282)	13.666(0.089)	0.291(0.034)	
(22)	C ₄ H	$N = 12 - 11, J = 23/2 - 21/2$	114221.040	9.75(1.046)	-26.19(1.282)	13.859(0.079)	0.327(0.036)	
(23)	C ₄ H	$^2\Pi_{1/2} J = 19/2 - 17/2, \nu 7 = 1f$	93863.300	3.36(0.551)	×	×	0.080(0.019)	B1
(24)	C ₄ H	$^2\Pi_{1/2} J = 21/2 - 19/2, \nu 7 = 1e$	103266.081	2.66(0.609)	-27.09(1.418)	14.154(0.289)	0.090(0.021)	
(25)	C ₄ H	$^2\Pi_{1/2} J = 23/2 - 21/2, \nu 7 = 1e$	112922.500	1.59(0.580)	-26.95(1.296)	13.801(0.339)	0.061(0.020)	
(26)	C ₄ H	$^2\Pi_{1/2} J = 23/2 - 21/2, \nu 7 = 1f$	113265.900	2.48(0.667)	-26.49(1.292)	13.919(0.233)	0.084(0.023)	
(27)	C ₄ H	$^2\Pi_{3/2} J = 23/2 - 21/2, \nu 7 = 1e$	105838.000	1.96(0.475)	-25.52(1.383)	13.801(0.193)	0.090(0.016)	
(28)	C ₄ H	$^2\Pi_{3/2} J = 23/2 - 21/2, \nu 7 = 1f$	106132.800	1.48(0.551)	-26.54(1.379)	13.048(0.286)	0.057(0.019)	
(29)	C ₄ H	$^2\Pi_{3/2} J = 25/2 - 23/2, \nu 7 = 1f$	115216.800	2.09(0.638)	-25.68(1.271)	14.674(0.331)	0.068(0.022)	
(30)	CN	$N = 1 - 0, J = 3/2 - 1/2, F = 3/2 - 1/2$	113488.140	86.4(0.841)	1.916(0.029)	1
(31)	CN	$N = 1 - 0, J = 3/2 - 1/2, F = 5/2 - 3/2$	113490.982	
(32)	CN	$N = 1 - 0, J = 3/2 - 1/2, F = 1/2 - 1/2$	113499.639	
(33)	CN	$N = 1 - 0, J = 3/2 - 1/2, F = 3/2 - 3/2$	113508.944	
(34)	CN	$N = 1 - 0, J = 3/2 - 1/2, F = 1/2 - 3/2$	113520.414	
(35)	CN	$N = 1 - 0, J = 1/2 - 1/2, F = 1/2 - 1/2$	113123.337	6.24(0.696)	-25.91(0.647)	14.363(0.051)	0.235(0.024)	
(36)	CN	$N = 1 - 0, J = 1/2 - 1/2, F = 1/2 - 3/2$	113144.192	20.00(0.957)	-26.01(0.647)	13.350(0.057)	0.789(0.033)	

Table B1 continued on next page

Table B1 (continued)

No.	Molecule	Transitions	Rest Freq.	$\int T_{\text{mb}} dv$	V_{lsr}	V_{exp}	T_{mb}	Notes
			(MHz)	(K km s ⁻¹)	(km s ⁻¹)	(km s ⁻¹)	(K)	
(37)	CN	$N = 1 - 0, J = 1/2 - 1/2, F = 3/2 - 1/2$	113170.528	15.80(0.783)	-25.96(0.647)	13.594(0.061)	0.679(0.027)	
(38)	CN	$N = 1 - 0, J = 1/2 - 1/2, F = 3/2 - 3/2$	113191.317	18.60(1.218)	-25.81(0.647)	13.264(0.080)	0.804(0.042)	
(39)	C ₃ N	$N = 9 - 8, J = 19/2 - 17/2$	89045.590	9.71(0.879)	-26.28(0.822)	13.807(0.049)	0.320(0.030)	
(40)	C ₃ N	$N = 9 - 8, J = 17/2 - 15/2$	89064.360	9.41(0.963)	-25.80(0.822)	13.891(0.053)	0.315(0.033)	
(41)	C ₃ N	$N = 10 - 9, J = 21/2 - 19/2$	98940.020	8.84(0.883)	-25.67(0.740)	13.734(0.049)	0.297(0.031)	
(42)	C ₃ N	$N = 10 - 9, J = 19/2 - 17/2$	98958.780	10.40(0.835)	-25.88(0.740)	13.781(0.043)	0.358(0.029)	
(43)	C ₃ N	$N = 11 - 10, J = 23/2 - 21/2$	108834.270	5.63(0.546)	-25.81(0.673)	14.027(0.049)	0.193(0.019)	
(44)	C ₃ N	$N = 11 - 10, J = 21/2 - 19/2$	108853.020	5.51(0.491)	-26.09(0.672)	14.365(0.041)	0.185(0.017)	
(45)	HC ₃ N	$J = 10 - 9$	90978.989	56.30(1.018)	-25.88(0.402)	13.854(0.014)	2.448(0.035)	
(46)	HC ₃ N	$J = 11 - 10$	100076.386	45.20(0.744)	-25.22(1.463)	13.399(0.047)	1.938(0.026)	
(47)	HC ₃ N	$J = 12 - 11$	109173.638	41.10(0.745)	-25.96(1.341)	13.435(0.047)	1.764(0.026)	
(48)	H ¹³ CCCN	$J = 10 - 9$	88166.808	2.19(0.626)	-27.68(1.660)	14.177(0.311)	0.076(0.022)	
(49)	H ¹³ CCCN	$J = 13 - 12$	114615.021	3.17(0.918)	-27.34(1.277)	14.173(0.271)	0.094(0.031)	NS
(50)	HC ¹³ CCN	$J = 10 - 9$	90593.059	×	×	×	×	B2
(51)	HCC ¹³ CN	$J = 10 - 9$	90601.791	4.56(0.551)	×	×	0.077(0.019)	B2
(52)	HC ¹³ CCN	$J = 11 - 10$	99651.863	2.55(0.435)	×	×	0.045(0.015)	B3
(53)	HCC ¹³ CN	$J = 11 - 10$	99661.471	×	×	×	×	B3
(54)	HC ¹³ CCN	$J = 12 - 11$	108710.523	2.63(0.406)	×	×	0.048(0.014)	B4
(55)	HCC ¹³ CN	$J = 12 - 11$	108721.008	×	×	×	×	B4
(56)	HC ₅ N	$J = 32 - 31$	85201.346	4.43(0.434)	-26.10(1.718)	14.345(0.130)	0.148(0.015)	
(57)	HC ₅ N	$J = 33 - 32$	87863.630	4.75(0.645)	-26.30(1.666)	14.042(0.160)	0.166(0.022)	
(58)	HC ₅ N	$J = 34 - 33$	90525.890	3.54(0.460)	-26.81(1.617)	13.911(0.156)	0.124(0.016)	
(59)	HC ₅ N	$J = 35 - 34$	93188.123	3.22(0.750)	-26.45(1.571)	13.336(0.230)	0.118(0.026)	
(60)	HC ₅ N	$J = 36 - 35$	95850.335	3.30(0.641)	-28.05(1.527)	13.111(0.181)	0.112(0.022)	
(61)	HC ₅ N	$J = 37 - 36$	98512.524	1.96(0.414)	-25.21(1.486)	13.377(0.172)	0.074(0.014)	
(62)	HC ₅ N	$J = 38 - 37$	101174.677	2.66(0.577)	-27.46(1.447)	13.756(0.232)	0.096(0.020)	
(63)	HC ₅ N	$J = 39 - 38$	103836.817	2.25(0.513)	-26.59(1.410)	13.266(0.181)	0.089(0.018)	
(64)	HC ₅ N	$J = 40 - 39$	106498.910	2.42(0.530)	-25.02(1.374)	14.428(0.288)	0.067(0.018)	
(65)	c-C ₃ H ₂	$J_{K_a, K_c} = 2_{1,2} - 1_{0,1}$	85338.906	2.97(0.509)	-25.77(1.715)	13.869(0.202)	0.099(0.018)	
(66)	HNC	$J = 1 - 0, F = 0 - 1$	90663.450	
(67)	HNC	$J = 1 - 0, F = 2 - 1$	90663.574	22.30(0.702)	-25.93(0.807)	13.740(0.019)	0.199(0.024)	1
(68)	HNC	$J = 1 - 0, F = 1 - 1$	90663.656	
(69)	HCN	$J = 1 - 0, F = 1 - 1$	88630.416	
(70)	HCN	$J = 1 - 0, F = 2 - 1$	88631.847	174(9.918)	-22.87(0.159)	16.211(0.052)	8.135(0.342)	1
(71)	HCN	$J = 1 - 0, F = 0 - 1$	88633.936	
(72)	H ¹³ CN	$J = 1 - 0, F = 1 - 1$	86338.737	
(73)	H ¹³ CN	$J = 1 - 0, F = 2 - 1$	86340.176	60.70(3.915)	-24.16(0.424)	16.925(0.055)	2.645(0.135)	1
(74)	H ¹³ CN	$J = 1 - 0, F = 0 - 1$	86342.255	
(75)	CO	$J = 1 - 0$	115271.202	228.00(2.697)	-26.02(0.159)	14.220(0.006)	9.673(0.093)	

Table B1 continued on next page

Table B1 (*continued*)

No.	Molecule	Transitions	Rest Freq.	$\int T_{\text{mb}} dv$	V_{lsr}	V_{exp}	T_{mb}	Notes
			(MHz)	(K km s $^{-1}$)	(km s $^{-1}$)	(km s $^{-1}$)	(K)	
(76)	^{13}CO	$J = 1 - 0$	110201.354	21.80(0.732)	-26.07(0.664)	14.547(0.009)	0.455(0.025)	
(77)	SiO	$J = 2 - 1, \nu = 0$	86846.995	18.20(0.921)	-25.81(0.843)	13.518(0.040)	0.722(0.032)	
(78)	^{29}SiO	$J = 2 - 1, \nu = 0$	85759.188	1.63(0.551)	-27.88(1.707)	13.460(0.047)	0.058(0.019)	
(79)	^{29}SiS	$J = 5 - 4, \nu = 0$	89103.720	1.70(0.551)	-25.84(1.643)	14.044(0.266)	0.065(0.019)	
(80)	Si^{34}S	$J = 6 - 5, \nu = 0$	105941.503	1.97(0.609)	-24.42(1.382)	14.679(0.231)	0.070(0.021)	
(81)	SiS	$J = 5 - 4, \nu = 0$	90771.561	30.40(0.725)	-25.93(0.843)	13.742(0.018)	1.102(0.025)	
(82)	SiS	$J = 6 - 5, \nu = 0$	108924.297	23.80(0.551)	-26.22(1.344)	13.466(0.043)	1.009(0.019)	
(83)	SiC $_2$	$J_{K_a, K_c} = 4_{0,4} - 3_{0,3}$	93063.639	14.30(0.986)	-26.95(0.787)	13.845(0.037)	0.501(0.034)	
(84)	SiC $_2$	$J_{K_a, K_c} = 4_{2,3} - 3_{2,2}$	94245.393	9.44(0.838)	-25.40(1.553)	13.987(0.069)	0.332(0.029)	
(85)	SiC $_2$	$J_{K_a, K_c} = 4_{2,2} - 3_{2,1}$	95579.381	10.30(0.559)	-25.98(0.153)	13.815(0.059)	0.335(0.019)	
(86)	SiC $_2$	$J_{K_a, K_c} = 5_{0,5} - 4_{0,4}$	115382.375	13.40(0.870)	-25.92(1.269)	13.855(0.029)	0.468(0.030)	
(87)	CS	$J = 2 - 1$	97980.953	61.20(4.421)	-25.85(0.187)	13.275(0.015)	2.522(0.049)	
(88)	^{13}CS	$J = 2 - 1$	92494.270	2.36(0.696)	-23.24(1.583)	13.908(0.310)	0.079(0.024)	
(89)	C^{34}S	$J = 2 - 1$	96412.950	5.46(0.638)	-25.59(1.518)	14.292(0.134)	0.197(0.022)	
(90)	C $_2$ S	$N = 8 - 7, J = 7 - 6$	93870.098	×	×	×	×	B1
(91)	C $_2$ S	$N = 9 - 8, J = 8 - 7$	106347.740	1.94(0.405)	-27.16(1.376)	13.352(0.253)	0.070(0.014)	
(92)	C $_3$ S	$J = 18 - 17$	104048.451	1.71(0.535)	-23.46(1.759)	13.553(0.394)	0.057(0.018)	
(93)	MgNC	$N = 9 - 8, J = 19/2 - 17/2$	107399.420	1.67(0.609)	-25.97(0.682)	14.001(0.230)	0.064(0.021)	
(94)	CH $_3$ CN	$J_K = 6_2 - 5_2, F = 7 - 6$	110375.049	2.01(0.783)	0.081(0.026)	1
(95)	CH $_3$ CN	$J_K = 6_1 - 5_1, F = 7 - 6$	110381.400	
(96)	CH $_3$ CN	$J_K = 6_0 - 5_0, F = 7 - 6$	110383.518	

NOTE—The numbers in parentheses represent the 1σ error. The rms noise on a main beam brightness temperature scale is obtained by statistics in areas without clear spectral lines, and the measurement uncertainty of the integrated intensities is the product of the rms noise and the width of the line, about 29 km s $^{-1}$. The error in the expansion velocity is obtained by shell function fitting, and the error in the LSR velocity is the velocity width of a channel. The information for each column in the table is as follows, Col. (1) : Number; Col. (2) : Molecule name; Col. (3) : Quantum numbers; Col. (4) : Rest frequency (Rest frequency are adopted from JPL (Pickett et al. 1998), CDMS (Müller et al. 2005), and splatalogue databases as well as the online Lovas line list (Lovas 2004) for astronomical spectroscopy.); Col. (5) : Integrated intensity (in main beam brightness temperature); Col. (6) : LSR velocity; Col. (7) : Expansion velocity; Col. (8) : Main beam brightness temperature. ... means the values cannot be obtained because of unresolved hyperfine structure, × implies that the values cannot be obtained due to two blended spin-rotation components. * addresses values that cannot be derived from our detection. (1) The hyperfine structure is not resolved. (B1) $^2\Pi_{1/2}$ C $_4$ H $J = 19/2 - 17/2, \nu 7 = 1f$ blended with C $_2$ S $N = 8 - 7, J = 7 - 6$. (B2) HC 13 CCN $J = 10 - 9$ is blend with HCC 13 CN $J = 10 - 9$. (B3) HC 13 CCN $J = 11 - 10$ is blended with HCC 13 CN $J = 11 - 10$. (B4) HC 13 CCN $J = 12 - 11$ is blended with HCC 13 CN $J = 12 - 11$. (NS) Transitions that are detected for the first time toward the source are marked with “NS”.

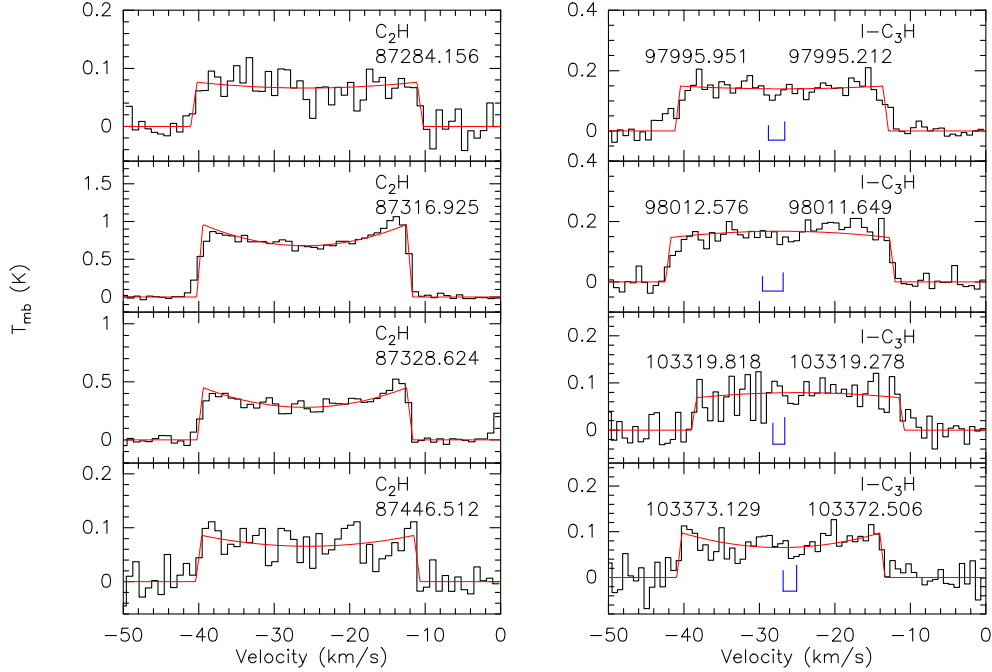


Figure C1. Same as Figure 2 but for C_2H and $l-C_3H$. The solid blue line indicates the hyperfine structure components of the molecule. The rest frequencies in MHz are shown in each panel’s upper right corner for single, and in the upper left and right corners for lines with two fine structure components.

C. SPECTRAL LINE PROFILES OF THE DETECTED SPECIES

In this appendix, we give all the observed spectral profiles of the identified species in Figs. C1 – C10. Note that we have fitted each spectrum by one of the four line profiles shown in Figure 2.

D. DETECTED SPECIES

A detailed description of the detected molecules, together with their previous observations, is provided in this appendix.

C_2H . The ethynyl radical C_2H was first detected and identified by Tucker et al. (1974) in several galactic sources, including IRC+10216. In this source, the $N = 1 - 0$ to $N = 4 - 3$ and $N = 6 - 5$ to $N = 9 - 8$ transitions of C_2H have been reported by De Beck et al. (2012). We detected the two spin-rotation fine structure components of C_2H $N = 1 - 0$ ($J = 3/2 - 1/2$ and $J = 1/2 - 1/2$) in which the nuclear spin of hydrogen further causes the spin-rotation to split into six hyperfine components: ($J = 3/2 - 1/2$, $F = 1 - 1$), ($J = 3/2 - 1/2$, $F = 2 - 1$), ($J = 3/2 - 1/2$, $F = 1 - 0$), ($J = 1/2 - 1/2$, $F = 1 - 1$ and $F = 0 - 1$) and ($J = 1/2 - 1/2$, $F = 1 - 0$). Among these components, C_2H ($J = 1/2 - 1/2$, $F = 1 - 1$) is blended with C_2H ($J = 1/2 - 1/2$, $F = 0 - 1$), producing two blended U-shaped spectral lines with the overlapping part showing stronger intensity than both sides. The transitions are presented in the left panel of Figure C1 and the top left panel of Figure C3. These spectral lines have also been detected by Johansson et al. (1984), Truong-Bach et al. (1987), and Kahane et al. (1988).

$l-C_3H$. The linear propynylidyne radical $l-C_3H$ was initially identified by Thaddeus et al. (1985a) in IRC+10216 and TMC-1. Interestingly, Johansson et al. (1984) had previously detected $l-C_3H$ at frequencies of 76202, 97995, and 98011 MHz, but had classified these spectral lines as U-lines and presumptively attributed them to transitions of $l-C_3H$. The $J = 3/2 - 1/2$, $J = 13/2 - 11/2$ and $J = 21/2 - 19/2$ transitions of this molecule have also been detected in other line surveys in this source (Kawaguchi et al. 1995; He et al. 2008). The right panel of Figure C1 shows eight hyperfine components that we have identified from the $l-C_3H$ rotational lines ${}^2\Pi_{1/2}$ $J = 9/2 - 7/2$ ($F = 5 - 4e$, $F = 4 - 3e$, $F = 5 - 4f$, $F = 4 - 3f$) and ${}^2\Pi_{3/2}$ $J = 9/2 - 7/2$ ($F = 5 - 4f$, $F = 4 - 3f$, $F = 5 - 4e$, $F = 4 - 3e$). These transitions have been previously reported by Thaddeus et al. (1985a), Yamamoto et al. (1987), and Nyman et al. (1993).

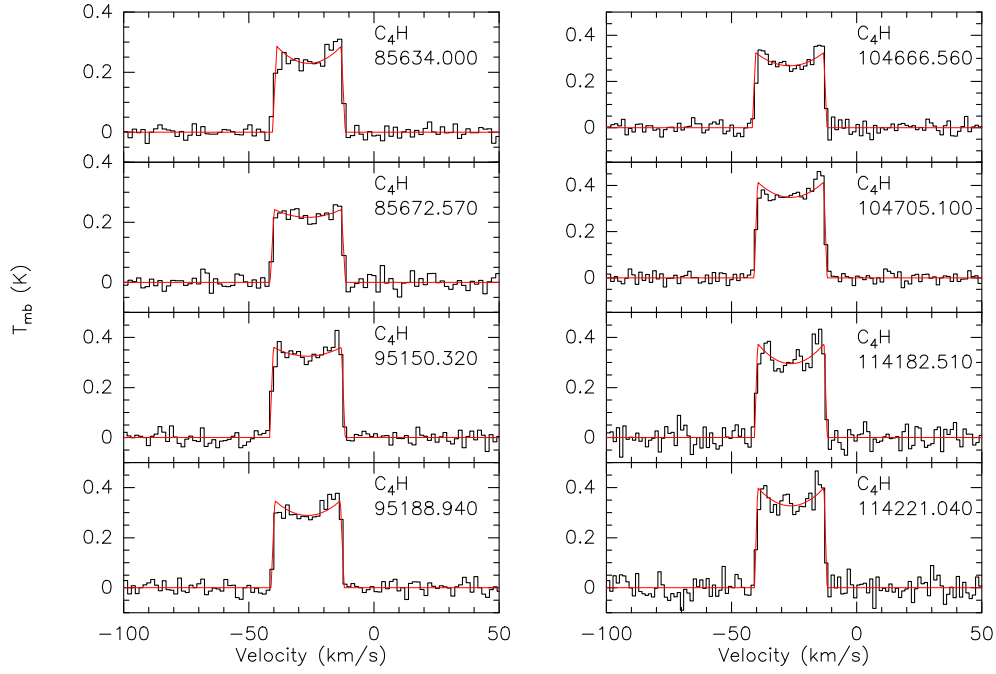


Figure C2. Same as Figure 2 but for C_4H .

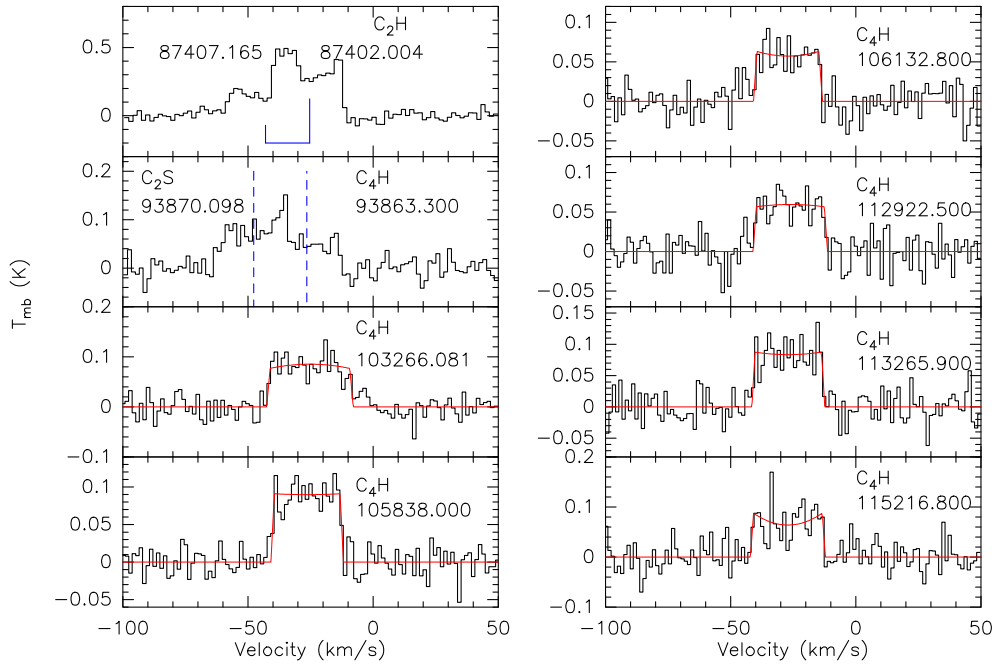


Figure C3. Same as Figure 2 and Figure C1 but for C_2H , C_4H ($\nu = 1$), C_2S , and CN . The blue dashed lines are the blended spectral lines.

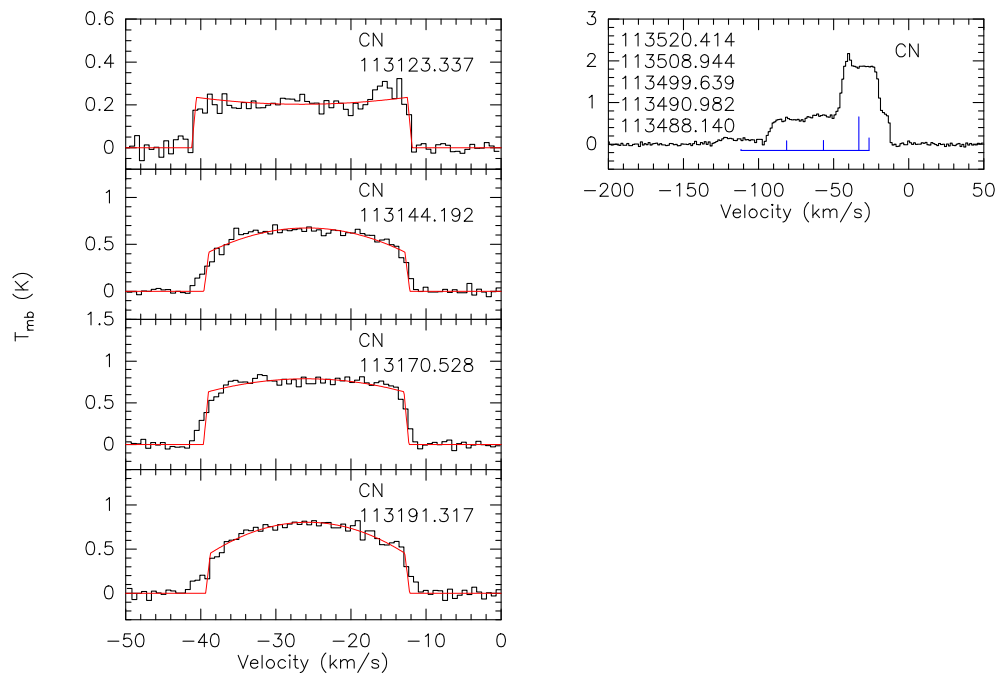


Figure C4. Same as Figure 2 and Figure C1 but for CN. The rest frequencies in MHz of spectral lines of more than two fine structure components are displayed in the upper left corner of each panel.

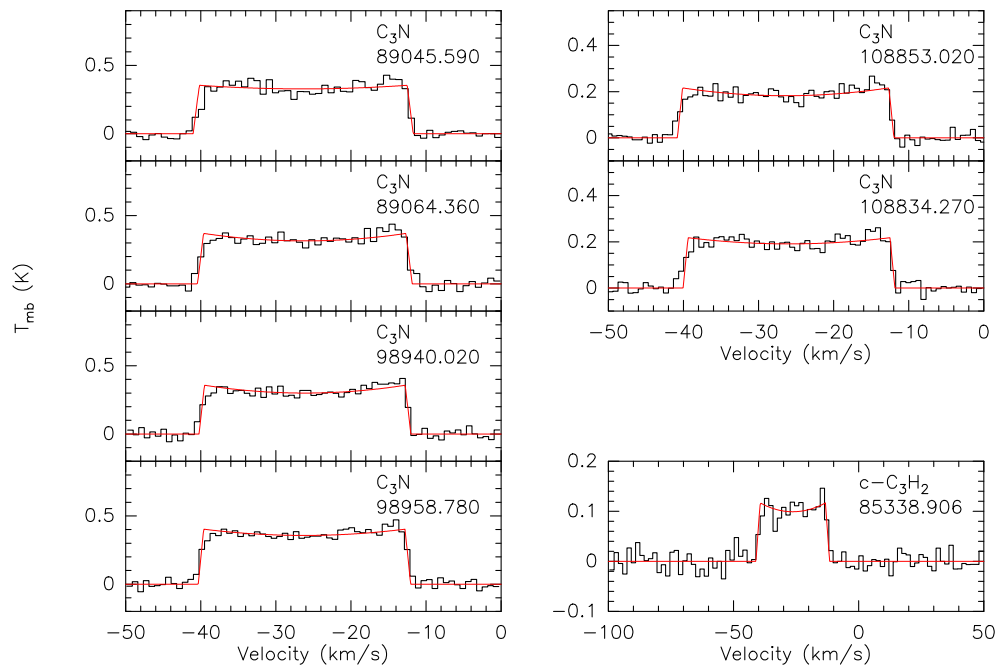


Figure C5. Same as Figure 2 but for C_3N and $c-C_3H_2$.

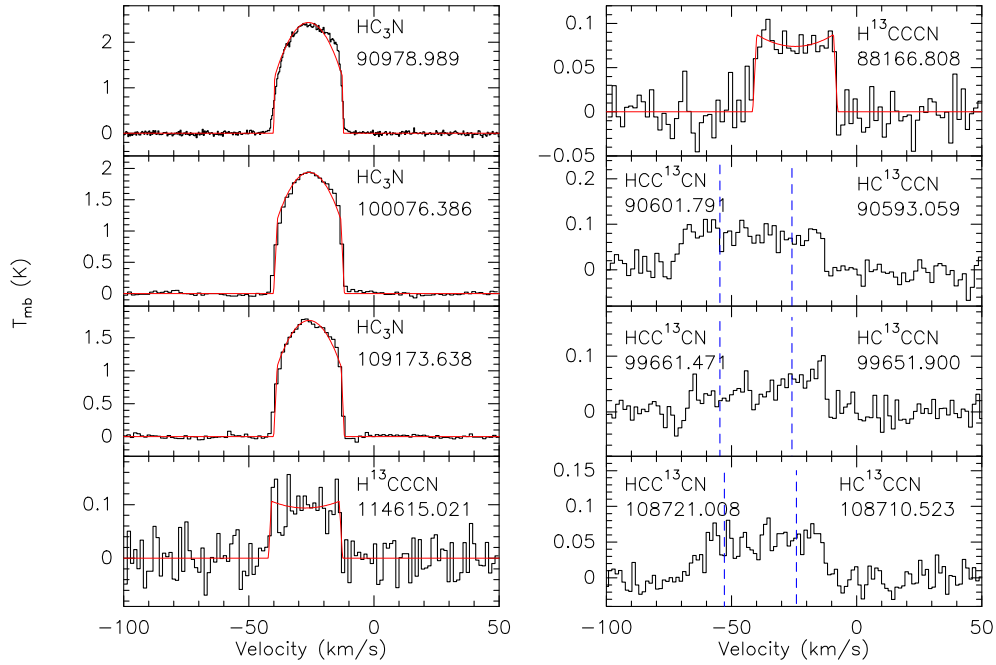


Figure C6. Same as Figure 2 and Figure C3 but for HC_3N , and its isotopologues.

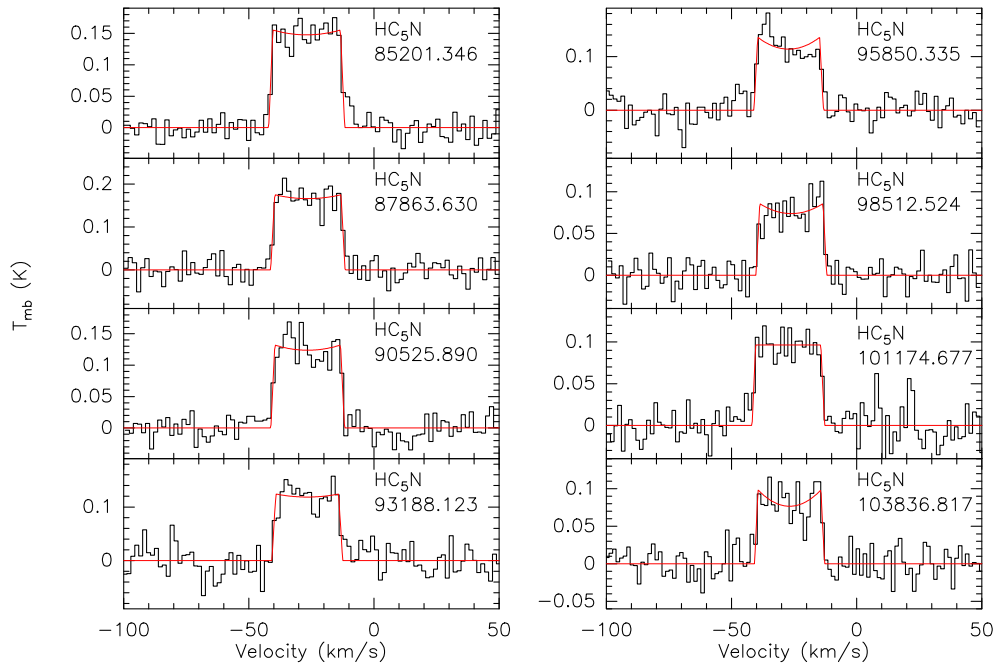


Figure C7. Same as Figure 2 but for HC_5N .

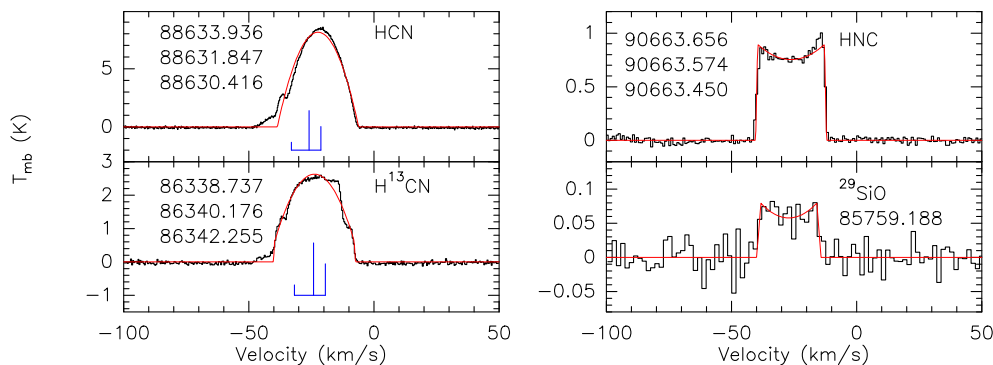


Figure C8. Same as Figure 2 and Figure C1 but for HCN, H¹³CN, HNC, and ²⁹SiO.

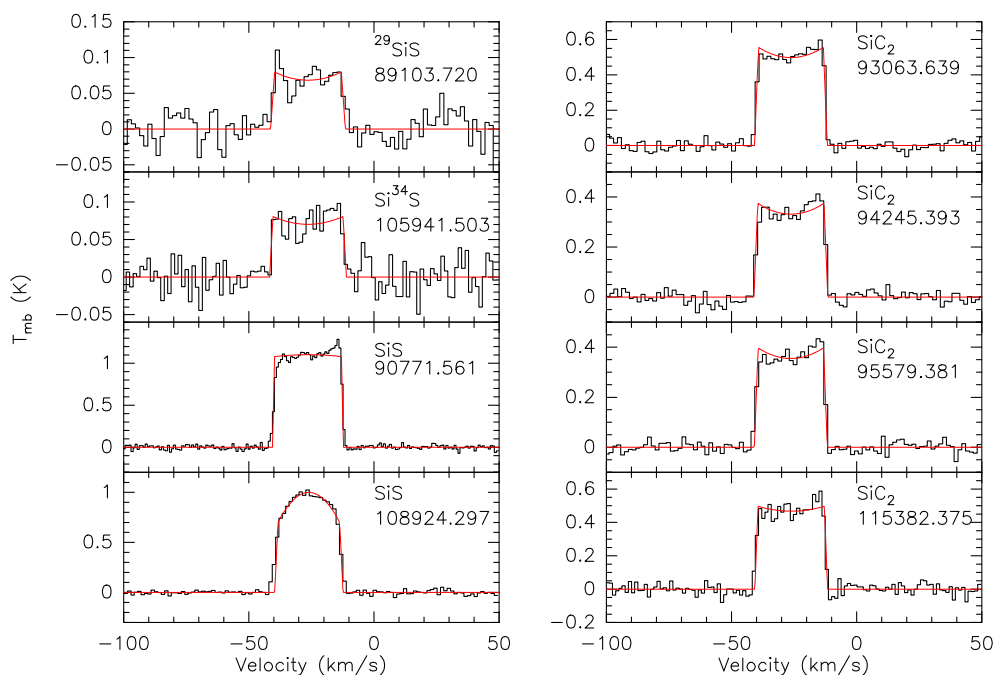


Figure C9. Same as Figure 2 but for SiS, ²⁹SiS, Si³⁴S, and SiC₂.

C₄H. The butadiynyl radical C₄H ($\nu = 0$) was first identified by Guélin et al. (1978) in the CSE of IRC +10216. Yamamoto et al. (1987) subsequently confirmed the transitions of C₄H in the CSE of IRC +10216 caused by the ²Π_{1/2}, ²Π_{3/2}, and Δ states through the use of experimental microwave spectroscopy. Further, other transitions of C₄H have also been detected in this source such as $N = 2 - 1$, $N = 3 - 2$ through $N = 5 - 4$, $N = 8 - 7$, $N = 14 - 13$ through $N = 16 - 15$ and $N = 24 - 23$ through $N = 28 - 27$ (Johansson et al. 1984; Kawaguchi et al. 1995; He et al. 2008; Gong et al. 2015). A total of 15 transitions of C₄H have been detected in our work. There are four rotational transitions ($N = 9 - 8$ through $N = 12 - 11$) of C₄H ($\nu = 0$), each of these rotational transitions is split into spin-rotation doublets due to fine-structure, and these are presented in Figure C2. Additionally, seven transitions of C₄H ($\nu = 1$) are shown in Figure C3. However, the ²Π_{1/2} C₄H $J = 19/2 - 17/2$, $\nu 7 = 1f$ line (93863.300 MHz) is blended with C₂S $N = 8 - 7$, $J = 7 - 6$ (93870.098 MHz), as shown in the second figure on the left panel of Figure C3.

CN. The rotational emission from the cyanide radical CN was first detected by Jefferts et al. (1970a) toward W 51. Subsequently, the $N = 1 - 0$ transition of this molecule was also detected in IRC +10216 (Wilson et al. 1971). Further

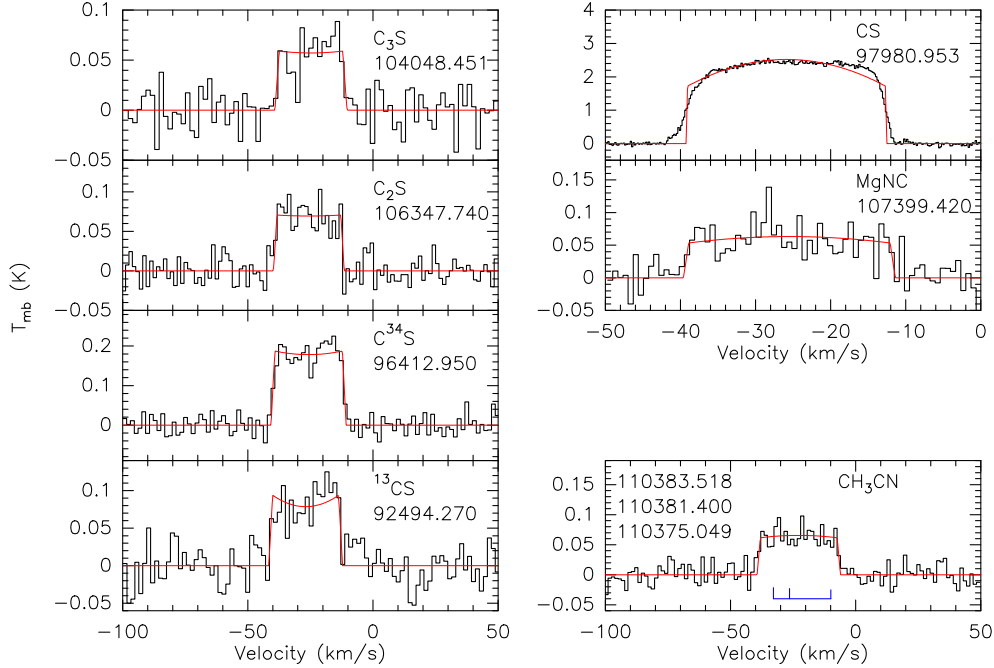


Figure C10. Same as Figure 2 and Figure C1 but for CS, ^{13}CS , C^{34}S , C_2S , C_3S , MgNC, and CH_3CN .

transitions such as $N = 2 - 1$ and $N = 3 - 2$ of CN were also detected in this source by Avery et al. (1992). We have detected the two spin-rotation fine structure lines of CN $N = 1 - 0$ ($J = 3/2 - 1/2$ and $J = 1/2 - 1/2$), which are then further split into nine hyper-fine components due to the nuclear spin of nitrogen. These components include $J = 3/2 - 1/2$ ($F = 3/2 - 1/2$, $F = 5/2 - 3/2$, $F = 1/2 - 1/2$, $F = 3/2 - 3/2$, $F = 1/2 - 3/2$) and $J = 1/2 - 1/2$ ($F = 1/2 - 1/2$, $F = 1/2 - 3/2$, $F = 3/2 - 1/2$, $F = 3/2 - 3/2$). The spectral line profiles are shown in Figure C4, although we note that the five hyper-fine lines of CN $N = 1 - 0$, $J = 3/2 - 1/2$ are blended.

C_3N . Guélin & Thaddeus (1977) detected a new molecule toward the CSE of IRC+10216, identifying it as the cyanoethynyl radical C_3N based on theoretical considerations. The $N = 2 - 1$, $N = 3 - 2$ through $N = 5 - 4$, $N = 8 - 7$ through $N = 11 - 10$, $N = 13 - 12$, $N = 14 - 13$ through $N = 17 - 16$, $N = 23 - 22$, $N = 24 - 23$, and $N = 27 - 26$ transition lines of C_3N in this source have been reported (Guélin & Thaddeus 1977; Johansson et al. 1984; Henkel et al. 1985; Kawaguchi et al. 1995; Cernicharo et al. 2000; He et al. 2008; Thaddeus et al. 2008; Gong et al. 2015). A total of six fine-structure lines of C_3N have been detected in our work, and displayed in Figure C5. These lines derive from three rotational transitions ($N = 9 - 8$ through $N = 11 - 10$) of C_3N . All of the detected rotational transition lines are split into spin-rotation doublets due to the interactions of fine structure.

$c\text{-C}_3\text{H}_2$. A strong unidentified line at 85.339 GHz was first detected by Thaddeus et al. (1981) toward Ori A, Sgr B2 (OH), and TMC-1. This line was subsequently identified as cyclopropenylidene $c\text{-C}_3\text{H}_2$ by Thaddeus et al. (1985b). The rotational transitions of $c\text{-C}_3\text{H}_2$ have also been detected in other spectral line surveys of this source (Kawaguchi et al. 1995; Cernicharo et al. 2000; He et al. 2008; Gong et al. 2015; Zhang et al. 2017). In our work, we have detected one transition of $c\text{-C}_3\text{H}_2$, shown at the bottom of the right panel in Figure C5.

HC_3N . Cyanoacetylene HC_3N was detected by Turner (1970) and Turner (1971) toward Sgr B2. Morris et al. (1975) also detected this molecule in IRC+10216 using the NRAO-11 m telescope. Various transitions of HC_3N and its isotopologues have been reported in this source. For instance, the $J = 2 - 1$ transitions of HC_3N , H^{13}CCCN , HC^{13}CCN and HCC^{13}CN were detected by Zhang et al. (2017), the $J = 4 - 3$ and $J = 5 - 4$ transitions of HC_3N and its isotope were detected by Kawaguchi et al. (1995) and the $J = 9 - 8$ and $J = 10 - 9$ transitions of HC_3N and its isotope were detected by Johansson et al. (1984). Nyman et al. (1993) detected HC_3N $J = 10 - 9$ and $J = 12 - 11$ in this source, as well as HC^{13}CCN and HCC^{13}CN . We detected three lines ($J = 10 - 9$ through $J = 12 - 11$) of HC_3N and two relatively weak isotopic lines (H^{13}CCCN $J = 10 - 9$ and H^{13}CCCN $J = 13 - 12$). We also detected three transitions of HC^{13}CCN ($J = 10 - 9$ through $J = 12 - 11$) and three transitions of HCC^{13}CN ($J = 10 - 9$

through $J = 12 - 11$), but all detected HC^{13}CCN lines are blended with HCC^{13}CN transitions. These lines are shown in Figure C6. To our knowledge, the $J = 13 - 12$ transition of H^{13}CCCN is detected in IRC +10216 for the first time.

HC₅N. Cyanodiacetylene HC_5N is a linear molecule, which was observed in Sgr B2 by Avery et al. (1976). In IRC +10216, Winnewisser & Walmsley (1978) confirmed the HC_5N transition reported by Churchwell et al. (1978). The $J = 2 - 1$, $J = 5 - 4$ to $J = 9 - 8$, $J = 28 - 27$ to $J = 40 - 39$ and $J = 49 - 48$ to $J = 54 - 53$ transitions of HC_5N have been detected in IRC +10216 (Johansson et al. 1984; Cernicharo et al. 1986b, 2000; Araya et al. 2003; Gong et al. 2015; Agúndez et al. 2017; Zhang et al. 2017). We have detected nine rotational transition lines of HC_5N from $J = 32 - 31$ to $J = 40 - 39$. These lines are shown in Figure 2 and Figure C7.

HCN. Hydrogen cyanide HCN was first detected in W49, W51, W3 (OH), Orion A, DR 21 (OH) and Sgr A (NH_3A) (Howard et al. 1970; Snyder & Buhl 1971). HCN has been detected in IRC +10216 by Morris et al. (1971). The transitions of $J = 2 - 1$ (Menten et al. 2018), $J = 3 - 2$ and $J = 4 - 3$ (Avery et al. 1992) of HCN , and the $J = 1 - 0$, $J = 3 - 2$, $J = 4 - 3$, and $J = 8 - 7$ transitions of H^{13}CN (Schöier et al. 2007) have been detected as well. The $J = 1 - 0$ transitions from HCN and H^{13}CN were detected in our line survey. The $\text{HCN } J = 1 - 0$ transition contains hyperfine structure, the frequency intervals between the individual features are too small (Olofsson et al. 1982) causing us to detect both absorption and emission in the line profile in Figure C8 (see also Dayal & Biegging 1995).

HNC. An unidentified emission line at 89.190 GHz was detected by Buhl & Snyder (1970) in W3 (OH), Orion, L134, Sgr A (NH_3A) and W 51, first attributed by Snyder & Buhl (1972) to the $J = 1 - 0$ transition of hydrogen isocyanide HNC . Brown et al. (1976) reported that HNC had been detected in IRC +10216. Using the IRAM-30 m telescope and the HIFI instrument onboard the Herschel Space Observatory, the transitions of $\text{HNC } J = 3 - 2$, $J = 1 - 0$ and $J = 6 - 5$ through $J = 12 - 11$ were detected in IRC +10216 (Daniel et al. 2012). In our work, we detected the $J = 1 - 0$ transition from HNC , as shown in Figure C8. Although $\text{HNC } J = 1 - 0$ contains hyper-fine structures, the frequency interval between these structures is too small to detect in IRC +10216 (Olofsson et al. 1982).

CO. Carbon monoxide CO at 115 GHz was observed by Jefferts et al. (1970b) in at least five galactic sources, including Orion A, Sgr A, Sgr B2, W39, and W51. Subsequently, CO was also observed in IRC +10216 (Solomon et al. 1971). Other transitions of CO and ^{13}CO in IRC +10216 had also been reported (Avery et al. 1992; Cernicharo et al. 2015a). In our work, we have detected the $J = 1 - 0$ transitions from CO and ^{13}CO , as shown in Figure 2.

SiO. The $J = 3 - 2$ transition of silicon monoxide SiO was detected in Sgr B2 by Wilson et al. (1971). Subsequently, Morris et al. (1975) observed the $J = 2 - 1$ transition of SiO in the CSE of IRC +10216. The transitions observed by previous research include $J = 1 - 0$ through $J = 8 - 7$ (Avery et al. 1992; Kawaguchi et al. 1995; Cernicharo et al. 2000; He et al. 2008; Tenenbaum et al. 2010b; Agúndez et al. 2012). In our study, we detected the $J = 2 - 1$ rotational transitions of SiO and ^{29}SiO , and their line profiles are illustrated in Figure 2 and Figure C8.

SiS. Silicon monosulfide SiS was first detected by Morris et al. (1975) toward IRC +10216. The maser and quasi-thermal emission of the $\text{SiS } J = 1 - 0$, and $J = 2 - 1$ lines in the CSE of IRC +10216 have been studied by Gong et al. (2017). The transitions of SiS and ^{29}SiS observed by Agúndez et al. (2012) include $J = 5 - 4$, $J = 6 - 5$ and $J = 8 - 7$ through $J = 19 - 18$. Among them, the $J = 11 - 10$, $J = 14 - 13$, and $J = 15 - 14$ transitions are masers, which was also reported by Fonfría Expósito et al. (2006) and Fonfría et al. (2018). The $J = 5 - 4$, $J = 6 - 5$ and $J = 8 - 7$ through $J = 20 - 19$ from Si^{34}S were also detected by Agúndez et al. (2012). We have detected the $J = 5 - 4$ and $J = 6 - 5$ lines from SiS , as well as the $J = 5 - 4$ transitions from ^{29}SiS and the $J = 6 - 5$ line from Si^{34}S . The line profiles are presented in Figure C9.

SiC₂. Silacyclopropylylidene, SiC_2 , was the first ring molecule identified in an astronomical source. Its millimeter- and centimeter-wave transitions were identified by Thaddeus et al. (1984) and Snyder et al. (1985), respectively, in the CSE of IRC +10216. High resolution spectra (channel width 195 kHz) of SiC_2 at 70–350 GHz (Cernicharo et al. 2018), 554.5–636.5 GHz (Cernicharo et al. 2010b) and the spatial distribution of SiC_2 in IRC +10216 (Fonfría et al. 2014; Velilla Prieto et al. 2015; Velilla-Prieto et al. 2019) have also been reported. We have detected the $J_{K_a, K_c} = 4_{0,4}-3_{0,3}$, $J_{K_a, K_c} = 4_{2,3}-3_{2,2}$, $J_{K_a, K_c} = 4_{2,2}-3_{2,1}$, and $J_{K_a, K_c} = 5_{0,5}-4_{0,4}$ transitions of SiC_2 , and the line profiles are shown in Figure C9.

CS. The $J = 3 - 2$ transition of carbon monosulfide CS was detected in IRC +10216, Orion A, W51 and DR 21 by Penzias et al. (1971). The transitions of $J = 1 - 0$ through $J = 7 - 6$ from CS and the transitions of $J = 1 - 0$ through $J = 3 - 2$ and $J = 5 - 4$ through $J = 7 - 6$ from ^{13}CS and C^{34}S in the CSE of IRC +10216 have also been extensively reported (Johansson et al. 1984; Avery et al. 1992; Lucas et al. 1995; Kawaguchi et al. 1995; He et al. 2008; Agúndez et al. 2012; Velilla-Prieto et al. 2019). We detected strong $\text{CS } J = 2 - 1$ emission and its isotopic lines, $^{13}\text{CS } J = 2 - 1$ and $\text{C}^{34}\text{S } J = 2 - 1$. The line profiles of CS , ^{13}CS and C^{34}S are depicted in Figure C10.

C₂S. An unknown interstellar line at 45.379 GHz from Sgr B2, TMC-1, TMC-1 (NH₃), and TMC2 was detected by Suzuki et al. (1984). Kaifu et al. (1987) detected seven unknown strong lines in the frequency regions of 22–24 and 36–50 GHz from TMC-1. The four unknown lines at 45.379, 43.981, 38.866 and 22.344 GHz were identified to trace the linear C₂S radical (Saito et al. 1987). Twelve spectral lines of C₂S in the frequency range of 81–157 GHz have also been detected by Cernicharo et al. (1987a) towards IRC +10216. In our work, we have detected two transitions of C₂S, $N = 9 - 8$, $J = 8 - 7$ and $N = 8 - 7$, $J = 7 - 6$, but the transition of C₂S $N = 8 - 7$, $J = 7 - 6$ is blended with the $^2\Pi_{1/2}$ C₄H $\nu_7 = 1$ f line. The second figure in the left panel of Figure C3 shows the C₂S spectral line blended with C₄H. Figure C10 shows a single C₂S spectral line.

C₃S. Kaifu et al. (1987) detected seven unknown strong lines in the frequency regions of 22–24 and 36–50 GHz from TMC-1, of which three were identified as linear C₃S radicals at 3.123, 40.465, and 46.246 GHz by Yamamoto et al. (1987). Meanwhile, Cernicharo et al. (1987a) used the IRAM 30 m telescope to detect 11 transition lines of C₃S between 75 and 168 GHz in IRC +10216. Only one transition line of C₃S $J = 18 - 17$ was detected in our work, and the spectral line is shown in Figure C10.

MgNC. Guélin et al. (1986) observed six unidentified spectral lines in IRC +10216 with the IRAM–30 m telescope, and they considered that these molecules were likely to be HSiCC (or its isomer HCCSi) or HSCC. Subsequently, Kawaguchi et al. (1993) detected linear MgNC radicals for the first time using microwave spectroscopy in the laboratory, and they confirmed that these unrecognized lines were linear MgNC free radicals. The $N = 2 - 1$ through $N = 4 - 3$ rotational transitions, as well as the rotational transitions of $N = 12 - 11$ and $N = 13 - 12$ of MgNC in the CSE of IRC +10216 have been observed by Kawaguchi et al. (1995), He et al. (2008), and Gong et al. (2015). In our work, we only detected the $N = 8 - 7$ $J = 19/2 - 17/2$ rotational transition of MgNC, which is displayed in the second sub-picture of the right panel of Figure C10.

CH₃CN. Methyl cyanide CH₃CN has been detected by Solomon et al. (1971) in Sgr B and Sgr A. Johansson et al. (1984) detected CH₃CN, the first species containing the methyl group, in IRC +10216. In this source, the $J = 2 - 1$ transitions in the $K = 0$ and $K = 1$ states of CH₃CN were detected by Kawaguchi et al. (1995). The $J = 8 - 7$, $J = 12 - 11$ and $J = 13 - 12$ transitions in the $K = 0, 1, 2, 3$ states and the $J = 14 - 13$ transitions in the $K = 0$ and $K = 1$ states of CH₃CN were detected by He et al. (2008). Other higher J lines of CH₃CN in the frequency range 293.9 – 354.8 GHz were observed by Patel et al. (2011). We only detected the $J = 6 - 5$ transitions in the $K = 0$, $K = 1$, and $K = 2$ states of CH₃CN and these blended emission lines are shown in the last sub-picture on the right panel of Figure C10.

E. ROTATIONAL DIAGRAMS FOR THE IDENTIFIED SPECIES

The rotational diagrams for the identified species from this survey are shown in Figs. E1 – E5.

F. MULTI-COMPONENTS OF THE CSE SPECIES

Both HC₃N and HC₅N in the CSE of IRC +10216 have two temperature components, tracing a warm region probed by high energy rotational lines and a cooler region probed by low energy lines. Bell et al. (1992b) find that HC₃N has a cold component with $T_{\text{ex}} = 12.7 \pm 1$ K, $N = (7.9 \pm 0.2) \times 10^{14} \text{ cm}^{-2}$, and a warm component with $T_{\text{ex}} = 48 \pm 6$ K, and $N = (2.1 \pm 1.4) \times 10^{14} \text{ cm}^{-2}$. Meanwhile, they find that HC₅N has a cold component with $T_{\text{ex}} \sim 13$ K and $N = 3.2 \times 10^{14} \text{ cm}^{-2}$ and a warm component with $T_{\text{ex}} \sim 25$ K and $N = 3.7 \times 10^{14} \text{ cm}^{-2}$. Zhang et al. (2017) also compared the excitation temperatures of HC₅N, HC₇N, and HC₉N at different frequency ranges and find that the excitation temperature obtained by fitting the high rotation transition of these molecules was correspondingly higher, indicating that the high rotational transitions of these molecules in the CSE of IRC +10216 trace the warm inner molecular region. We also compare the excitation temperatures of HC₃N and HC₅N at different upper-state energy levels. Our results show that the excitation temperatures gradually increase with higher excited rotational transitions.

In Figures F1 and F2, we compare the excitation temperatures obtained from different upper-state energy levels. For HC₃N, the ratios of these are estimated to be scaled as: HC₃N ($E_u/k < 10$ K) : HC₃N ($20 \text{ K} < E_u/k < 35$ K) : HC₃N ($50 \text{ K} < E_u/k < 80$ K) : HC₃N ($E_u/k > 140$ K) = 1 : 1.7 : 3.4 : 5.9. The excitation temperatures of HC₅N are estimated to be scaled as: HC₅N ($E_u/k < 3$ K) : HC₅N ($3 \text{ K} < E_u/k < 6$ K) : HC₅N ($8 \text{ K} < E_u/k < 25$ K) : HC₅N ($60 \text{ K} < E_u/k < 105$ K) : HC₅N ($E_u/k > 150$ K) = 1 : 2.8 : 5.2 : 6.5 : 10.4. This indicates that the high-J transitions of the HC₃N molecules in the CSE of IRC +10216 also trace the warmer molecular regions.

Bell et al. (1993) find that C₃S also has at least two excitation temperature components, of which the excitation temperature of the low energy part is about 17 K and that of the high energy part is about 47 K. We also compare

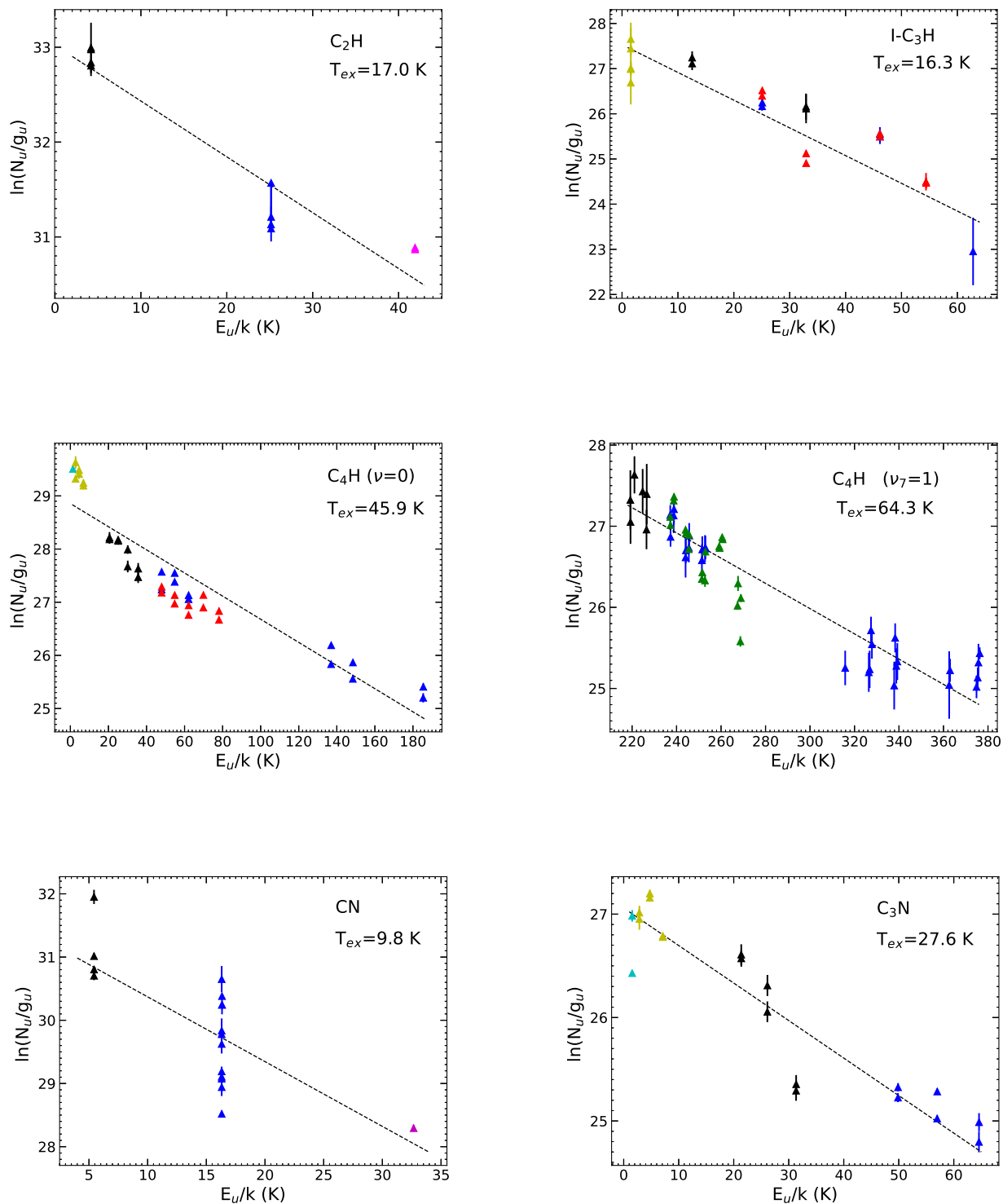


Figure E1. Rotational diagrams for the identified molecules in IRC+10216 in the λ 3 mm wavelength band. The results obtained from the linear least-squares fitting are plotted in black dashed lines. The adopted data points with error bars are from our PMO-13.7 m observations (black triangles), He et al. (2008) (blue triangles), Gong et al. (2015) (cyan triangles), Zhang et al. (2017) (dark-orange triangles), Kawaguchi et al. (1995) (yellow-green triangles), Cernicharo et al. (2000) (red triangles), Agúndez et al. (2012) (green triangles), and Groesbeck et al. (1994) (magenta triangles), respectively. Note that the error bars are invisible if their values are smaller than the adopted data points.

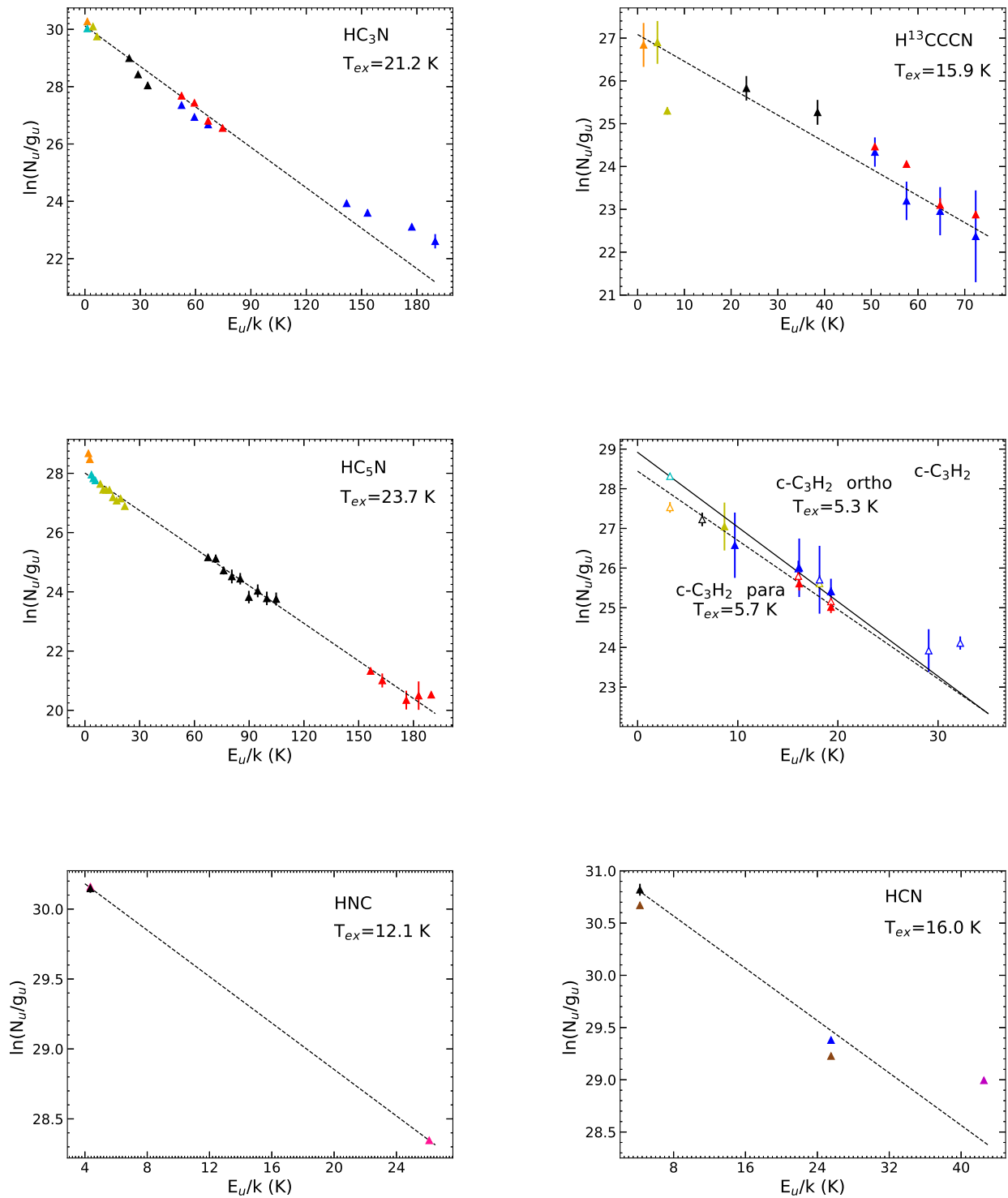


Figure E2. Same as Figure E1, but for different molecular species. Note, molecular c -C₃H₂ is separated into ortho (open triangles) and para (filled triangles) states and fitted in solid (ortho) and dotted (para) lines. The data in saddle-brown triangles with error bars are obtained from Nyman et al. (1993).

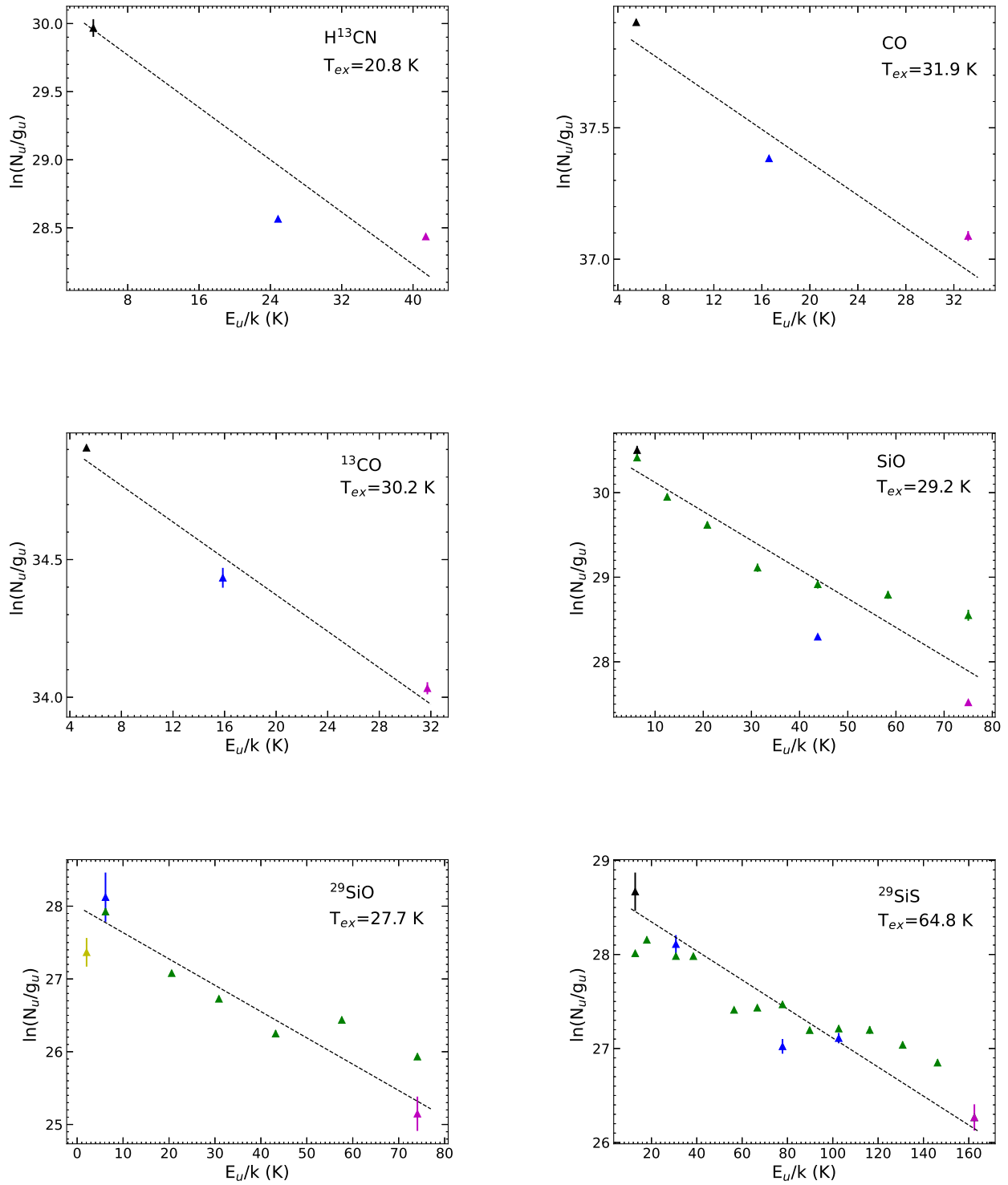


Figure E3. Same as Figure E1.

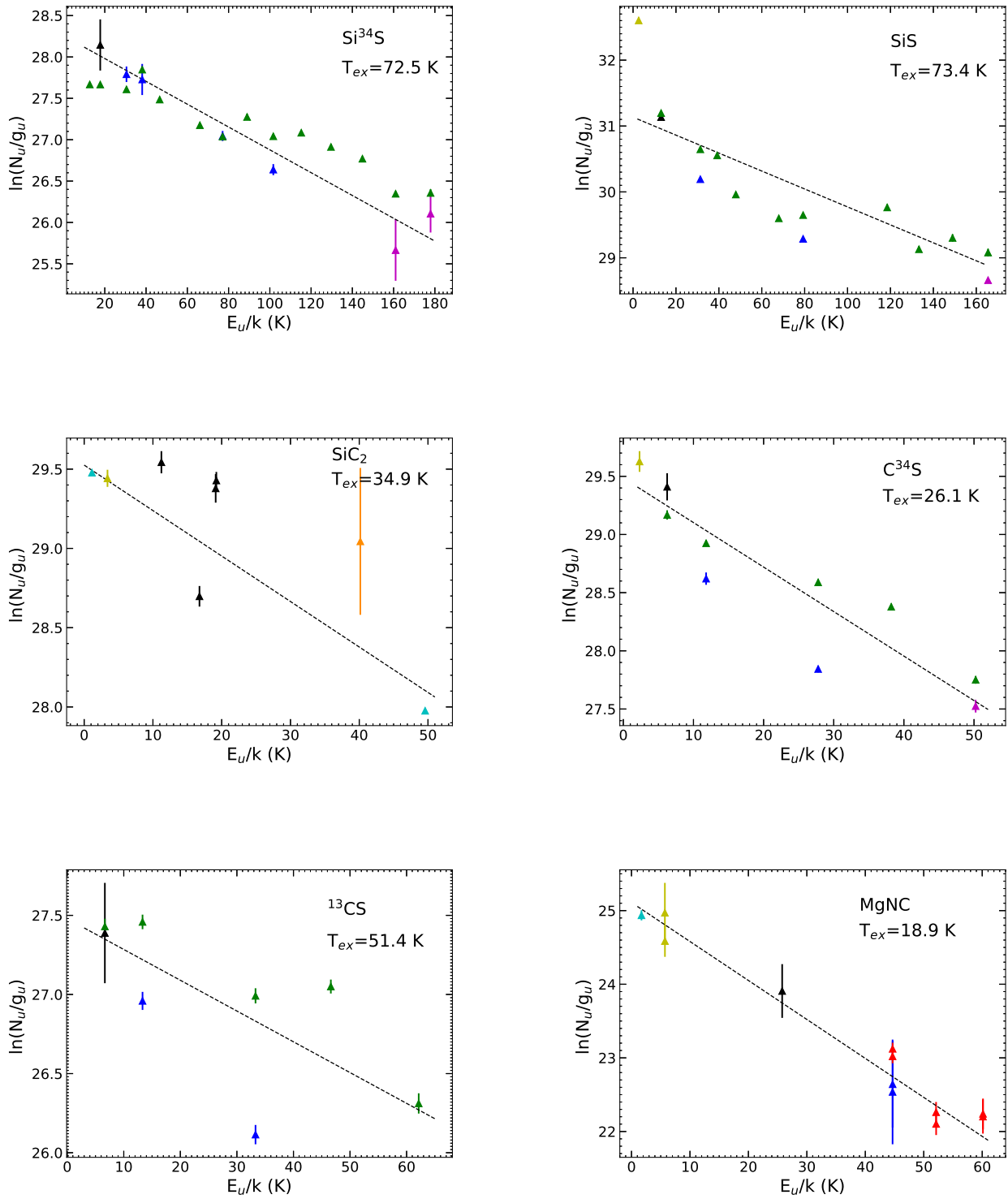


Figure E4. Same as Figure E1.

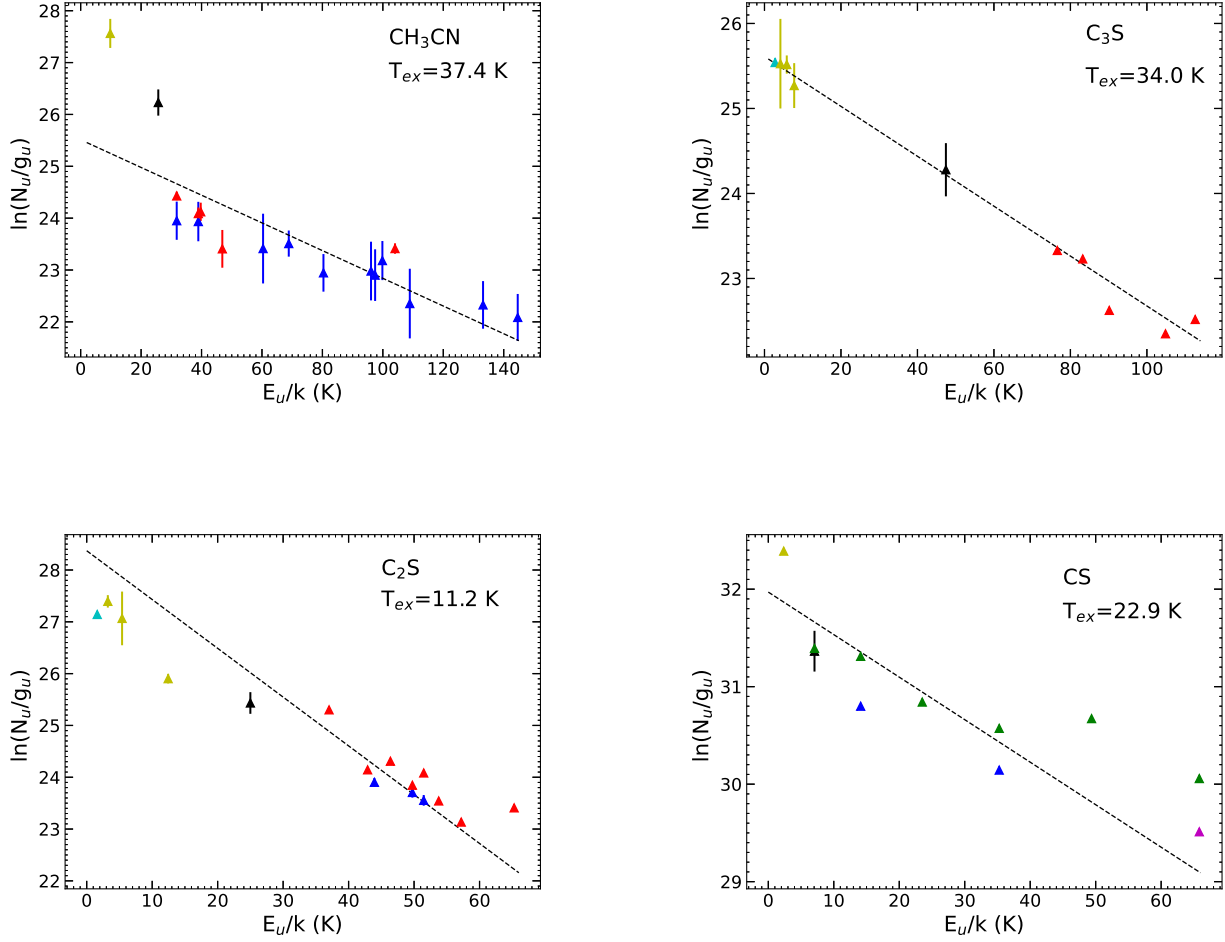


Figure E5. Same as Figure E1.

the excitation temperature of C_3S at different upper-state energies. When E_u/k is less than 10 K, the excitation temperature is 15.4 K, and when E_u/k is greater than 40 K, the excitation temperature is 34.1 K.

Our analysis using the rotational diagram method shows that C_4H ($\nu = 0$), C_4H ($\nu = 1$), CH_3CN and SiS also have different excitation temperature components. Therefore, we also compared the excitation temperatures of these molecules at different upper-state energies. For CH_3CN , the scaled ratios are estimated to be $CH_3CN (E_u/k < 30 \text{ K}) : CH_3CN (30 \text{ K} < E_u/k < 50 \text{ K}) : CH_3CN (E_u/k > 50 \text{ K}) = 1 : 1.4 : 3.5$. For SiS , these are estimated to be $SiS (E_u/k < 15 \text{ K}) : SiS (20 \text{ K} < E_u/k < 80 \text{ K}) : SiS (E_u/k > 115 \text{ K}) = 1 : 6.1 : 10.5$. For C_4H ($\nu = 0$), these are estimated to be $C_4H (E_u/k < 10 \text{ K}) : C_4H (20 \text{ K} < E_u/k < 40 \text{ K}) : C_4H (40 \text{ K} < E_u/k < 80 \text{ K}) : C_4H (E_u/k > 130 \text{ K}) = 1 : 1.6 : 3.6 : 5.7$. The excitation temperatures of C_4H ($\nu = 1$) are estimated to be $C_4H (E_u/k < 260 \text{ K}) : C_4H (E_u/k > 315 \text{ K}) = 1 : 6.8$.

Table F1 gives information about the excitation temperature, column density in specific levels, and fractional abundances of the molecules, relative to H_2 , for C_4H ($\nu = 0$), C_4H ($\nu = 1$), HC_3N , HC_5N , CH_3CN , C_3S , and SiS , at different upper energy levels. Figure F1 and Figure F2 show that the thermal structures of HC_3N , HC_5N , C_3S , CH_3CN , SiS , C_4H ($\nu = 0$) and C_4H ($\nu = 1$) are stratified (Chau et al. 2012). Similarly to HC_3N and HC_5N , their excitation temperatures increase with the increase of rotational energy level. Therefore, like HC_5N , HC_7N , and HC_9N , the high-J transitions of these molecules in the CSE of IRC+10216 can trace the warmer molecular regions. The column density and abundance derived from different transitions of the same molecule are different, which may be due to opacity effects (Zhang et al. 2017).

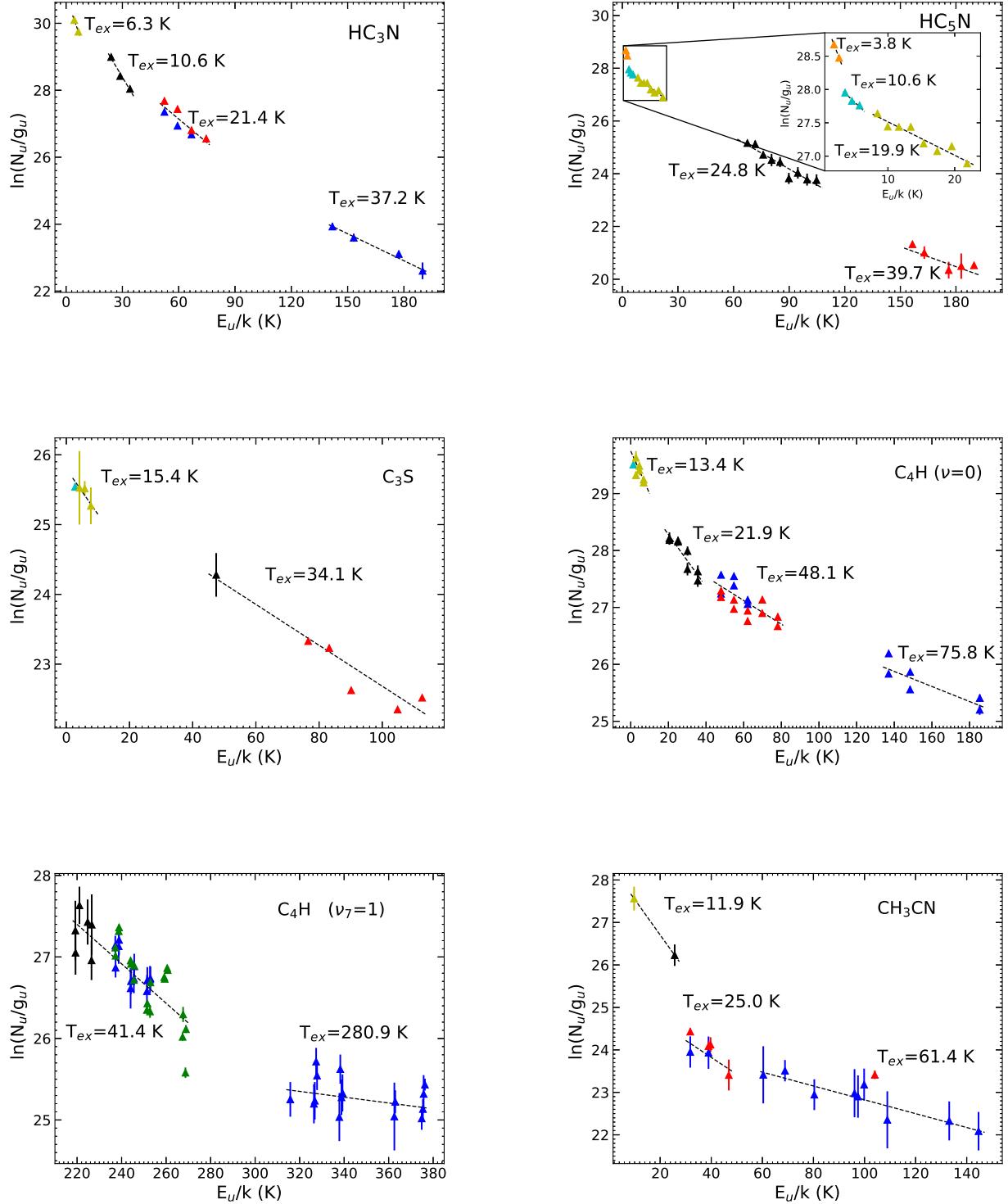


Figure F1. Multi-components revealed in the rotational diagrams of several species: HC₃N, HC₅N, C₃S, C₄H ($\nu = 0$), C₄H ($\nu = 1$) and CH₃CN. The results obtained from the linear least-squares fitting are plotted in black dashed lines. The adopted data points with error bars are from our PMO–13.7 m observations (black triangles), He et al. (2008) (blue triangles), Gong et al. (2015) (cyan triangles), Zhang et al. (2017) (dark-orange triangles), Kawaguchi et al. (1995) (yellow-green triangles), Cernicharo et al. (2000) (red triangles), Agúndez et al. (2012) (green triangles), and Groesbeck et al. (1994) (magenta triangles), respectively. Note that the error bars are invisible if their values are smaller than the adopted data points.

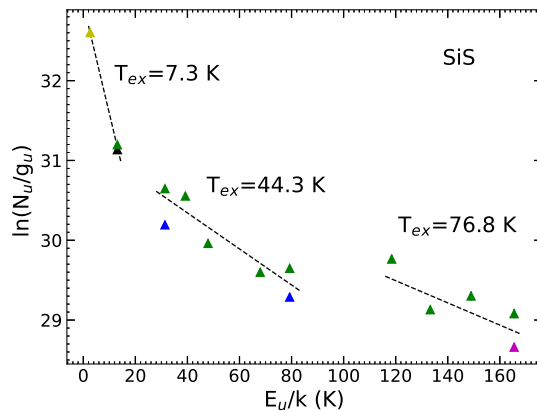


Figure F2. Same as Figure F1 but for SiS.

The low rotational lines observed in the CSE of AGB stars are seen to trace the low temperature region, while the information on warmer regions is determined by the higher energy lines. Some molecules with stratified excitation temperatures have already been mapped with high resolution, allowing us to determine the extended ranges of the cold and warm components based on the results. These findings have been summarized in Table F2.

Thanks to previously obtained maps of C_4H ($\nu=0$) by high resolution telescopes or interferometers, we have discovered that the spatial distribution of low-rotational transitions ($N = 9 - 8$ through $N = 12 - 11$) form a hollow shell structure with a width of about $3''$ and a radius of about $15''$ (Agúndez et al. 2017). In contrast, high rotational transitions ($N = 36 - 35$) show a compact spatial distribution (radius $\leq 2.7''$) (Patel et al. 2011). The spatial distribution between low- and the high-rotational transitions ($N = 27 - 26$) has both characteristics, that is, there is a compact distribution in the center and a bright shell structure outside (Cooksey et al. 2015).

The molecule at issue is CH_3CN . Agúndez et al. (2015) observed the spatial distribution of CH_3CN ($J = 14 - 13$) using the ALMA telescope, which showed a hollow shell with a radius of about $2''$ and a width of about $1''$. However, the CH_3CN observed by Patel et al. (2011) using SMA ($J = 16 - 15$ to $J = 19 - 18$) indicated a compact spatial distribution with a radius of about $3''$. Agúndez et al. (2015) points out that the higher rotational transition lines observed with the SMA may cause the emission to shift inward, and that the compact distribution in the center may be due to the insufficient resolution of the SMA. There are chemical models that predict that most CH_3CN should be distributed at a large radius (about $18''$, see Agúndez et al. 2008b; Li et al. 2014), and other chemical models predict that most CH_3CN is located within a radius of about $15''$, but with a compact distribution of about $1''$ in the center (Agúndez et al. 2015), inconsistent with the ALMA observations. We speculate that the low- J transitions of CH_3CN are likely distributed over a large radius, and the emission may move gradually inwards as the rotational energy level increases, similar to C_4H ($\nu=0$).

G. DETAILED COMPARISON OF EMISSION LINES OBTAINED WITH DIFFERENT ANGULAR RESOLUTIONS

Here, we provide a comparison of the line intensities and line shapes of the same transition of a molecule obtained by telescopes with different angular resolutions, including IRAM-30m, Onsala-20m, FCRAO-14m, TRA0-14m, PMO-13.7m, NRAO-11m, the Number Two 10.4m telescope of the Owens Valley Radio Observatory, and the 7m Bell Laboratories Antenna at Crawford Hill.

(1) The impact of different angular resolutions on the integrated line intensities. Comparison of emission lines observed with different angular resolutions is more uncertain if any of the observed lines are weak and we suggest that

Table F1. Multi-components fits for C₄H, HC₃N, HC₅N, CH₃CN, C₃S, and SiS.

Species	E_u/k (K)	T_{ex} (K)	N (cm ⁻²)	$f(N/N_{\text{H}_2})$
HC ₃ N	$E_u/k < 10$	6.3 (0.0)	$6.88 (0.01) \times 10^{14}$	2.67×10^{-7}
	$20 < E_u/k < 35$	10.6 (1.4)	$1.78 (0.70) \times 10^{15}$	6.92×10^{-7}
	$50 < E_u/k < 80$	21.4 (4.7)	$1.00 (0.67) \times 10^{15}$	3.89×10^{-7}
HC ₅ N	$E_u/k > 140$	37.1 (3.0)	$1.93 (0.74) \times 10^{14}$	7.51×10^{-8}
	$E_u/k < 3$	3.8 (0.0)	$2.81 (0.00) \times 10^{14}$	1.09×10^{-7}
	$3 < E_u/k < 6$	10.6 (2.1)	$3.19 (0.69) \times 10^{14}$	1.24×10^{-7}
	$8 < E_u/k < 25$	19.9 (2.8)	$4.59 (0.82) \times 10^{14}$	1.78×10^{-7}
C ₃ S	$60 < E_u/k < 105$	24.8 (3.3)	$4.65 (2.28) \times 10^{14}$	1.81×10^{-7}
	$E_u/k > 150$	39.7 (17.4)	$4.53 (9.00) \times 10^{13}$	1.76×10^{-8}
	$E_u/k < 10$	15.4 (4.0)	$1.79 (0.49) \times 10^{13}$	9.25×10^{-9}
C ₄ H ($\nu = 0$)	$E_u/k > 40$	34.1 (2.4)	$3.29 (0.46) \times 10^{13}$	1.70×10^{-8}
	$E_u/k < 10$	13.4 (5.2)	$1.96 (0.81) \times 10^{15}$	7.60×10^{-7}
	$20 < E_u/k < 40$	21.9 (3.7)	$1.84 (0.51) \times 10^{15}$	7.14×10^{-7}
C ₄ H ($\nu = 1$)	$40 < E_u/k < 80$	48.1 (12.3)	$1.77 (0.71) \times 10^{15}$	6.87×10^{-7}
	$E_u/k > 130$	75.8 (20.1)	$1.46 (0.92) \times 10^{15}$	5.67×10^{-7}
	$E_u/k < 260$	41.4 (4.2)	$1.67 (1.00) \times 10^{17}$	6.49×10^{-5}
CH ₃ CN	$E_u/k > 315$	280.9 (209.1)	$3.59 (4.68) \times 10^{15}$	1.39×10^{-6}
	$E_u/k < 30$	11.9 (0.0)	$2.07 (0.27) \times 10^{14}$	8.03×10^{-8}
	$30 < E_u/k < 50$	25.0 (10.4)	$3.35 (3.10) \times 10^{13}$	1.30×10^{-8}
SiS	$E_u/k > 50$	61.4 (10.9)	$5.06 (2.30) \times 10^{13}$	1.97×10^{-8}
	$E_u/k < 15$	7.3 (0.3)	$3.17 (0.32) \times 10^{15}$	9.02×10^{-7}
	$20 < E_u/k < 80$	44.3 (8.5)	$3.84 (1.28) \times 10^{15}$	1.09×10^{-6}
	$E_u/k > 115$	76.8 (33.3)	$6.32 (5.96) \times 10^{15}$	1.80×10^{-6}

Table F2. The cold and warm components of the extended radius of molecular C₄H, HC₃N, HC₅N, CH₃CN, and SiS.

Species	Radial extent (r) (")	Telescope	Comments
HC ₃ N (warm)	$r \leq 5$ ⁽¹⁾	ALMA	$J = 28 - 27, J = 30 - 29, \text{ and } J = 38 - 37$
HC ₃ N (cool)	$7 \leq r \leq 18.5$ ⁽²⁾	ALMA	$J = 10 - 9 \text{ to } J = 12 - 11$
HC ₅ N (warm)	$13 \leq r \leq 18$ ⁽²⁾	ALMA	$J = 32 - 31 \text{ to } J = 43 - 42$
C ₄ H ($\nu=0$) (warm)	$r \leq 2.7$ ⁽³⁾	SMA	$N = 36 - 35$
C ₄ H ($\nu=0$) (cool)	$12 \leq r \leq 20$ ⁽²⁾	ALMA	$N = 9 - 8 \text{ to } N = 12 - 11$
C ₄ H ($\nu=1$) (cool)	$12 \leq r \leq 18$ ^(4,5)	IRAM, SMA	$N = 27 - 26$
CH ₃ CN (warm)	$r \leq 3.2$ ⁽³⁾	SMA	$J = 16 - 15 \text{ to } J = 19 - 18$
SiS (warm)	$r \leq 2$ ⁽⁶⁾	CARMA	$J = 14 - 13$
SiS (cool)	$r \leq 10$ ^(7,8,9)	ALMA, BIMA, IRAM	$J = 5 - 4, J = 6 - 5, J = 8 - 7, J = 9 - 8, \text{ and } J = 12 - 11$

NOTE—The radial extent was estimated to be the value at which the brightness distribution had fallen to half its peak value. References : (1) Siebert et al. (2022); (2) Agúndez et al. (2017); (3) Patel et al. (2011); (4) Guélin et al. (1999); (5) Cooksy et al. (2015); (6) Fonfría et al. (2014); (7) Velilla-Prieto et al. (2019); (8) Bieging & Tafalla (1993); (9) Lucas et al. (1995).

such comparisons be made only if the S/N of the lines are greater than or equal to 5. For the strong lines (S/N \geq 5), the integrated intensity of the same molecular line from different angular resolutions is approximately identical, i.e., $\int T_{\text{R}} dv \approx \text{Constant}$, where $T_{\text{R}} = \frac{T_{\text{mb}}}{\eta_{\text{BD}}}$, $\eta_{\text{BD}} = \frac{\theta_s^2}{\theta_s^2 + \theta_{\text{beam}}^2}$ (see Section 4.1.1), $T_{\text{mb}} = T_{\text{A}}^*/\eta$ (see Section 2). In other words, the ratio of the integrated line intensity ($\int T_{\text{R}} dv$) between the same molecular transition from different angular resolutions is close to unity. For instance, Zhang et al. (2017) found that the ratios of the integrated intensities observed with the TMRT-65 m for HC₇N ($\nu = 0, J = 16 - 15$), SiS ($\nu = 0, J = 1 - 0$), and HC₃N ($\nu = 0, J = 2 - 1$)

to those values derived by Gong et al. (2015) using the Effelsberg–100 m telescope were 1 : (0.863 ± 0.121), 1 : (0.928 ± 0.029), and 1 : (0.899 ± 0.020), respectively. We compare the integrated intensities of SiS, HNC, and HCN in IRC +10216 observed by the PMO–13.7 m, TRAO–14 m, and IRAM–30 m telescopes, and find that the ratios among SiS ($J = 5 - 4$), HNC ($J = 1 - 0$), and HCN ($J = 1 - 0$) are 1 : 0.82 : 0.72, 1 : 0.88 : 0.86, and 1 : 0.83 : 1.08, respectively. The ratio of the integrated intensities of ^{13}CO deduced by the observations from PMO–13.7 m, TRAO–14 m, and 7 m Bell Laboratories Antenna at Crawford Hill telescopes is 1:0.88:0.96.

(2) The impact of different angular resolutions on the line shapes. For the strong emission lines ($S/N \geq 5$), the observed spectral line shape is the same for the same transition of the same molecule with different angular resolutions. If the S/N is less than 5, the observed line profiles might differ. Take molecular C_4H as an example. Using the PMO–13.7 m telescope, we observed double-peaked structures of C_4H lines in all the $N = 9 - 8, 10 - 9, 11 - 10, 12 - 11$ transitions with $S/N \geq 5$, as shown in Figure C2. Guélin et al. (1978) observed similar transitions of C_4H via the NRAO–11 m telescope with the S/N less than 5, and obtained different conclusions: the shapes of the $N = 9 - 8$ and $N = 10 - 9$ lines were difficult to judge due to the poor S/N ; the $N = 11 - 10$ line showed a flat-topped structure; the $N = 12 - 11$ line exhibited a double-peaked structure. The C_4H ($N = 9 - 8$) observed by the Onsala–20 m telescope (Johansson et al. 1984) and the C_4H ($N = 10 - 9$) observed by the IRAM–30 m telescope (Cernicharo et al. 1986a) both possess double-peaked line shapes.

(3) The impact of different angular resolutions on the double peaked spectra. For the optically thin species that exhibit double-peaked line shapes, a more considerable intensity contrast can be found between the line wings and the line center while using a telescope with higher spatial resolution (Olofsson et al. 1982). For instance, the C_2H $N = 1 - 0, J = 3/2 - 1/2, F = 2 - 1$ was observed by the IRAM–30 m (De Beck et al. 2012), Onsala–20 m (Truong-Bach et al. 1987), TRAO–14 m (Park et al. 2008), and PMO–13.7 m (this work) telescopes towards IRC +10216. All of these spectra showed double-peaked shapes while $S/N \geq 5$. The calculated intensity contrasts between the line wings and the line center are 2.3, 1.4, 1.3, and 1.8. These values for HNC ($J = 1 - 0$) are 1.8, 1.7, 1.2, and 1.4, respectively. Similarly, for ^{13}CO observed by the IRAM–30 m (Kahane et al. 1992), Onsala–20 m (Olofsson et al. 1982), TRAO–14 m (Park et al. 2008), PMO–13.7 m (this work), NRAO–11 m (Kuiper et al. 1976; Wannier & Linke 1978), and the 7 m Bell Laboratories Antenna at Crawford Hill (Knapp & Chang 1985) telescopes, these values are obtained to be 3.4, 2.6, 2.2, 2.4, 1.9, and 1.8, respectively.

REFERENCES

- Agúndez, M., & Cernicharo, J. 2006, *ApJ*, 650, 374, doi: [10.1086/506313](https://doi.org/10.1086/506313)
- Agúndez, M., Cernicharo, J., & Guélin, M. 2007, *ApJL*, 662, L91, doi: [10.1086/519561](https://doi.org/10.1086/519561)
- . 2014, *A&A*, 570, A45, doi: [10.1051/0004-6361/201424542](https://doi.org/10.1051/0004-6361/201424542)
- Agúndez, M., Cernicharo, J., Pardo, J. R., Guélin, M., & Phillips, T. G. 2008a, *A&A*, 485, L33, doi: [10.1051/0004-6361:200810193](https://doi.org/10.1051/0004-6361:200810193)
- Agúndez, M., Cernicharo, J., Quintana-Lacaci, G., et al. 2015, *ApJ*, 814, 143, doi: [10.1088/0004-637X/814/2/143](https://doi.org/10.1088/0004-637X/814/2/143)
- Agúndez, M., Cernicharo, J., Waters, L. B. F. M., et al. 2011, *A&A*, 533, L6, doi: [10.1051/0004-6361/201117578](https://doi.org/10.1051/0004-6361/201117578)
- Agúndez, M., Fonfría, J. P., Cernicharo, J., et al. 2012, *A&A*, 543, A48, doi: [10.1051/0004-6361/201218963](https://doi.org/10.1051/0004-6361/201218963)
- Agúndez, M., Fonfría, J. P., Cernicharo, J., Pardo, J. R., & Guélin, M. 2008b, *A&A*, 479, 493, doi: [10.1051/0004-6361:20078956](https://doi.org/10.1051/0004-6361:20078956)
- Agúndez, M., Cernicharo, J., Guélin, M., et al. 2010, *A&A*, 517, L2, doi: [10.1051/0004-6361/201015186](https://doi.org/10.1051/0004-6361/201015186)
- Agúndez, M., Cernicharo, J., Quintana-Lacaci, G., et al. 2017, *A&A*, 601, A4, doi: [10.1051/0004-6361/201630274](https://doi.org/10.1051/0004-6361/201630274)
- Anderson, J. K., & Ziurys, L. M. 2014, *ApJL*, 795, L1, doi: [10.1088/2041-8205/795/1/L1](https://doi.org/10.1088/2041-8205/795/1/L1)
- Andrews, H., De Beck, E., & Hirvonen, P. 2022, *MNRAS*, 510, 383, doi: [10.1093/mnras/stab3244](https://doi.org/10.1093/mnras/stab3244)
- Apponi, A. J., McCarthy, M. C., Gottlieb, C. A., & Thaddeus, P. 1999, *ApJL*, 516, L103, doi: [10.1086/311998](https://doi.org/10.1086/311998)
- Araya, E., Hofner, P., Goldsmith, P., Slysh, S., & Takano, S. 2003, *ApJ*, 596, 556, doi: [10.1086/377533](https://doi.org/10.1086/377533)
- Asplund, M., Grevesse, N., Sauval, A. J., & Scott, P. 2009, *ARA&A*, 47, 481, doi: [10.1146/annurev.astro.46.060407.145222](https://doi.org/10.1146/annurev.astro.46.060407.145222)
- Avery, L. W., Broten, N. W., MacLeod, J. M., Oka, T., & Kroto, H. W. 1976, *ApJL*, 205, L173, doi: [10.1086/182117](https://doi.org/10.1086/182117)
- Avery, L. W., Amano, T., Bell, M. B., et al. 1992, *ApJS*, 83, 363, doi: [10.1086/191742](https://doi.org/10.1086/191742)
- Bakker, E. J., van Dishoeck, E. F., Waters, L. B. F. M., & Schoenmaker, T. 1997, *A&A*, 323, 469, <https://arxiv.org/abs/astro-ph/9610063>

- Battino, U., Pignatari, M., Tattersall, A., Denissenkov, P., & Herwig, F. 2022, *Universe*, 8, 170, doi: [10.3390/universe8030170](https://doi.org/10.3390/universe8030170)
- Becklin, E. E., Frogel, J. A., Hyland, A. R., Kristian, J., & Neugebauer, G. 1969, *ApJL*, 158, L133, doi: [10.1086/180450](https://doi.org/10.1086/180450)
- Bell, M. B. 1993, *ApJ*, 417, 305, doi: [10.1086/173313](https://doi.org/10.1086/173313)
- Bell, M. B., Avery, L. W., & Feldman, P. A. 1993, *ApJL*, 417, L37, doi: [10.1086/187088](https://doi.org/10.1086/187088)
- Bell, M. B., Avery, L. W., MacLeod, J. M., & Matthews, H. E. 1992a, *ApJ*, 400, 551, doi: [10.1086/172017](https://doi.org/10.1086/172017)
- Bell, M. B., Feldman, P. A., & Avery, L. W. 1992b, *ApJ*, 396, 643, doi: [10.1086/171745](https://doi.org/10.1086/171745)
- Bernath, P. F., Hinkle, K. H., & Keady, J. J. 1989, *Science*, 244, 562, doi: [10.1126/science.244.4904.562](https://doi.org/10.1126/science.244.4904.562)
- Betz, A. L. 1981, *ApJL*, 244, L103, doi: [10.1086/183490](https://doi.org/10.1086/183490)
- Betz, A. L., McLaren, R. A., & Spears, D. L. 1979, *ApJL*, 229, L97, doi: [10.1086/182937](https://doi.org/10.1086/182937)
- Bieging, J. H., & Nguyen-Quang-Rieu. 1989, *ApJL*, 343, L25, doi: [10.1086/185502](https://doi.org/10.1086/185502)
- Bieging, J. H., & Rieu, N.-Q. 1988, *ApJL*, 329, L107, doi: [10.1086/185187](https://doi.org/10.1086/185187)
- Bieging, J. H., & Tafalla, M. 1993, *AJ*, 105, 576, doi: [10.1086/116455](https://doi.org/10.1086/116455)
- Brown, R. D., Godfrey, P. D., Storey, J. W. V., & Clark, F. O. 1976, *Nature*, 262, 672, doi: [10.1038/262672a0](https://doi.org/10.1038/262672a0)
- Buhl, D., & Snyder, L. E. 1970, *Nature*, 228, 267, doi: [10.1038/228267a0](https://doi.org/10.1038/228267a0)
- Bujarrabal, V., Guélin, M., Morris, M., & Thaddeus, P. 1981, *A&A*, 99, 239
- Busso, M., Gallino, R., & Wasserburg, G. J. 1999, *ARA&A*, 37, 239, doi: [10.1146/annurev.astro.37.1.239](https://doi.org/10.1146/annurev.astro.37.1.239)
- Cabezas, C., Cernicharo, J., Alonso, J. L., et al. 2013, *ApJ*, 775, 133, doi: [10.1088/0004-637X/775/2/133](https://doi.org/10.1088/0004-637X/775/2/133)
- Cabezas, C., Pardo, J. R., Agúndez, M., et al. 2023, *A&A*, 672, L12, doi: [10.1051/0004-6361/202346462](https://doi.org/10.1051/0004-6361/202346462)
- Cernicharo, J., Agúndez, M., & Guélin, M. 2011, in *The Molecular Universe*, ed. J. Cernicharo & R. Bachiller, Vol. 280, 237–248, doi: [10.1017/S1743921311025014](https://doi.org/10.1017/S1743921311025014)
- Cernicharo, J., Daniel, F., Castro-Carrizo, A., et al. 2013, *ApJL*, 778, L25, doi: [10.1088/2041-8205/778/2/L25](https://doi.org/10.1088/2041-8205/778/2/L25)
- Cernicharo, J., Gottlieb, C. A., Guélin, M., et al. 1991a, *ApJL*, 368, L39, doi: [10.1086/185943](https://doi.org/10.1086/185943)
- . 1991b, *ApJL*, 368, L43, doi: [10.1086/185944](https://doi.org/10.1086/185944)
- Cernicharo, J., Gottlieb, C. A., Guélin, M., Thaddeus, P., & Vrtilik, J. M. 1989, *ApJL*, 341, L25, doi: [10.1086/185449](https://doi.org/10.1086/185449)
- Cernicharo, J., & Guélin, M. 1987, *A&A*, 183, L10
- . 1996, *A&A*, 309, L27
- Cernicharo, J., Guélin, M., Agúndez, M., et al. 2007, *A&A*, 467, L37, doi: [10.1051/0004-6361:20077415](https://doi.org/10.1051/0004-6361:20077415)
- Cernicharo, J., Guélin, M., Agúndez, M., McCarthy, M. C., & Thaddeus, P. 2008, *ApJL*, 688, L83, doi: [10.1086/595583](https://doi.org/10.1086/595583)
- Cernicharo, J., Guélin, M., Hein, H., & Kahane, C. 1987a, *A&A*, 181, L9
- Cernicharo, J., Guélin, M., & Kahane, C. 2000, *A&AS*, 142, 181, doi: [10.1051/aas:2000147](https://doi.org/10.1051/aas:2000147)
- Cernicharo, J., Guélin, M., Kahane, C., Bogey, M., & Demuyne, C. 1991c, *A&A*, 246, 213
- Cernicharo, J., Guélin, M., Menten, K. M., & Walmsley, C. M. 1987b, *A&A*, 181, L1
- Cernicharo, J., Guélin, M., & Pardo, J. R. 2004, *ApJL*, 615, L145, doi: [10.1086/426439](https://doi.org/10.1086/426439)
- Cernicharo, J., Kahane, C., Gomez-Gonzalez, J., & Guélin, M. 1986a, *A&A*, 164, L1
- . 1986b, *A&A*, 167, L5
- . 1986c, *A&A*, 167, L9
- Cernicharo, J., Marcelino, N., Agúndez, M., & Guélin, M. 2015a, *A&A*, 575, A91, doi: [10.1051/0004-6361/201424565](https://doi.org/10.1051/0004-6361/201424565)
- Cernicharo, J., Decin, L., Barlow, M. J., et al. 2010a, *A&A*, 518, L136, doi: [10.1051/0004-6361/201014553](https://doi.org/10.1051/0004-6361/201014553)
- Cernicharo, J., Waters, L. B. F. M., Decin, L., et al. 2010b, *A&A*, 521, L8, doi: [10.1051/0004-6361/201015150](https://doi.org/10.1051/0004-6361/201015150)
- Cernicharo, J., McCarthy, M. C., Gottlieb, C. A., et al. 2015b, *ApJL*, 806, L3, doi: [10.1088/2041-8205/806/1/L3](https://doi.org/10.1088/2041-8205/806/1/L3)
- Cernicharo, J., Agúndez, M., Velilla Prieto, L., et al. 2017, *A&A*, 606, L5, doi: [10.1051/0004-6361/201731672](https://doi.org/10.1051/0004-6361/201731672)
- Cernicharo, J., Guélin, M., Agúndez, M., et al. 2018, *A&A*, 618, A4, doi: [10.1051/0004-6361/201833335](https://doi.org/10.1051/0004-6361/201833335)
- Cernicharo, J., Velilla-Prieto, L., Agúndez, M., et al. 2019a, *A&A*, 627, L4, doi: [10.1051/0004-6361/201936040](https://doi.org/10.1051/0004-6361/201936040)
- Cernicharo, J., Cabezas, C., Pardo, J. R., et al. 2019b, *A&A*, 630, L2, doi: [10.1051/0004-6361/201936372](https://doi.org/10.1051/0004-6361/201936372)
- . 2023a, *A&A*, 672, L13, doi: [10.1051/0004-6361/202346467](https://doi.org/10.1051/0004-6361/202346467)
- Cernicharo, J., Pardo, J. R., Cabezas, C., et al. 2023b, *A&A*, 670, L19, doi: [10.1051/0004-6361/202245816](https://doi.org/10.1051/0004-6361/202245816)
- Changala, P. B., Gupta, H., Cernicharo, J., et al. 2022, *ApJL*, 940, L42, doi: [10.3847/2041-8213/aca144](https://doi.org/10.3847/2041-8213/aca144)
- Chapovsky, P. L. 2021, *MNRAS*, 503, 1773, doi: [10.1093/mnras/stab407](https://doi.org/10.1093/mnras/stab407)
- Charbonnel, C. 1995, *ApJL*, 453, L41, doi: [10.1086/309744](https://doi.org/10.1086/309744)
- Chau, W., Zhang, Y., Nakashima, J.-i., Deguchi, S., & Kwok, S. 2012, *ApJ*, 760, 66, doi: [10.1088/0004-637X/760/1/66](https://doi.org/10.1088/0004-637X/760/1/66)
- Churchwell, E., Winnewisser, G., & Walmsley, C. M. 1978, *A&A*, 67, 139
- Clegg, R. E. S., Hinkle, K. H., & Lambert, D. L. 1982, *MNRAS*, 201, 95, doi: [10.1093/mnras/201.1.95](https://doi.org/10.1093/mnras/201.1.95)

- Cooksy, A. L., Gottlieb, C. A., Killian, T. C., et al. 2015, *ApJS*, 216, 30, doi: [10.1088/0067-0049/216/2/30](https://doi.org/10.1088/0067-0049/216/2/30)
- Cordiner, M. A., & Millar, T. J. 2009, *ApJ*, 697, 68, doi: [10.1088/0004-637X/697/1/68](https://doi.org/10.1088/0004-637X/697/1/68)
- Cristallo, S., Straniero, O., Gallino, R., et al. 2009, *ApJ*, 696, 797, doi: [10.1088/0004-637X/696/1/797](https://doi.org/10.1088/0004-637X/696/1/797)
- Crosas, M., & Menten, K. M. 1997, *ApJ*, 483, 913, doi: [10.1086/304256](https://doi.org/10.1086/304256)
- Daniel, F., Agúndez, M., Cernicharo, J., et al. 2012, *A&A*, 542, A37, doi: [10.1051/0004-6361/201118449](https://doi.org/10.1051/0004-6361/201118449)
- Dayal, A., & Biegging, J. H. 1995, *ApJ*, 439, 996, doi: [10.1086/175237](https://doi.org/10.1086/175237)
- De Beck, E., Decin, L., de Koter, A., et al. 2010, *A&A*, 523, A18, doi: [10.1051/0004-6361/200913771](https://doi.org/10.1051/0004-6361/200913771)
- De Beck, E., Lombaert, R., Agúndez, M., et al. 2012, *A&A*, 539, A108, doi: [10.1051/0004-6361/201117635](https://doi.org/10.1051/0004-6361/201117635)
- Decin, L., Justtanont, K., De Beck, E., et al. 2010, *A&A*, 521, L4, doi: [10.1051/0004-6361/201015069](https://doi.org/10.1051/0004-6361/201015069)
- Draine, B. T. 1978, *ApJS*, 36, 595, doi: [10.1086/190513](https://doi.org/10.1086/190513)
- Epchtein, N., Le Bertre, T., Lepine, J. R. D., et al. 1987, *A&AS*, 71, 39
- Fonfría, J. P., Cernicharo, J., Richter, M. J., et al. 2015, *MNRAS*, 453, 439, doi: [10.1093/mnras/stv1634](https://doi.org/10.1093/mnras/stv1634)
- Fonfría, J. P., Fernández-López, M., Agúndez, M., et al. 2014, *MNRAS*, 445, 3289, doi: [10.1093/mnras/stu1968](https://doi.org/10.1093/mnras/stu1968)
- Fonfría, J. P., Hinkle, K. H., Cernicharo, J., et al. 2017, *ApJ*, 835, 196, doi: [10.3847/1538-4357/835/2/196](https://doi.org/10.3847/1538-4357/835/2/196)
- Fonfría, J. P., Fernández-López, M., Pardo, J. R., et al. 2018, *ApJ*, 860, 162, doi: [10.3847/1538-4357/aac5e3](https://doi.org/10.3847/1538-4357/aac5e3)
- Fonfría Expósito, J. P., Agúndez, M., Tercero, B., Pardo, J. R., & Cernicharo, J. 2006, *ApJL*, 646, L127, doi: [10.1086/507104](https://doi.org/10.1086/507104)
- Fong, D., Meixner, M., & Shah, R. Y. 2003, *ApJL*, 582, L39, doi: [10.1086/346034](https://doi.org/10.1086/346034)
- Fong, D., Meixner, M., Sutton, E. C., Zalucha, A., & Welch, W. J. 2006, *ApJ*, 652, 1626, doi: [10.1086/508127](https://doi.org/10.1086/508127)
- Ford, K. E. S., Neufeld, D. A., Goldsmith, P. F., & Melnick, G. J. 2003, *ApJ*, 589, 430, doi: [10.1086/374552](https://doi.org/10.1086/374552)
- Ford, K. E. S., Neufeld, D. A., Schilke, P., & Melnick, G. J. 2004, *ApJ*, 614, 990, doi: [10.1086/423886](https://doi.org/10.1086/423886)
- Gallardo Cava, I., Bujarrabal, V., Alcolea, J., Gómez-Garrido, M., & Santander-García, M. 2022, *A&A*, 659, A134, doi: [10.1051/0004-6361/202142339](https://doi.org/10.1051/0004-6361/202142339)
- Gensheimer, P. D. 1997a, *Ap&SS*, 251, 199, doi: [10.1023/A:1000744924767](https://doi.org/10.1023/A:1000744924767)
- . 1997b, *ApJL*, 479, L75, doi: [10.1086/310576](https://doi.org/10.1086/310576)
- Goldhaber, D. M., & Betz, A. L. 1984, *ApJL*, 279, L55, doi: [10.1086/184255](https://doi.org/10.1086/184255)
- Goldhaber, D. M., Betz, A. L., & Ottusch, J. J. 1987, *ApJ*, 314, 356, doi: [10.1086/165066](https://doi.org/10.1086/165066)
- Gong, Y., Henkel, C., Spezzano, S., et al. 2015, *A&A*, 574, A56, doi: [10.1051/0004-6361/201424819](https://doi.org/10.1051/0004-6361/201424819)
- Gong, Y., Henkel, C., Ott, J., et al. 2017, *ApJ*, 843, 54, doi: [10.3847/1538-4357/aa7853](https://doi.org/10.3847/1538-4357/aa7853)
- Groesbeck, T. D., Phillips, T. G., & Blake, G. A. 1994, *ApJS*, 94, 147, doi: [10.1086/192076](https://doi.org/10.1086/192076)
- Guélin, M., & Cernicharo, J. 1991, *A&A*, 244, L21
- Guélin, M., Cernicharo, J., Kahane, C., & Gomez-Gonzales, J. 1986, *A&A*, 157, L17
- Guélin, M., Cernicharo, J., Paubert, G., & Turner, B. E. 1990, *A&A*, 230, L9
- Guélin, M., Green, S., & Thaddeus, P. 1978, *ApJL*, 224, L27, doi: [10.1086/182751](https://doi.org/10.1086/182751)
- Guélin, M., Lucas, R., & Cernicharo, J. 1993, *A&A*, 280, L19
- Guélin, M., Lucas, R., & Neri, R. 1997, *IAU Symposium*, 170, 359
- Guélin, M., Muller, S., Cernicharo, J., et al. 2000, *A&A*, 363, L9
- Guélin, M., Muller, S., Cernicharo, J., McCarthy, M. C., & Thaddeus, P. 2004, *A&A*, 426, L49, doi: [10.1051/0004-6361:200400074](https://doi.org/10.1051/0004-6361:200400074)
- Guélin, M., Neininger, N., & Cernicharo, J. 1998, *A&A*, 335, L1. <https://arxiv.org/abs/astro-ph/9805105>
- Guélin, M., Neininger, N., Lucas, R., & Cernicharo, J. 1999, in *The Physics and Chemistry of the Interstellar Medium*, ed. V. Ossenkopf, J. Stutzki, & G. Winnewisser, 326
- Guélin, M., & Thaddeus, P. 1977, *ApJL*, 212, L81, doi: [10.1086/182380](https://doi.org/10.1086/182380)
- Habing, H. J., & Olofsson, H. 2004, *Asymptotic Giant Branch Stars*, doi: [10.1007/978-1-4757-3876-6](https://doi.org/10.1007/978-1-4757-3876-6)
- Halfen, D. T., Clouthier, D. J., & Ziurys, L. M. 2008, *ApJL*, 677, L101, doi: [10.1086/588024](https://doi.org/10.1086/588024)
- Hall, D. N. B., & Ridgway, S. T. 1978, *Nature*, 273, 281, doi: [10.1038/273281a0](https://doi.org/10.1038/273281a0)
- He, J. H., Dinh-V-Trung, & Hasegawa, T. I. 2017, *ApJ*, 845, 38, doi: [10.3847/1538-4357/aa7e76](https://doi.org/10.3847/1538-4357/aa7e76)
- He, J. H., Dinh-V-Trung, Kwok, S., et al. 2008, *ApJS*, 177, 275, doi: [10.1086/587142](https://doi.org/10.1086/587142)
- He, J. H., Kamiński, T., Mennickent, R. E., et al. 2019, *ApJ*, 883, 165, doi: [10.3847/1538-4357/ab3d37](https://doi.org/10.3847/1538-4357/ab3d37)
- Henkel, C., Matthews, H. E., Morris, M., Terebey, S., & Fich, M. 1985, *A&A*, 147, 143
- Herwig, F. 2005, *ARA&A*, 43, 435, doi: [10.1146/annurev.astro.43.072103.150600](https://doi.org/10.1146/annurev.astro.43.072103.150600)
- Hinkle, K. W., Keady, J. J., & Bernath, P. F. 1988, *Science*, 241, 1319, doi: [10.1126/science.241.4871.1319](https://doi.org/10.1126/science.241.4871.1319)
- Howard, W. E., Buhl, D., & Snyder, L. E. 1970, *IAUC*, 2251, 1

- Jefferts, K. B., Penzias, A. A., & Wilson, R. W. 1970a, ApJL, 161, L87, doi: [10.1086/180576](https://doi.org/10.1086/180576)
- Jefferts, K. B., Penzias, N. J., Penzias, A. A., & Wilson, R. W. 1970b, IAUC, 2231, 1
- Jeste, M., Wiesemeyer, H., Menten, K. M., & Wyrowski, F. 2023, A&A, 675, A139, doi: [10.1051/0004-6361/202346034](https://doi.org/10.1051/0004-6361/202346034)
- Jewell, P. R., & Snyder, L. E. 1984, ApJ, 278, 176, doi: [10.1086/161779](https://doi.org/10.1086/161779)
- Johansson, L. E. B., Andersson, C., Ellder, J., et al. 1984, A&A, 130, 227
- Johansson, L. E. B., Andersson, C., Elder, J., et al. 1985, A&AS, 60, 135
- Kahane, C., Cernicharo, J., Gomez-Gonzalez, J., & Guélin, M. 1992, A&A, 256, 235
- Kahane, C., Gomez-Gonzalez, J., Cernicharo, J., & Guélin, M. 1988, A&A, 190, 167
- Kaifu, N., Suzuki, H., Ohishi, M., et al. 1987, ApJL, 317, L111, doi: [10.1086/184922](https://doi.org/10.1086/184922)
- Kasai, Y., Kagi, E., & Kawaguchi, K. 2007, ApJL, 661, L61, doi: [10.1086/518555](https://doi.org/10.1086/518555)
- Kawaguchi, K., Kagi, E., Hirano, T., Takano, S., & Saito, S. 1993, ApJL, 406, L39, doi: [10.1086/186781](https://doi.org/10.1086/186781)
- Kawaguchi, K., Kasai, Y., Ishikawa, S.-I., & Kaifu, N. 1995, PASJ, 47, 853
- Kawaguchi, K., Fujimori, R., Aimi, S., et al. 2007, PASJ, 59, L47, doi: [10.1093/pasj/59.5.L47](https://doi.org/10.1093/pasj/59.5.L47)
- Keene, J., Young, K., Phillips, T. G., Buettgenbach, T. H., & Carlstrom, J. E. 1993, ApJL, 415, L131, doi: [10.1086/187050](https://doi.org/10.1086/187050)
- Keller, D., Menten, K. M., Kamiński, T., & Claussen, M. J. 2015, in *Astronomical Society of the Pacific Conference Series*, Vol. 497, *Why Galaxies Care about AGB Stars III: A Closer Look in Space and Time*, ed. F. Kerschbaum, R. F. Wing, & J. Hron, 123
- Khoury, T., de Koter, A., Decin, L., et al. 2014, A&A, 570, A67, doi: [10.1051/0004-6361/201424298](https://doi.org/10.1051/0004-6361/201424298)
- Knapp, G. R., & Chang, K. M. 1985, ApJ, 293, 281, doi: [10.1086/163235](https://doi.org/10.1086/163235)
- Koelmay, L. A., & Ziurys, L. M. 2023, ApJL, 958, L6, doi: [10.3847/2041-8213/ad0899](https://doi.org/10.3847/2041-8213/ad0899)
- Kuiper, T. B. H., Knapp, G. R., Knapp, S. L., & Brown, R. L. 1976, ApJ, 204, 408, doi: [10.1086/154183](https://doi.org/10.1086/154183)
- Le Gal, R., Xie, C., Herbst, E., et al. 2017, A&A, 608, A96, doi: [10.1051/0004-6361/201731566](https://doi.org/10.1051/0004-6361/201731566)
- Li, J., Wang, J. Z., Gu, Q. S., & Zheng, X. W. 2013, A&A, 555, A18, doi: [10.1051/0004-6361/201220943](https://doi.org/10.1051/0004-6361/201220943)
- Li, X., Millar, T. J., Walsh, C., Heays, A. N., & van Dishoeck, E. F. 2014, A&A, 568, A111, doi: [10.1051/0004-6361/201424076](https://doi.org/10.1051/0004-6361/201424076)
- Linke, R. A., Goldsmith, P. F., Wannier, P. G., Wilson, R. W., & Penzias, A. A. 1977, ApJ, 214, 50, doi: [10.1086/155229](https://doi.org/10.1086/155229)
- Lovas, F. J. 2004, *Journal of Physical and Chemical Reference Data*, 33, 177, doi: [10.1063/1.1633275](https://doi.org/10.1063/1.1633275)
- Lucas, R., Guélin, M., Kahane, C., Audinos, P., & Cernicharo, J. 1995, Ap&SS, 224, 293, doi: [10.1007/BF00667860](https://doi.org/10.1007/BF00667860)
- Massalkhi, S., Agúndez, M., Cernicharo, J., et al. 2018, A&A, 611, A29, doi: [10.1051/0004-6361/201732038](https://doi.org/10.1051/0004-6361/201732038)
- McCarthy, M. C., Gottlieb, C. A., Gupta, H., & Thaddeus, P. 2006, ApJL, 652, L141, doi: [10.1086/510238](https://doi.org/10.1086/510238)
- McElroy, D., Walsh, C., Markwick, A. J., et al. 2013, A&A, 550, A36, doi: [10.1051/0004-6361/201220465](https://doi.org/10.1051/0004-6361/201220465)
- McGuire, B. A. 2018, ApJS, 239, 17, doi: [10.3847/1538-4365/aae5d2](https://doi.org/10.3847/1538-4365/aae5d2)
- . 2022, ApJS, 259, 30, doi: [10.3847/1538-4365/ac2a48](https://doi.org/10.3847/1538-4365/ac2a48)
- Melnick, G. J., Neufeld, D. A., Ford, K. E. S., Hollenbach, D. J., & Ashby, M. L. N. 2001, *Nature*, 412, 160, <https://arxiv.org/abs/astro-ph/0107212>
- Menten, K. M., Reid, M. J., Kamiński, T., & Claussen, M. J. 2012, A&A, 543, A73, doi: [10.1051/0004-6361/201219422](https://doi.org/10.1051/0004-6361/201219422)
- Menten, K. M., Wyrowski, F., Keller, D., & Kamiński, T. 2018, A&A, 613, A49, doi: [10.1051/0004-6361/201732296](https://doi.org/10.1051/0004-6361/201732296)
- Milam, S. N., Halfen, D. T., Tenenbaum, E. D., et al. 2008, ApJ, 684, 618, doi: [10.1086/589135](https://doi.org/10.1086/589135)
- Milam, S. N., Woolf, N. J., & Ziurys, L. M. 2009, ApJ, 690, 837, doi: [10.1088/0004-637X/690/1/837](https://doi.org/10.1088/0004-637X/690/1/837)
- Millar, T. J. 2020, *Chinese Journal of Chemical Physics*, 33, 668, doi: [10.1063/1674-0068/cjcp2008145](https://doi.org/10.1063/1674-0068/cjcp2008145)
- Millar, T. J., Herbst, E., & Bettens, R. P. A. 2000, MNRAS, 316, 195, doi: [10.1046/j.1365-8711.2000.03560.x](https://doi.org/10.1046/j.1365-8711.2000.03560.x)
- Morisawa, Y., Fushitani, M., Kato, Y., et al. 2006, ApJ, 642, 954, doi: [10.1086/501041](https://doi.org/10.1086/501041)
- Morris, M., Gilmore, W., Palmer, P., Turner, B. E., & Zuckerman, B. 1975, ApJL, 199, L47, doi: [10.1086/181846](https://doi.org/10.1086/181846)
- Morris, M., Zuckerman, B., Palmer, P., & Turner, B. E. 1971, ApJL, 170, L109, doi: [10.1086/180850](https://doi.org/10.1086/180850)
- Müller, H. S. P., Schlöder, F., Stutzki, J., & Winnewisser, G. 2005, *Journal of Molecular Structure*, 742, 215, doi: [10.1016/j.molstruc.2005.01.027](https://doi.org/10.1016/j.molstruc.2005.01.027)
- Nguyen-Q-Rieu, Graham, D., & Bujarrabal, V. 1984, A&A, 138, L5
- Nyman, L. A., Olofsson, H., Johansson, L. E. B., et al. 1993, A&A, 269, 377
- Ohishi, M., Kaifu, N., Kawaguchi, K., et al. 1989, ApJL, 345, L83, doi: [10.1086/185558](https://doi.org/10.1086/185558)

- Olofsson, H. 1996, *Ap&SS*, 245, 169, doi: [10.1007/BF00642225](https://doi.org/10.1007/BF00642225)
- Olofsson, H., Johansson, L. E. B., Hjalmarsen, A., & Nguyen-Quang-Rieu. 1982, *A&A*, 107, 128
- Pardo, J. R., Cabezas, C., Fonfría, J. P., et al. 2021, *A&A*, 652, L13, doi: [10.1051/0004-6361/202141671](https://doi.org/10.1051/0004-6361/202141671)
- Pardo, J. R., Cernicharo, J., Goicoechea, J. R., Guélin, M., & Asensio Ramos, A. 2007, *ApJ*, 661, 250, doi: [10.1086/513734](https://doi.org/10.1086/513734)
- Pardo, J. R., Cernicharo, J., Velilla Prieto, L., et al. 2018, *A&A*, 615, L4, doi: [10.1051/0004-6361/201833303](https://doi.org/10.1051/0004-6361/201833303)
- Pardo, J. R., Cernicharo, J., Tercero, B., et al. 2022, *A&A*, 658, A39, doi: [10.1051/0004-6361/202142263](https://doi.org/10.1051/0004-6361/202142263)
- Park, I. H., Wakelam, V., & Herbst, E. 2006, *A&A*, 449, 631, doi: [10.1051/0004-6361:20054420](https://doi.org/10.1051/0004-6361:20054420)
- Park, J. A., Cho, S.-H., Lee, C. W., & Yang, J. 2008, *AJ*, 136, 2350, doi: [10.1088/0004-6256/136/6/2350](https://doi.org/10.1088/0004-6256/136/6/2350)
- Patel, N. A., Young, K. H., Brünken, S., et al. 2009, *ApJ*, 692, 1205, doi: [10.1088/0004-637X/692/2/1205](https://doi.org/10.1088/0004-637X/692/2/1205)
- Patel, N. A., Young, K. H., Gottlieb, C. A., et al. 2011, *ApJS*, 193, 17, doi: [10.1088/0067-0049/193/1/17](https://doi.org/10.1088/0067-0049/193/1/17)
- Peng, T. C., Humphreys, E. M. L., Testi, L., et al. 2013, *A&A*, 559, L8, doi: [10.1051/0004-6361/201322466](https://doi.org/10.1051/0004-6361/201322466)
- Penzias, A. A., Solomon, P. M., Wilson, R. W., & Jefferts, K. B. 1971, *ApJL*, 168, L53, doi: [10.1086/180784](https://doi.org/10.1086/180784)
- Pickett, H. M., Poynter, R. L., Cohen, E. A., et al. 1998, *JQSRT*, 60, 883, doi: [10.1016/S0022-4073\(98\)00091-0](https://doi.org/10.1016/S0022-4073(98)00091-0)
- Portinari, L., Chiosi, C., & Bressan, A. 1998, *A&A*, 334, 505, doi: [10.48550/arXiv.astro-ph/9711337](https://doi.org/10.48550/arXiv.astro-ph/9711337)
- Pulliam, R. L., Edwards, J. L., & Ziurys, L. M. 2011, *ApJ*, 743, 36, doi: [10.1088/0004-637X/743/1/36](https://doi.org/10.1088/0004-637X/743/1/36)
- Pulliam, R. L., Savage, C., Agúndez, M., et al. 2010, *ApJL*, 725, L181, doi: [10.1088/2041-8205/725/2/L181](https://doi.org/10.1088/2041-8205/725/2/L181)
- Qiu, J.-J., Zhang, Y., Zhang, J.-S., & Nakashima, J.-i. 2022, *ApJS*, 259, 56, doi: [10.3847/1538-4365/ac5180](https://doi.org/10.3847/1538-4365/ac5180)
- Quintana-Lacaci, G., Agúndez, M., Cernicharo, J., et al. 2016, *A&A*, 592, A51, doi: [10.1051/0004-6361/201527688](https://doi.org/10.1051/0004-6361/201527688)
- Reach, W. T., Ruaud, M., Wiesemeyer, H., et al. 2022, *ApJ*, 926, 69, doi: [10.3847/1538-4357/ac4162](https://doi.org/10.3847/1538-4357/ac4162)
- Remijan, A. J., Hollis, J. M., Lovas, F. J., et al. 2007, *ApJL*, 664, L47, doi: [10.1086/520704](https://doi.org/10.1086/520704)
- Ridgway, S. T., Hall, D. N. B., Wojslaw, R. S., Kleinmann, S. G., & Weinberger, D. A. 1976, *Nature*, 264, 345, doi: [10.1038/264345a0](https://doi.org/10.1038/264345a0)
- Sahai, R., Wootten, A., & Clegg, R. E. S. 1984, *ApJ*, 284, 144, doi: [10.1086/162394](https://doi.org/10.1086/162394)
- Saito, S., Kawaguchi, K., Yamamoto, S., et al. 1987, *ApJL*, 317, L115, doi: [10.1086/184923](https://doi.org/10.1086/184923)
- Schöier, F. L., Fong, D., Bieging, J. H., et al. 2007, *ApJ*, 670, 766, doi: [10.1086/522196](https://doi.org/10.1086/522196)
- Shan, W., Yang, J., Shi, S., et al. 2012, *IEEE Transactions on Terahertz Science and Technology*, 2, 593, doi: [10.1109/TTHZ.2012.2213818](https://doi.org/10.1109/TTHZ.2012.2213818)
- Siebert, M. A., Van de Sande, M., Millar, T. J., & Remijan, A. J. 2022, *ApJ*, 941, 90, doi: [10.3847/1538-4357/ac9e52](https://doi.org/10.3847/1538-4357/ac9e52)
- Smith, C. L., Zijlstra, A. A., & Fuller, G. A. 2015, *MNRAS*, 454, 177, doi: [10.1093/mnras/stv1934](https://doi.org/10.1093/mnras/stv1934)
- Snyder, L. E., & Buhl, D. 1971, *ApJL*, 163, L47, doi: [10.1086/180664](https://doi.org/10.1086/180664)
- . 1972, *Annals of the New York Academy of Sciences*, 194, 17, doi: [10.1111/j.1749-6632.1972.tb12687.x](https://doi.org/10.1111/j.1749-6632.1972.tb12687.x)
- Snyder, L. E., Henkel, C., Hollis, J. M., & Lovas, F. J. 1985, *ApJL*, 290, L29, doi: [10.1086/184436](https://doi.org/10.1086/184436)
- Solomon, P., Jefferts, K. B., Penzias, A. A., & Wilson, R. W. 1971, *ApJL*, 163, L53, doi: [10.1086/180665](https://doi.org/10.1086/180665)
- Suzuki, H., Kaifu, N., Miyaji, T., et al. 1984, *ApJ*, 282, 197, doi: [10.1086/162191](https://doi.org/10.1086/162191)
- Tenenbaum, E. D., Apponi, A. J., Ziurys, L. M., et al. 2006, *ApJL*, 649, L17, doi: [10.1086/508166](https://doi.org/10.1086/508166)
- Tenenbaum, E. D., Dodd, J. L., Milam, S. N., Woolf, N. J., & Ziurys, L. M. 2010a, *ApJL*, 720, L102, doi: [10.1088/2041-8205/720/1/L102](https://doi.org/10.1088/2041-8205/720/1/L102)
- . 2010b, *ApJS*, 190, 348, doi: [10.1088/0067-0049/190/2/348](https://doi.org/10.1088/0067-0049/190/2/348)
- Tenenbaum, E. D., & Ziurys, L. M. 2008, *ApJL*, 680, L121, doi: [10.1086/589973](https://doi.org/10.1086/589973)
- Tercero, F., López-Pérez, J. A., Gallego, J. D., et al. 2021, *A&A*, 645, A37, doi: [10.1051/0004-6361/202038701](https://doi.org/10.1051/0004-6361/202038701)
- Thaddeus, P., Cummins, S. E., & Linke, R. A. 1984, *ApJL*, 283, L45, doi: [10.1086/184330](https://doi.org/10.1086/184330)
- Thaddeus, P., Gottlieb, C. A., Gupta, H., et al. 2008, *ApJ*, 677, 1132, doi: [10.1086/528947](https://doi.org/10.1086/528947)
- Thaddeus, P., Gottlieb, C. A., Hjalmarsen, A., et al. 1985a, *ApJL*, 294, L49, doi: [10.1086/184507](https://doi.org/10.1086/184507)
- Thaddeus, P., Guélin, M., & Linke, R. A. 1981, *ApJL*, 246, L41, doi: [10.1086/183549](https://doi.org/10.1086/183549)
- Thaddeus, P., Vrtilek, J. M., & Gottlieb, C. A. 1985b, *ApJL*, 299, L63, doi: [10.1086/184581](https://doi.org/10.1086/184581)
- Truong-Bach, Nguyen-Q-Rieu, Omont, A., Olofsson, H., & Johansson, L. E. B. 1987, *A&A*, 176, 285
- Tsuge, M., Kouchi, A., & Watanabe, N. 2021, *ApJ*, 923, 71, doi: [10.3847/1538-4357/ac2a33](https://doi.org/10.3847/1538-4357/ac2a33)
- Tucker, K. D., Kutner, M. L., & Thaddeus, P. 1974, *ApJL*, 193, L115, doi: [10.1086/181646](https://doi.org/10.1086/181646)
- Turner, B. E. 1970, *IAUC*, 2268, 2
- . 1971, *ApJL*, 163, L35, doi: [10.1086/180662](https://doi.org/10.1086/180662)
- . 1992, *ApJL*, 388, L35, doi: [10.1086/186324](https://doi.org/10.1086/186324)
- Turner, B. E., Steimle, T. C., & Meerts, L. 1994, *ApJL*, 426, L97, doi: [10.1086/174043](https://doi.org/10.1086/174043)

- Van de Sande, M., & Millar, T. J. 2019, *ApJ*, 873, 36, doi: [10.3847/1538-4357/ab03d4](https://doi.org/10.3847/1538-4357/ab03d4)
- . 2022, *MNRAS*, 510, 1204, doi: [10.1093/mnras/stab3282](https://doi.org/10.1093/mnras/stab3282)
- Van de Sande, M., Walsh, C., & Millar, T. J. 2021, *MNRAS*, 501, 491, doi: [10.1093/mnras/staa3689](https://doi.org/10.1093/mnras/staa3689)
- van der Veen, W. E. C. J., Huggins, P. J., & Matthews, H. E. 1998, *ApJ*, 505, 749, doi: [10.1086/306191](https://doi.org/10.1086/306191)
- Velilla-Prieto, L., Cernicharo, J., Agúndez, M., et al. 2019, *A&A*, 629, A146, doi: [10.1051/0004-6361/201834717](https://doi.org/10.1051/0004-6361/201834717)
- Velilla Prieto, L., Cernicharo, J., Quintana-Lacaci, G., et al. 2015, *ApJL*, 805, L13, doi: [10.1088/2041-8205/805/2/L13](https://doi.org/10.1088/2041-8205/805/2/L13)
- Velilla Prieto, L., Sánchez Contreras, C., Cernicharo, J., et al. 2017, *A&A*, 597, A25, doi: [10.1051/0004-6361/201628776](https://doi.org/10.1051/0004-6361/201628776)
- Wannier, P. G., & Linke, R. A. 1978, *ApJ*, 225, 130, doi: [10.1086/156474](https://doi.org/10.1086/156474)
- Wasserburg, G. J., Karakas, A. I., & Lugaro, M. 2017, *ApJ*, 836, 126, doi: [10.3847/1538-4357/836/1/126](https://doi.org/10.3847/1538-4357/836/1/126)
- Wilson, R. W., Solomon, P. M., Penzias, A. A., & Jefferts, K. B. 1971, *ApJL*, 169, L35, doi: [10.1086/180809](https://doi.org/10.1086/180809)
- Wilson, T. L., & Rood, R. 1994, *ARA&A*, 32, 191, doi: [10.1146/annurev.aa.32.090194.001203](https://doi.org/10.1146/annurev.aa.32.090194.001203)
- Winnewisser, G., & Walmsley, C. M. 1978, *A&A*, 70, L37
- Woods, P. M., Schöier, F. L., Nyman, L. Å., & Olofsson, H. 2003, *A&A*, 402, 617, doi: [10.1051/0004-6361:20030190](https://doi.org/10.1051/0004-6361:20030190)
- Wootten, A., Lichten, S. M., Sahai, R., & Wannier, P. G. 1982, *ApJ*, 257, 151, doi: [10.1086/159973](https://doi.org/10.1086/159973)
- Yamamoto, S., Saito, S., Guélin, M., et al. 1987, *ApJL*, 323, L149, doi: [10.1086/185076](https://doi.org/10.1086/185076)
- Yan, Y. T., Henkel, C., Kobayashi, C., et al. 2023, *A&A*, 670, A98, doi: [10.1051/0004-6361/202244584](https://doi.org/10.1051/0004-6361/202244584)
- Yang, K., Zhang, Y., Qiu, J., Ao, Y., & Li, X. 2023, *PASJ*, 75, 853, doi: [10.1093/pasj/psad043](https://doi.org/10.1093/pasj/psad043)
- Zack, L. N., Halfen, D. T., & Ziurys, L. M. 2011, *ApJL*, 733, L36, doi: [10.1088/2041-8205/733/2/L36](https://doi.org/10.1088/2041-8205/733/2/L36)
- Zhang, X.-Y., Zhu, Q.-F., Li, J., et al. 2017, *A&A*, 606, A74, doi: [10.1051/0004-6361/201730791](https://doi.org/10.1051/0004-6361/201730791)
- Zhang, Y., Chau, W., Nakashima, J.-i., & Kwok, S. 2020, *PASJ*, 72, 46, doi: [10.1093/pasj/psaa032](https://doi.org/10.1093/pasj/psaa032)
- Zhang, Y., Kwok, S., & Dinh-V-Trung. 2008, *ApJ*, 678, 328, doi: [10.1086/529428](https://doi.org/10.1086/529428)
- . 2009a, *ApJ*, 691, 1660, doi: [10.1088/0004-637X/691/2/1660](https://doi.org/10.1088/0004-637X/691/2/1660)
- Zhang, Y., Kwok, S., & Nakashima, J.-i. 2009b, *ApJ*, 700, 1262, doi: [10.1088/0004-637X/700/2/1262](https://doi.org/10.1088/0004-637X/700/2/1262)
- Zhang, Y., Kwok, S., Nakashima, J.-i., Chau, W., & Dinh-V-Trung. 2013, *ApJ*, 773, 71, doi: [10.1088/0004-637X/773/1/71](https://doi.org/10.1088/0004-637X/773/1/71)
- Ziurys, L. M., Apponi, A. J., Guélin, M., & Cernicharo, J. 1995, *ApJL*, 445, L47, doi: [10.1086/187886](https://doi.org/10.1086/187886)
- Ziurys, L. M., Apponi, A. J., & Phillips, T. G. 1994, *ApJ*, 433, 729, doi: [10.1086/174682](https://doi.org/10.1086/174682)
- Ziurys, L. M., Savage, C., Highberger, J. L., et al. 2002, *ApJL*, 564, L45, doi: [10.1086/338775](https://doi.org/10.1086/338775)
- Zuckerman, B. 1987, in *Astrochemistry*, ed. M. S. Vardya & S. P. Tarafdar, Vol. 120, 345–355